

## **A Mobile Deformable Barrier Test for the Front Crash Assessment of Future Urban Microcars**

**Ernö Dux, Lutz Eckstein**

Institut für Kraftfahrzeuge, RWTH Aachen University  
Germany

**Maja Wolkenstein, Gian Antonio d'Addetta**

Robert Bosch GmbH  
Germany

**Peter Luttenberger**

Institut für Fahrzeugsicherheit, Graz University of Technology  
Austria

Paper Number 15-0343

### **ABSTRACT**

A rising share of electric microcars (with mass well below 800kg) is predicted for the future urban vehicle fleet. Therefore the relevance of safety hazards due to mass incompatibility in case of front crashes will increase significantly. The front crash test according to ECE regulation no.94 initially defined for M class vehicles does not allow to reproduce the predicted real-world crash severity for light vehicles. This paper describes an alternative test for front crash assessment of microcars using a mobile progressive deformable barrier (MPDB) with adjusted mass properties. Since the long term development of the vehicle fleet is unclear, a test set-up with parameterized barrier mass properties having the potential to reproduce variable car-to-car front crash constellations is proposed.

The relevant test parameters for a microcar front crash test are chosen based on predicted future trends from literature, expert surveys and car-to-car crash sensitivity tests. Based on that, a finite element (FE) model of a parametric MPDB is proposed, reproducing the mass properties of various possible front crash opponents. To quantify the use potential of the test, a comparison of MPDB test outputs for three types of possible microcar concepts with car-to-car crash outputs using FE Generic Car Models from the FIMCAR project as opponents is carried out. The main focus of this comparison is on structural crash performance and occupant injury. In order to bridge these two, an adequate crash restraint system triggering based on the acceleration sensing system is proposed.

As conclusion general use recommendations for the parametric MPDB test configuration are formulated.

The study presented within this document was executed within the EC co-financed project SafeEV (Safe Small Electric Vehicles through Advanced Simulation Methodologies) – [www.project-safeev.eu](http://www.project-safeev.eu)

### **INTRODUCTION**

The small cars segments (A/B) are predicted to show highest global growth rates in a mid-term perspective (*Kalmbach et al., 2011*). In an urban environment cars showing special features globally attributed to the term microcar – such as reduced overall dimensions, low fuel consumption due to reduced engine capacity, limited seating and storage space and in case of electric powering also local emission free usage – can become especially attractive.

Until now cars showing these properties can either be classified as M class vehicles (*Directive 2007/46/EC*) or as heavy quadricycles belonging to the category L7e-CP (*Regulation (EU) No 168/2013*) on the European market. The main distinction between these classifications with respect to passive safety is the lack of crash test assessment, that a L7e-CP vehicle has to fulfil for homologation, while M class vehicles are required to pass several crash tests. In addition, there is an upper speed limit of 90 km/h and an upper weight limit of 450 kg (without battery system) set to vehicles attributed to the L7e-CP class. M class listing is not related to a lower weight limit. Nevertheless current M class vehicles weight generally more than approximately 800 kg, due to the weight-increasing fulfilment of comfort and functionality requirements, partly not relevant in an urban use environment. The present study is focussing on future urban microcars defined as being placed in the weight gap between L7e-CP class and the virtual lower limit of 800 kg for current M class vehicles.

The main front crash passive safety hazard identified for light vehicles is the potential crash against heavier opponent vehicles (*O'Brien, 2010*) due to the high significance of mass incompatibility. This results in higher velocity change for the lighter crash partner and therefore in higher crash severity. Current European front crash testing procedures, either related to M class according to *UN-ECE Regulation No. 94* or related to L7e-C vehicles as seen in Euro NCAP's most recent test series for heavy quadricycles (*Euro NCAP, 2014*), are not addressing the issues of mass incompatibility by testing against fixed crash barriers. These test conditions do not reproduce the energy balance of a vehicle-to-vehicle crash and the possible influence of the mass ratio on crash severity for the assessed vehicle. Higher reproduction potential is attributed to mobile deformable barrier (MDB) tests according to different studies (e.g. *O'Brien, 2010* or *Uittenbogaard and Versmissen, 2013*), due to the more realistic energy balance.

The use profile of these future urban microcars is not yet clear on midterm forecasting level: Will their use be restricted to urban areas? With what kind of possible crash opponents will they share the traffic environment and what developments will influence closing speed and impact direction in case of front crash? Resulting from that, precise parameters of the relevant real world safety hazard related to vehicle-to-vehicle front crash cannot yet be defined. Fixed testing conditions with a static logic behind the crash severity definition do not have the flexibility to respond to changes in the target crash scenario.

### **USE POTENTIAL OF THE MOBILE PROGRESSIVE DEFORMABLE BARRIER (MPDB)**

Previous studies have identified the high use potential of MDBs for the front crash assessment of light vehicles. MDB tests show good reproduction potential of the real world crash kinematic. In addition, the structural interaction between crash partners is also suitably reproduced, when a deformable barrier element is chosen with stiffness properties that are comparable to those of a crash opponent's vehicle front.

The MPDB, introduced by *Bosch-Rekvelde et al., 2006* and further developed during the 'Frontal Impact and Compatibility Assessment Research (FIMCAR)' project is the most recent European development in the field of MDBs for front crash assessment. The weight is adjusted to represent the European fleet average with inertia properties according to US vehicle fleet mass properties. The progressive deformable barrier (PDB) as energy absorption element has stiffness properties that are comparable the those of recent vehicles tested in EuroNCAP's offset front crash configuration (*Uittenbogaard and Versmissen, 2013*). First analysis of the influence of the barrier weight on crash severity was already executed by *Bosch-Rekvelde et al., 2006*, identifying a mayor influence on crash pulse and energy dissipation level of the tested vehicle. The test set-up investigated during the FIMCAR project for the 1,500 kg MPDB has the following parameters: 50 % overlap, 50 km/h-50 km/h impact speed, 0 ° impact angle.

Test configurations using a mobile test barrier offer the highest number of crash configuration parameters, therefore being most suitable for a flexible adjustment of the test in case of target scenario shift. In this way the current MPDB test set-up can easily be adapted to a configuration relevant for microcar assessment.

### **DEFINITION OF A PARAMETRIC MOBILE PROGRESSIVE DEFORMABLE BARRIER (P-MPDB)**

Concerning the future real-world vehicle-to-vehicle crash target scenario for microcars, only general trends can be discussed:

- Relevant crash opponent mass: The arguments related to fuel saving and emission reductions specially in urban traffic environment lead to significant lightweighting efforts in vehicle development, possibly leading to lower average vehicle weight (*Luttenberger et al., 2013*). *Wismans et al. 2013* identify 1,150 kg curb weight as average front crash opponent weight for possible future urban microcars.
- Impact speed: It is unclear, how far the use profile of future urban microcars will be restricted to urban traffic environment, resulting in lower relevant crash speeds. In the same form the future penetration of advanced driver assistance systems related to collision mitigation into the vehicle fleet might have an impact speed reducing effect.
- Impact angle: with a possible use concentration of microcars to urban areas, the relevance of accidents with oblique impact direction in turning and crossing traffic is supposed to grow in relation to conventional head-on collisions (*Wismans et al., 2013*).

The current MDPB test configuration requires a parametric adaptation to fit more to the possible traffic scenario developments and the resulting real world vehicle-to-vehicle front crashes involving microcars.

For a better understanding of the relevance of different vehicle-to-vehicle crash parameters (opponent vehicle mass properties and configuration parameters like impact speed and angle) on the resulting crash severity for the lighter crash partner, vehicle-to-vehicle crash sensitivity tests are executed on a virtual level. To eliminate the influence of specific structural properties of exemplary vehicle models on crash severity output parameters, vehicles with idealized form and force compatibility properties are used for these tests. For this purpose vehicle models with homogeneous energy absorbing honeycomb structures filling the front vehicle are defined (c.f. *Figure 1, left*). These idealized front vehicles show progressive stiffness comparable to the lower load path within the PDB. The only remaining incompatibility property within the sensitivity test set is related to mass, representing different vehicle-to-vehicle crashes with mass ratio between 1:1 and 1:2.8.

The executed sensitivity testing allows the formulation of approximately linear dependencies between crash configuration parameters and the crash severity output. Based on this assessment, the implementation of the following parameters into a parametric model of the MPDB FE model is decided (c.f. *Figure 1, right*):

- Centre-of gravity in x-direction (driving direction),
- Total barrier mass and
- Inertia properties of barrier (defined as dependent on total barrier mass).

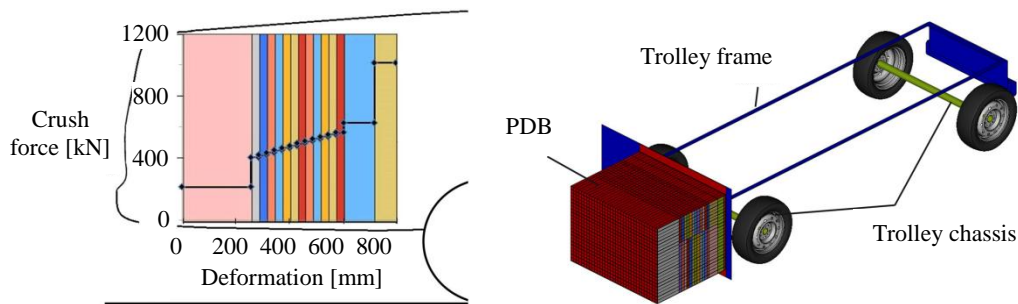


**Figure 1** Idealized vehicle front model (left) and its correspondence to the P-MPDB FE model (right)

The barrier model's main property is to represent real front crash opponent vehicles of different possible total mass. To model the mass-dependent inertia properties of a broad range of vehicles, the inertia values expressed as function of mass are implemented into the FE model of the barrier, based on fleet measurements as discussed by *Bosch-Rekvelde et al., 2006* (c.f. Equations 1-3).

$$I_{XY} = 0.0497 \cdot m^{1.4879} \quad (1.)$$

$$I_{XZ} = 0.0289 \cdot m^{1.5572} \quad (2.)$$

$$I_{YZ} = 0.0256 \cdot m^{1.3644} \quad (3.)$$

with  $m$  [kg];  $I_{ij}$  [ $\text{kg} \cdot \text{m}^2$ ]

Besides this adjustability of the barrier itself, also the influence of change of crash configuration parameters is to be analyzed. Therefore a range of impact speeds and angles are to be considered to represent different possible front crash scenarios. The barrier overlap is fixed to 50 % of the vehicle width, to allow a meaningful assessment of microcars structural performance in case of one sided loading of its energy absorbing structures.

## DEMONSTRATION OF P-MPDB USE POTENTIAL - STRUCTURAL CRASH BEHAVIOUR

In a next step, the use potential of the P-MPDB test configuration is to be quantified. The focus of this analysis is double:

- Show the advantages of this test set-up for microcar assessment in comparison to conventional offset crash test procedures.
- Identify the capacities and limitations of the test set-up to reproduce different crash severity aspects of vehicle-to-vehicle crash in different possible crash configurations.

For this assessment, three reference electric vehicle examples, being potential representatives of future urban microcars, are analysed in FE modelling environment concerning relevant structural crash severity output parameters in front crash situations:

Reference electric vehicle model 1 (REVM1) represents a light weight vehicle (curb weight = 685 kg), designed according to M class vehicle standards and therefore dimensioned to fulfil M class front crash regulation targets (Puppini *et al.*, 2013).

Reference electric vehicle model 2 subversion 8 (REVM2\_V8) is representative for vehicles situated at the borderline of the L7e-CP vehicle category (curb weight = 513 kg, including battery system weight), using conventional design tools and materials not considering any structural passive safety requirement. This design strategy results in a behaviour comparable to the ones of current heavy quadricycles (*c.f. Euro NCAP, 2014*), showing weak structures resulting in high crash deformations but soft deceleration pulses. Reference electric vehicle model 2 subversion 9 (REVM2\_V9) shows the same structure and weight properties as REVM2\_V8, but applies high performance materials, therefore showing stiff structural design resulting in low crash deformations but hard deceleration pulses. (Hinc, 2015)

Possible M class crash opponent vehicles to simulate real world vehicle-to-vehicle front crash are taken from the FE vehicle model pool of generic car models (GCM) (Stein *et al.*, 2012).

### P-MPDB use benefit in baseline crash configuration

The first step of the use potential assessment of the P-MPDB consists of a comparison between a chosen baseline vehicle-to-vehicle front crash, different standard barrier front crash tests and front crash against P-MPDB in a mass property version adjusted to the chosen crash opponent vehicle. This assessment step allows to proof whether the defined test set-up shows a higher potential to reproduce the baseline real-world front crash than known standard laboratory tests. For this purpose the baseline vehicle-to-vehicle front crash configuration is chosen to be the same as the reference for the definition of the 56 km/h ODB front crash according to ECE regulation No. 94 (Lowne, 1994):

- 50 % horizontal overlap
- 50 km/h impact speed (100 km/h closing speed)
- 0 deg impact (in-line impacting)

The generic car model 2A (GCM2A) is selected as reference opponent (curb weight: 1,186 kg), at is has a weight comparable to the average front crash opponent weight for future urban microcars identified above. Standard front crash tests (ODB front crash test, according to *UN-ECE Regulation No. 94* and the PDB front crash test as described in *Regulation No. 94 – Proposal for draft amendments*) and the MPDB test are compared to the P-MPDB test (*c.f. Table 1*). For every assessed microcar in each barrier crash configuration the percentile variation of the structural crash severity parameters is calculated in comparison to the vehicle-to-vehicle reference crash output according to Equation 4.

$$Variation = \frac{(parameter_{veh-to-barrier} - parameter_{veh-to-veh})}{parameter_{veh-to-veh}} \cdot 100 \quad (4.)$$

To condense the percentile variation for the three used microcar types into one index value per crash severity parameter, the root mean square (RMS) of the percentile variation of each parameter is calculated (*c.f. Table 1*). The RMS was chosen because it penalizes big differences with few occurrences over small differences with many occurrences and prevents that positive and negative values may compensate each other leading into unrealistic interpretations. The test set-up with the smallest parameter variation with respect to the vehicle-to-vehicle crash reference is highlighted in blue.

**Table 1**  
**RMS of crash severity parameter deviation between baseline vehicle-to-vehicle crash (opponent: GCM2A) and examined vehicle-to-barrier tests**

<b>REVMx vs.</b>	<b>P-MPDB</b>	<b>MPDB</b>	<b>ODB</b>	<b>PDB</b>
Barrier properties	MDB- 1,336 kg	MDB - 1,500 kg	Fixed barrier	Fixed barrier
Test configuration parameters	50 - 50 km/h 50 % overlap	50 - 50 km/h 50 % overlap	0 - 56 km/h 40% overlap	0 - 60 km/h 50% overlap
<b>Passenger compartment intrusions</b>				
Max. intrusion	20 %	21 %	70 %	37 %
<b>Kinematic behavior</b>				
$a_{x,max}$	10 %	10 %	36 %	29 %
$\Delta v_x$	3 %	6 %	6 %	6 %
Average z-rotation speed	10 %	28 %	25 %	26 %
<b>Crash energy balance</b>				
Deformation energy	12 %	17 %	64 %	45 %
Energy Equivalent Speed (EES)	6 %	8 %	40 %	26 %

Both fixed barrier tests show high deviation from the reference vehicle-to-vehicle crash behaviour, while the MDB tests show a good reproduction capacity. These high deviations are clearly related to the incapacity to reproduce the crash mechanic behaviour of a moving crash opponent vehicle with a fixed barrier test. Meanwhile, the reduction of the moving barrier's total mass from the MPDB mass level (1,500 kg) to the mass of the reference crash opponent GCM2A explains the highest reproduction accuracy of the P-MPDB test.

The calculations leading to the impact speed of 56 km/h in the ODB test (c.f. *Lowne, 1994*) to reproduce a 100 km/h closing speed reference crash between two vehicles assume that the involved vehicles are identical. This is no longer valid when the reference crash shows a high mass ratio between the crash partners. To overcome the intrinsic deficit of fixed barrier crash, not being able to reproduce the kinetic behaviour of a moving crash opponent, the impact speed for light vehicles could be increased. In accordance with this argument additional fixed barrier tests at higher impact speeds are executed for REVM2\_V8 and REVM2\_V9, representing the lightest microcars in the assessment, therefore showing the highest mass ratio in a crash against the GCM2A.

With increasing impact speed the crash severity is increasing for different types of microcars, as REVM2\_v8 represents a weak SEV structure, while REVM2\_v9 represents stiff structural response. Nevertheless, the severity increase is not proportional, resulting in improved reproduction capacity for energetic output parameters but only weak change to the kinematic outputs. Therefore no clear speed value can be identified, that would allow to overcome the intrinsic deficits of fixed barriers, not being able to reproduce the kinematic behaviour of a moving crash opponent.

### **Reproduction limitations for alternative vehicle-to-vehicle crash configurations**

Having identified the use benefit of a P-MPDB test to reproduce vehicle-to-vehicle crashes in baseline configuration, the next step of the examination addresses the oblique crash configuration identified as representative for accident scenarios in turning and crossing traffic within an urban environment (c.f. *Wismans et al., 2013*). It is to quantify how far a P-MPDB based oblique test set-up can reproduce the crash severities occurring for different microcar structures in an oblique crash against the selected crash GCM2A. Table 2 shows the comparison of crash severity output parameters between the two oblique impact configurations for the three examined microcars.

The P-MPDB is capable of producing crash severities that are very well comparable (max. 15 % deviation) or higher than within the comparable vehicle-to-vehicle crash for different types of microcars also under oblique impact direction. Even though the barrier front shows better structural interaction possibilities for the assessed vehicles, the resulting severities in the field of intrusion and deceleration are higher than in the vehicle-to-vehicle crash. This is a result of the large size of the loaded surface of the barrier front under oblique impact angle in comparison to the interacting structures of a crash opponent's vehicle front. The difference between the interacting structures of a homogeneously deforming barrier and any given vehicle front geometry represents the intrinsic deficit of a MDB

test to reproduce a vehicle-to-vehicle crash. The relevance of this limitation is dependent on the impact angle, as the relative position of the interacting structures is influenced by the orientation of the crash partners.

**Table 2**  
**Comparison of crash severity indicators: vehicle-to-vehicle and vehicle-to-P-MPDB crash**

Assessed microcar	REVM1		REVM2_V8		REVM2_V9	
	GCM2A	P-MPDB	GCM2A	P-MPDB	GCM2A	P-MPDB
Crash opponent	1,336 kg					
Crash configuration parameters: Overlap 50 %, impact speed 35 – 35 km/h, opponent impact angle 30 deg						
Passenger compartment intrusions						
Max. intrusion [mm]	67.2	170	197	270	53.1	51.8
Kinematic behaviour						
$a_{x,max}$ [g]	28.7	30.7	25.9	30.8	34.0	42.0
$\Delta v_x$ [m/s]	11.5	13.2	10.97	11.75	10.72	10.92
$\Delta v_y$ [m/s]	6.25	5.5	5.7	5.15	5.82	5.02
Crash energy balance						
Deformation energy [kJ]	28.3	38.6	41.0	43.9	30.8	24.6
EES [m/s]	8.22	9.61	11.1	11.5	9.59	8.58
Legend: green = deviation from reference <15 %; red = severity is > 15 % higher than in vehicle-to-vehicle crash; yellow = severity is > 15 % lower than in vehicle-to-vehicle crash						

## CRASH RESTRAINT SYSTEM TRIGGERING

Overall goal of vehicle to barrier tests is the reproduction of a real world vehicle to vehicle crash situation. Besides the right deformation of the vehicle it is also important to predict or rather assess the passive safety sensors and the restraint system of the tested vehicle. Comparable to a state-of-the-art vehicle development process the virtual sensor evaluation for front crash safety represents one key part within the SafeEV project development of an advanced simulation methodology for consistent safety analysis of electric microcars.

First step within the virtual sensor evaluation process is to define the sensor layout for the microcar. Therefore sensors have to be positioned at suitable areas within the vehicle. The typical sensor layout for small state-of-the-art vehicles is shown in *Figure 2*.

For accurate detection of frontal crashes at least one acceleration sensor for detection and one for the plausibility verification are used. The external satellite sensors (green in *Figure 2*) can be damaged or switched off during crash after the restraint system has been triggered. The electronic control unit (ECU) must remain intact even after the crash event because of crash data recording. The acceleration sensor should be mounted on a stiff structure within the vehicle. Regular driving mode and misuse crashes like driving through a pothole should not cause a high excitation at the sensor position. In state-of-the-art vehicles the sensors are typically mounted at the vehicle tunnel or the pillars. If the vehicle structure of microcars changes strongly compared to these types of vehicles, a sensor on the left and right rocker sill can be placed instead of a central sensor at the tunnel.

The most important requirement for the virtual application of the sensor system is a good matching of acceleration crash signals between the real-world vehicle and the virtual model. Therefore the crash signals should be compared with state-of-the-art vehicles to check the plausibility of the virtual crash data. After defining the sensor position within the vehicle a crash set of different crash types must be generated including fire (e.g. ODB 40%, 64kph), no-fire (e.g. RCAR Bumper Test) and misuse (e.g. driving through a pothole) crashes. Via a simplified application procedure the trigger times for the restraint system are determined. The applied algorithm procedure consists of a standalone core part, which provides a capable base performance, and support functions, which consider the vehicle specific characteristics (c.f. *Kärner et al., 2008*).

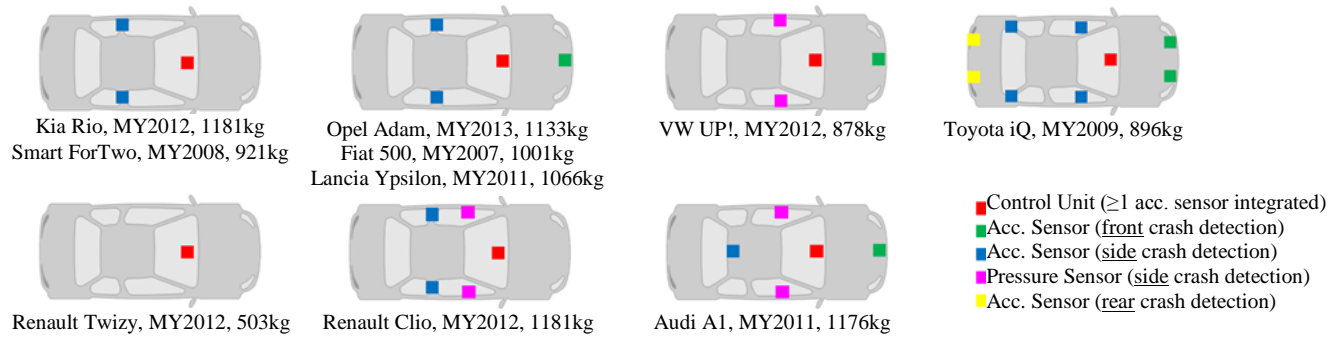


**Figure 2** Sensor layout in small state-of-the-art vehicles according to A2Mac1 database

Since the used vehicle FE models in the SafeEV project are not suitable for the simulation of certain misuse cases only fire and nofire crash types are taken into account for the simplified application procedure. The advantage of the used algorithm application procedure is that the calibration of the use crashes is independent of the misuse crashes. Thus trigger times can be estimated by using the fire and no fire crash signals in the application procedure. However for the final determination of the trigger times the misuse crash signals are absolutely necessary. If misuse crash signals are included in the application procedure, a later triggering of restraint system may be obtained.

The application process in today's series algorithm calibration works contrary to the above described procedure. Generally the vehicle manufacturer first performs occupant simulations, defines the necessary triggering times for belt pretensioner and airbag for each crash and delivers the trigger times to the airbag control unit supplier. Afterwards the supplier adapts his algorithm to the customer needs. Through in-depth analysis of the vehicle crash pulses according to an extended and customer defined crash set the required trigger times are realized through an advanced version of the described application procedure.

The determined trigger times for the belt pretensioner and the first and second deployment stage of the airbag are shown in the Table 3 for REVM2\_V9 as a result of the simplified crash signal calibration. The determined trigger times are compared with publicly available trigger times from state-of-the-art small vehicles like the Smart Fortwo and Fiat 500 (IIHS database) and Renault Twizy (EuroNCAP database). The determined trigger times for SafeEV's microcars are lower than the trigger times of above small vehicles. The main reason for this effect is the combination of REVM2\_V9 low weight and high stiffness. High acceleration signals are measured earlier at the vehicle tunnel during the crash process resulting in an earlier triggering of the restraint systems. Nevertheless it should be verified if available in-crash sensors are capable to generate adequate crash signals in order to realize such an earlier triggering. Additional possible solutions would be more sensors in the vehicle front (upfront sensors) or environment sensing coupled with reversible or irreversible restraint systems, like electronic belt tensioner. Another alternative is to adapt the restraint systems, i.e. overall shorter deployment times.

**Table 3**  
Crash set for REVM2\_V9 for assessment of restraint system triggering time for front crashes

Vehicle	Crash Type (Opponent)	Impact Velocity [km/h]	Belt Pretensioner / Airbag 1 <sup>st</sup> Stage [ms]	Airbag 2 <sup>nd</sup> Stage [ms]
Smart ForTwo	ODB 40%	64	22	-
Fiat 500	ODB 40%	64	20	-
Renault Twizy	FWDB, 0°	50	24	-
REVM2_V9	ODB 40%	64	16.6 - 17.6	21.6 - 22.6
REVM2_V9	P-MPDB 50%, 0°	50 / 50	8.8 - 9.3	13.8 - 14.3
REVM2_V9	P-MPDB 50%, 30°	35 / 35	20.3 - 20.8	25.3 - 25.8
REVM2_V9	GCM2A 50%, 0°	50 / 50	23.2 - 24.1	28.2 - 29.1

The analysis of the use potential of the P-MPDB has shown that the reproduction of a vehicle-to-vehicle crash is generally possible. Although a good correlation in vehicle deformation between REVM2\_V9 vs. P-MPDB and REVM2\_V9 vs. GCM2A can be shown (see section “P-MPDB use benefit in baseline crash configuration”), the obtained trigger times for the P-MPDB crash (cf. Table 3) are much lower than for the vehicle-to-vehicle crash. This can be attributed to the higher crash signal of the P-MPDB crash in the early stage of the crash (see *Figure 3*).

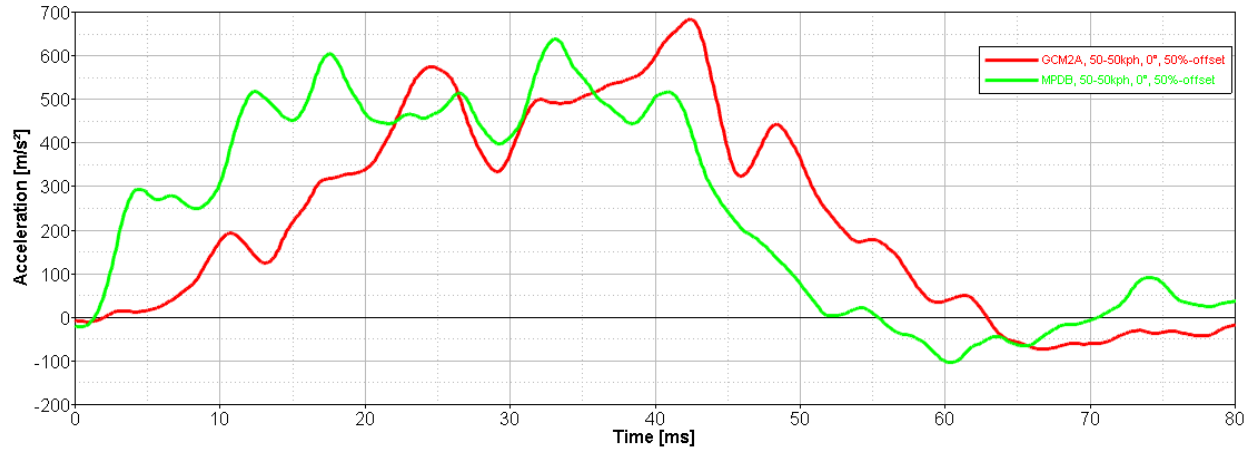


**Figure 3** Comparison of acceleration signal from REVM2\_V9 vs. GCM2A / P-MPDB

The estimated occupant forward displacements at the calculated trigger times for both crash types can be shown to be almost in the same range. In case of the REVM2\_V9 vs. GCM2A crash the triggering of the restraint system occurs later but the occupant forward displacement is also slower than in the P-MPDB crash. Thus the same safety level for the occupant can be realized. The vehicle deformation and occupant safety of vehicle to vehicle crashes can be well reproduced by vehicle to P-MPDB barrier crash. However for the calibration of the restraint system triggering algorithm it makes a difference, since the signals must be processed differently.

### MICROCAR OCCUPANT INJURY PREDICTION IN OBLIQUE CRASH CONFIGURATION

For the assessment of the crash severity for the occupant a reduced sled model and the Human Body Model (HBM) “THUMSv4.0” was used. The results are then assessed with an injury prediction tool developed at the Vehicle Safety Institute in Graz. First a short summary of the models will be given. Secondly a review of energy, strain and stress based prediction for injuries is shown for the oblique crash configuration identified as representative for accident scenarios in turning and crossing traffic within an urban environment (c.f. *Wismans et al., 2013*).

The THUMSv4.0 was introduced in 2010 and is the latest version of Toyota’s HBM research activities in this field. The geometric data was obtained from computed tomography scans of a human male (173 cm, 77.3 kg) and scaled to a 50 percentile human. Due to the more detailed model and improved bio-fidelity injuries and injury criteria can be assessed. The validation of the model was done by running different loading situations on the human body regions (i.e. head or abdomen) and parts. For example, translational impacts, belt loading, 3-point bending, dynamic and quasi static tests, etc. were simulated (*Toyota Motor Company, 2011*). The sled model was derived from the microcar REVM2\_V9 and was reduced to the most important components for occupant safety analysis. As the original vehicle model has no interior parts the used parts were extracted from a Ford Taurus, available at the *NCAC download area*.

The used restrain system within the model was implemented by a project partner. This system was not well optimized for the oblique crash configuration itself, but delivers sufficient response quality on injury severity to assess the output sensitivity on crash configuration parameter change. The usual restraint system models within the solver are used and the values for the numerical simulation runs were set to:

- Airbag Fire Time = 20.0 ms
- Pretensioner Fire Time = 20.0 ms
- Force Pretensioner = 1.5 kN
- Force Load Limiter = 4 kN

The assessment of the simulation results was performed with the injury tool. The development of the tool was necessary as already available post-processors are not capable of handling the amount of data caused by a detailed HBM and the evaluation procedure and injury criteria cannot be implemented easily. The injury tool includes following assessment groups in the latest version:

- Rib Fractures, Organ Damage, Bone Fractures, Head Injury, Ligament Elongation.

For the analyzed oblique front crash configuration the Strasbourg University Finite Elements Head Model (SUFEHM) criteria level is very low (probability of injury ~1 %). The Cumulative Strain Damage Measure (CSDM) criterion has an AIS3+ probability of 10 % for the load case. The probability for rib fracture was calculated with 83.6 % for 4 fractures and 16.4 % for 3 fractures. From the Abbreviated Injury Scale (AIS) codebook it is known that 4 fractured ribs would be classified as AIS3. The fractures occur in the shoulder area and next to the sternum. For the assessment of organ injuries the selected thresholds predict a probability of a possible damage varying from 38 % to  $\geq 100$  %.

In *Figure 4* the head and lower extremity assessment is shown. For the CSDM an injury risk curve is already available.

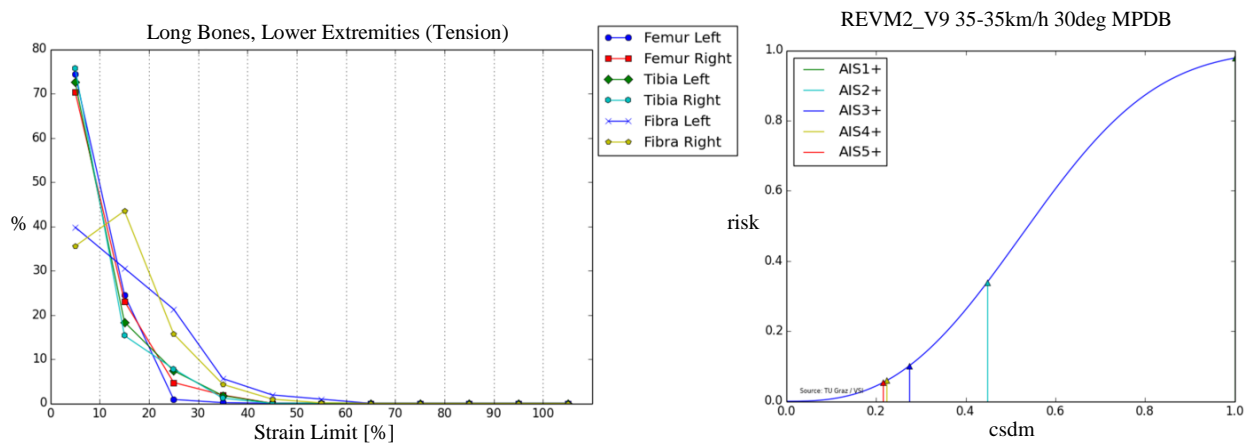


**Figure 4** Head and lower extremity assessment for REVM2\_V9

In case of the long bones and strain-stress based injury prediction no risk curve was found. For the bones only the cortical volume was used. 100 % of strain limit in the diagram is the predefined threshold for long bones. The ordinate shows the fraction of elements of the cortical parts reaching a certain value based on the threshold.

## GENERAL USE RECOMMENDATIONS FOR THE P-MPDB TEST CONFIGURATION

The proposed virtual test shows good ability to reproduce the hazards arising for microcars within a car-to-car front crash and exceeds the use potential of common tests using fixed deformable barriers as crash targets. The advantage of the defined set-up in comparison to conventional tests is growing with shrinking mass of the assessed microcar. All configuration parameters of a vehicle-to-vehicle crash can be implemented directly into the P-MPDB crash set-up.

The comparison between the P-MPDB test and vehicle-to-vehicle front crashes quantifies the capacities of barriers to reproduce vehicle crash opponents. Visible limitation appears due to the barrier's homogeneous energy absorption properties in planar direction in comparison to exemplary crash opponent front structures. The relevance of this limitation is dependent on the impact angle, as the relative position of the interacting structures is influenced by the orientation of the crash partners. This effect cannot be overcome as long as a neutral assessment of the vehicle

should be assured, inhibiting optimization related to single selected opponent structures. Furthermore the resulting higher structural crash severities in a P-MPDB test are supposed to be beneficial to the crashworthy development of future microcars.

Through a simplified algorithm procedure plausible trigger times for an adequate in-crash triggering of the restraint systems could be achieved for the proposed test set-up. In comparison to a vehicle-to-vehicle crash against M class opponents, a microcar's restraint system triggering has to occur earlier as the occupant's forward displacement is faster during a P-MPDB crash.

The deceleration based occupant injury predicted for the oblique impact crash appears to be well controlled with common restraint system functioning also for microcars showing stiff structural response. The lateral displacement and rotation effect of an oblique impact on the microcar nevertheless is challenging for the effective interaction between occupant and front airbag.

## REFERENCES

A2Mac1 database <https://www.a2mac1.com>

Bosch-Rekvelde, M.; Versmissen, T.; van der Zweep, C.; Mooi, H.; McEvoy, S., 2006. "The Development of a Load Sensing Trolley for Frontal Offset Testing". Conference ICrash 2006. Athens / Greece

Directive 2007/46/EC of the European Parliament and of the Council of 5 September 2007 establishing a framework for the approval of motor vehicles and their trailers, and of systems, components and separate technical units intended for such vehicles

EURO NCAP, 2014. Euro NCAP tests on Heavy Quadricycles, [www.euroncap.com](http://www.euroncap.com)

Hinc, K., 2015. „SafeEV Deliverable No. 3.7 – Report on final test configuration and evaluation criteria”. Graz/Austria

Kalmbach, R.; Bernhart, W.; Grosse Kleinmann, P.; Hoffmann, M., 2011. „Automotive landscape 2025 – Opportunities and challenges ahead”. Roland Berger Strategy Consultants, 03/2011

Kärner, C.; Körner, O.; Kolatschek, J., 2008. „Usage of FEA methods in order to ensure integration and application in the restraint system control in early development phase”. 9<sup>th</sup> International Symposium and Exhibition on Sophisticated Car Occupant Safety Systems. Karlsruhe/Germany

Lowne, R., 1994. "EEVC Working Group 11 report on the development of a frontal impact test procedure". 14th international technical conference on Enhanced Safety of Vehicles. Munich/Germany

Luttenberger, P.; Tomasch, E.; Willinger, R.; Bourdet, N.; Mayer, C.; Ewald, C., 2013. "SafeEV Deliverable No.1.1 – Methodical analysis on future accident scenarios involving SEVs". Graz/Austria

NCAC download area - <http://www.ncac.gwu.edu/>

O'Brien, S., 2010. "Measurement and Assessment of Passenger Vehicle Compatibility in Front and Side Collisions". Faculty of Engineering, RMIT University, Melbourne / Australia

Puppini, R.; Puleo, G.; Hinc, K. M., 2013. "SafeEV Deliverable No.3.1 – Reference Electric Vehicle Models". Graz/Austria

Regulation (EU) No 168/2013 of 15 January 2013 on the approval and market surveillance of two- or three-wheel vehicles and quadricycles

Regulation No. 94 – Proposal for draft amendments, 2007. Proposal submitted by France. Working Party on Passive Safety of GRSP, 42. Session. Geneva/Switzerland.

Safe Small Electric Vehicles through Advanced Simulation Methodologies – [www.project-safeev.eu](http://www.project-safeev.eu)

Stein, M.; Johannsen, H.; Puppini, R., 2012. „FIMCAR Models for the Assessment of Frontal Impact Compatibility” iCrash Conference 2012. Milan/Italy

Toyota Motor Company, Toyota Central R&D Labs, Inc. 2011. Documentation – AM50 Occupant Model: Academic Version 4.0

Uittenbogaard, J.; Versmissen, T., 2013. “FIMCAR-Frontal Impact and Compatibility Assessment Research, Part IX - MDB Test Procedure: Initial Test Protocol”. Technische Universität Berlin, Institut für Land- und Seeverkehr, Universitätsverlag der TU Berlin

UN-ECE Regulation No. 94, Revision 1, Uniform provisions concerning the approval of vehicles with regard to the protection of the occupants in the event of a frontal collision

Wismans, J.; Davidsson, J.; Carlsson, A.; Mayer, C.; Luttenberger, P.; D’Addetta, G. A.; Hinc, K. M.; Dux, E.; Nuss, F.; Willinger, R., 2013. “SafeEV Deliverable No.2 - Report on test conditions and evaluation criteria for occupant and vulnerable road user protection of small electric vehicles”. Graz/Austria

# NHTSA OBLIQUE CRASH TEST RESULTS: VEHICLE PERFORMANCE AND OCCUPANT INJURY RISK ASSESSMENT IN VEHICLES WITH SMALL OVERLAP COUNTERMEASURES

**James Saunders**

**Dan Parent**

**Eva Ames**

National Highway Traffic Safety Administration (NHTSA)

USA

Paper Number: 15-0108

## ABSTRACT

**Objective:** The National Highway Traffic Safety Administration (NHTSA) has been developing a research test protocol representative of real-world injury potential in frontal offset oblique impacts. This paper will address the vehicle and occupant responses from the latest research test series.

**Methods:** In this series, the Oblique Moving Deformable Barrier (OMDB) impacted stationary vehicles in both left and right side impacts. Vehicles were selected only if their performance in the Insurance Institute for Highway Safety (IIHS) Small Overlap (SOI) test condition earned a “Good” or “Acceptable” rating and had side curtain air bags meeting the requirements of Federal Motor Vehicle Safety Standard (FMVSS) No. 226, Ejection Mitigation. The vehicle responses studied included total velocity change (delta-V, DV), interior intrusion and steering wheel displacement, and the occupant responses studied included Brain Injury Criterion (BrIC), Multipoint Thoracic Injury Criterion, and Ankle Moment.

**Results:** Generally, delta-V (DV) in the X-direction decreased as the weight of the vehicle increased in both left and right side impacts, and the interior intrusion increased toward the center of the vehicle for both impact directions as well. A significant correlation between lap belt loads and vehicle mass was not found, but there was a general decreasing trend of peak lap belt loads with increase in vehicle mass. Occupant kinematics were generally mirror images for left and right side impacts, with the occupant’s head moving forward and toward the direction of impact. The near-side occupants’ heads moved toward the gap between the frontal and side curtain air bags, while the far-side occupants’ heads rotated off of the frontal air bag and impacted the center instrument panel.

**Discussion:** The Honda Accord showed the greatest difference between left and right side impact vehicle response. The highest probability of injury for both near- and far-side occupants was predicted to occur in the head, chest, and ankle, agreeing with the findings from previous real-world oblique crash injury analysis. The test mode predicted a high risk of ankle injury, primarily due to ankle inversion and/or eversion. Left and right side impacts resulted in similar magnitudes of vehicle response, but occupant responses differed enough that it may be important to consider both left and right side oblique impacts in restraint system design.

**Conclusions:** The interior intrusions on the toe pan increased towards vehicle center, and toe pan point TP3 consistently showed the highest intrusion measurement. Vehicle deformation from left and right side impacts can differ due to the stack up of non-symmetrical vehicle component layouts. The latest NHTSA Oblique test series involving vehicles with a “Good” or “Acceptable” rating in the IIHS SOI test condition and with side curtain air bags meeting the requirements of FMVSS No. 226 suggest that additional countermeasures may reduce injury risk in this test mode.

## INTRODUCTION

A September 2009 report from the National Highway Traffic Safety Administration (NHTSA) investigated why occupant fatalities still occur in frontal crashes despite the presence of air bags and seat belts and the crashworthy structures of late-model vehicles [1]. It concluded that, aside from exceedingly severe crashes, the main cause of these deaths was poor structural engagement between the vehicle and its collision partner: corner impacts, oblique crashes, impacts with narrow objects, and heavy vehicle underrides. In response, the agency initiated a research program to develop a crash test procedure capable of replicating the injury potentials from real-world frontal offset oblique crashes.

The NHTSA Research Oblique Crash Test Protocol, illustrated below in Figure 1, involves a moving deformable barrier (MDB) weighing 2,486 kg (5,480 lb) which impacts a stationary vehicle at a speed of 90 km/h (56 mph), a 15 degree angle, and a 35 percent overlap. For an average mass 1,497 kg (3,300 lb) target vehicle, this barrier-to-vehicle crash has a delta-V of 56 km/h (35 mph), which is equivalent to a crash between two average mass vehicles with the bullet vehicle striking the target vehicle at a speed of 113 km/h (70 mph), a 15 degree angle, and a 50 percent overlap. For this test, a THOR 50th percentile male anthropomorphic test device (ATD) is seated in both the driver’s and front passenger’s positions.

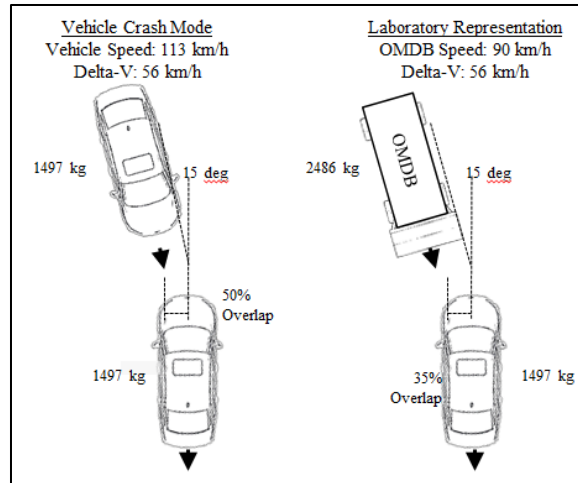


**Figure 1. Test Setup**

This test method is different from the existing New Car Assessment Program (NCAP) frontal tests in which the amount of test energy depends upon the mass of the vehicle. Because of the MDB impacting a stationary vehicle at the same speed regardless of the target vehicle’s mass, the NHTSA Research Oblique Test Protocol is a constant-energy test, which encourages comparison of vehicle safety results between vehicle classes. As explained in Saunders 2012, the test speed was selected for consistency with the test severity of the NCAP frontal crash [2]. Saunders 2012 mistakenly noted that the NCAP test speed was 90 km/h (56 mph), but the proper speed, 56 km/h (35 mph), was actually used for the derivation of the speed for the NHTSA Oblique Test Protocol.

The research program started with a series of full-scale vehicle-to-vehicle crash tests to establish a baseline understanding of vehicle interaction and occupant kinematics. These full-scale vehicle-to-vehicle tests were then compared to results obtained in crash tests using an MDB, where it was determined that the MDB already in use in Federal Motor Vehicle Safety Standard (FMVSS) No. 214 would require modifications to produce equivalent test results. The face plate was enlarged to a width greater than the outer barrier track width to prevent wheel damage, a suspension was added to prevent the assembly from bouncing at high speeds, and the barrier honeycomb stiffness and thickness were optimized to prevent the barrier face from bottoming out too soon [3]. This modified version of the FMVSS No. 214 MDB is called the Oblique Moving Deformable Barrier (OMDB).

Previously, test procedure repeatability was demonstrated [4] and vehicle crash tests of high sales volume vehicles were performed to expand the database of OMDB-to-vehicle crash tests with THOR 50th ATDs [5]. Testing of vehicles redesigned or introduced in 2010 and 2011 with the highest ratings in US consumer rating programs has shown that there is potential for additional vehicle design improvements to mitigate real-world injuries and fatalities in frontal oblique crashes [5]. When comparing the average injury assessment values (IAVs) for each body region, trends appeared which mirrored the real-world data, including the risk of knee-thigh-hip, lower extremity, head, and chest injuries. Rudd, et al. 2011 also found similar injury incidence when they reviewed oblique crashes included in the Crash Injury Research and Engineering Network (CIREN) and National Automotive Sampling System Crashworthiness Data System (NASS-CDS) databases [6].

The current study presents both vehicle and occupant results from the latest series of OMDB-to-vehicle crash tests, in which vehicle selection was limited to those which received a “Good” or “Acceptable” rating in the Insurance Institute for Highway Safety (IIHS) Small Overlap Impact (SOI) crash test and also had side curtain air bags meeting the requirements of Federal Motor Vehicle Safety Standard (FMVSS) No. 226, “Ejection mitigation.” These NHTSA Oblique tests were performed in both the left side impact (LSI) and right side impact (RSI) conditions, and kinematics for the occupants on both the struck and non-struck sides were evaluated.

## METHODOLOGY

### Oblique Crash Testing

Figure 21, in APPENDIX A, shows the left side impact (LSI) Oblique test procedure setup. In this setup, the OMDB impacts the target vehicle at 90 km/h (56 mph) and the stationary vehicle is positioned such that the angle between the OMDB and the vehicle is 15 degrees clockwise and the overlap is 35 percent on the driver side of the vehicle. For right side impacts (RSI) the OMDB impacts the target vehicle at 90 km/h (56 mph) and the stationary vehicle is positioned such that the angle between the OMDB and the stationary vehicle is 15 degrees counterclockwise and the overlap is 35 percent on the passenger side of the vehicle.

The vehicles were instrumented with a rear accelerometer on the left and right door sill to record the X and Y accelerations of the vehicle. APPENDIX B describes the intrusion points taken during the test. These points were placed according to IIHS “Moderate Overlap Frontal Crashworthiness Evaluation Crash Test Protocol (Version XV) dated May 2014. These points are listed in Table 3 and illustrated in Figure 23 and Figure 24, in APPENDIX B.

Table 1 shows the list of vehicles tested in the LSI condition, along with the naming convention for each vehicle, and Table 2 shows the list of vehicles tested in the RSI condition.

*Table 1: LSI matrix and vehicle naming convention*

NHTSA TEST NUMBER	MAKE	MODEL	YEAR	TEST WEIGHT (KG)
9043	Honda	Fit	2015	1426
8787	Mazda	3	2014	1588
8789	Honda	Accord	2014	1744
8788	Mazda	CX-5	2014	1769
8478	Subaru	Forester	2014	1803
8488	Volvo	S60	2012	1936

*Table 2: RSI matrix and vehicle naming convention*

NHTSA TEST NUMBER	MAKE	MODEL	YEAR	TEST WEIGHT (KG)
8999	Mazda	3	2014	1582
9042	Honda	Accord	2014	1749
8998	Mazda	CX-5	2014	1777

### Occupant Response Assessment

Previous OMDB crash tests have included either a single THOR (Test Device for Human Occupant Restraint) anthropomorphic test device (ATD) seated in the driver (near-side) position, or THOR ATDs in both the driver and right front passenger positions. The tests presented in this paper (Table 1 and Table 2) included two THOR ATDs, one in the driver position and one in the right front passenger position. Both THOR ATDs met the specifications of the Mod Kit [7] with the addition of the SD-3 shoulder, a derivation of the Chalmers shoulder [8] which was further developed through the European Union’s THORAX project [9]. For the LSI tests, the driver was on the near-side and the passenger on the far-side, while for the RSI tests, the passenger was on the near-side and the driver was on the far-side (further illustrated in Figure 22, APPENDIX A). In both the LSI and the RSI conditions, each ATD was positioned using the basic principles of the FMVSS No. 208 seating procedure, updated to account for the differences between THOR and Hybrid III.

### Injury Criteria

Occupant injury risk was assessed by determining the probability of given severity of injury based on the Abbreviated Injury Scale (AIS) [10] [11]. For the head, neck, chest, abdomen, femur, and acetabulum, the probability of an AIS score of three or higher ( $AIS \geq 3$ ) was calculated. For the lower extremity, the probability of an AIS score of two or higher ( $AIS \geq 2$ ) was calculated. As such, this injury assessment was limited to injury criteria for which injury risk functions were available in the literature. Table 8, in APPENDIX G, summarizes the calculation of each injury criterion, including the predictor variable, any intermediate variables and constant definitions, and the associated injury risk functions. Compared to previous NHTSA publications of Oblique test results and analysis, there are three notable changes to calculation of injury risk.

**BRIC.** Previous analysis of brain injury risk in the Oblique test condition was calculated using the kinematic brain injury criterion (BRIC) injury assessment metric calculated using the method and critical values described in Saunders et al., 2012 [2]. Since that publication, an updated methodology for brain injury assessment was published

by Takhounts et al., 2013 [12]. The revised rotational brain injury criterion (BrIC) does not consider angular acceleration, but does consider each individual local axis of angular velocity. The critical values are directionally dependent but not dummy-specific, so the critical values applicable to THOR are the average critical angular velocities for the BrIC formulation based on maximum principle strain (MPS), as summarized in Table 8 (APPENDIX G).

**Multipoint Thoracic Injury Criterion.** A relationship between chest deformation and injury risk was determined through a series of matched-pair sled tests conducted at the University of Virginia [13]. Sled tests were conducted in twelve conditions using the THOR ATD with SD-3 shoulder, for which thoracic biofidelity has been demonstrated [14]. The matched set of post-mortem human surrogate (PMHS) tests included 38 observations on 34 PMHS (four PMHS were subjected to a low-speed, non-injurious loading condition before injurious testing). A relationship was developed between the thoracic deflections measured in the THOR ATD tests to the incidence of injury in the PMHS in the same condition. Thoracic deflection was quantified by calculating the maximum resultant deflection at any of the four measurement locations on the THOR rib cage. Incidence of injury was quantified as AIS  $\geq$  3 thoracic injury to the PMHS, which represents three or more fractured ribs based on the 2005 (update 2008) version of AIS. The paired PMHS and THOR tests, along with associated test number in the NHTSA Biomechanics Database where available and the peak resultant deflection measured by the THOR ATD in each condition, are included in Table 7 (APPENDIX F).

**Ankle Moment.** Kuppala et al., 2001 proposed injury risk curves for the human lower extremity [15] and described their application to the lower extremity hardware of the THOR ATD [16]. Injury risk function were presented for the prediction of tibia plateau fractures (proximal or upper tibia axial force), tibia/fibula shaft fractures (Revised Tibia Index), calcaneus, talus, ankle, and midfoot fractures (distal or lower tibia axial force), and malleolar fractures and ankle ligament injuries (ankle rotation angle or moment). Previous analyses of ankle injury in the Oblique test condition were discarded due to measured ankle rotation data that were inconsistent with visual ankle kinematics from review of high-speed video. Since malleolar and ankle ligament injuries account for 60 percent of the lower extremity injuries in air bag equipped vehicles in frontal crashes, ankle injury risk was revisited by calculating ankle dorsiflexion moment and inversion/eversion moment as described by Kuppala et al., 2001 [16].

## **RESULTS**

### **Vehicle Response**

In general, the total velocity change (delta-V (DV)) in the X-direction decreased as the weight of the vehicle increased for both LSI and RSI (Figure 2). The DV in the X-direction for the vehicles impacted on the RSI was higher than the DV for LSI impacts, but the same trend held for weight.

Figure 3 and Figure 4 show the interior intrusion of the vehicles tested in both LSI and RSI. Generally, intrusion increased toward the center of the vehicle for both RSI and LSI. Also, for the toe pan, point TP3 always displayed the highest intrusion. There was no apparent trend for the Left IP, Right IP, bottom A-pillar, and rocker panel intrusions.

Figure 5 shows the residual displacement of the steering wheel in the X-Y plane of the vehicle. From this figure it can be seen that the steering wheel moves toward the driver's door, and the Forester had about 100 mm of displacement toward the door.



Figure 2. X DV

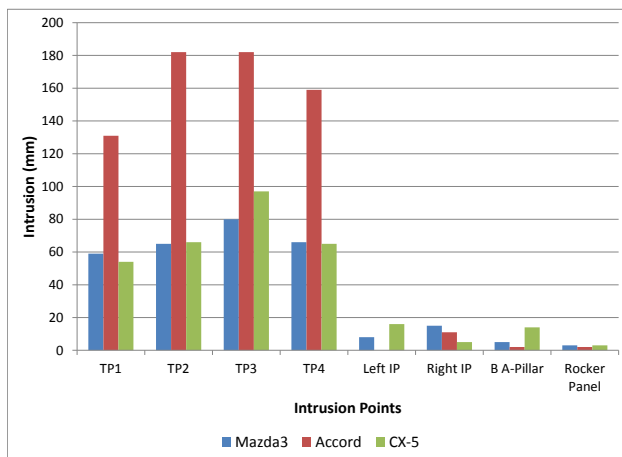


Figure 4 – Interior intrusions for RSI

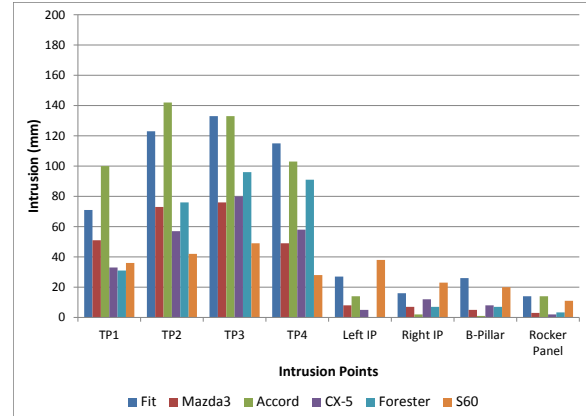


Figure 3 – Interior intrusions for LSI

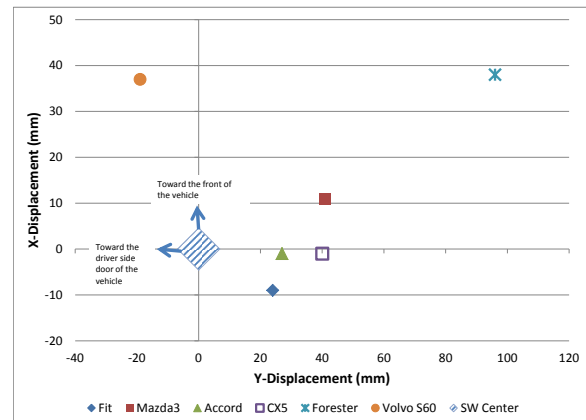


Figure 5 – Steering wheel motion in the X-Y plane

## Occupant Response

**Restraint Deployment.** In all nine tests presented in this paper (Table 1 and Table 2), the vehicles deployed retractor pretensioners, frontal air bags, and side curtain air bags to the near-side occupants. The vehicles deployed retractor pretensioners and frontal air bags to the far-side occupants. Since the far-side occupants primarily translated and rotated in the inboard direction, the far-side curtain air bags were disabled to allow for high-speed video coverage.

Frontal air bag deployment time varied across vehicles, but deployed no later than 22 milliseconds after barrier contact with the bumper of the target vehicle. Safety belt pretensioners triggered at roughly the same time as frontal air bag deployment, and triggered at the same time for both the driver and right front passenger. The side curtain air bags generally deployed later than the frontal air bags, the outliers being the Forester (25ms) and the S60 (18ms) which fired at similar times to the frontal air bags. Restraint deployment times and head contact locations are summarized in Table 4 (APPENDIX C). Note that in some cases, contact was not evidenced by paint transfer since either the air bag itself or the hand shielded the contact between the head and door panel or instrument panel, but there was evidence of contact in the high-speed video and head acceleration time-histories.

In this set of vehicles, there was a general decreasing trend of peak lap belt loads with increase in vehicle mass (Figure 7), likely resulting from the decrease in delta-V with increasing mass (Figure 2). Overall there is not a significant correlation between lap belt loads and vehicle mass. If the near-side occupants are isolated, there is a statistically-significant relationship between peak lap belt force and vehicle mass ( $p = 0.036$ ), but not for the far-side

occupants ( $p = 0.154$ ). The far-side occupant saw a higher peak lap belt load than the near-side occupant in all but one vehicle, which had the highest shoulder belt load of the group (Forester, as seen in Figure 6). Despite the shoulder of the far-side occupant slipping out of the shoulder belt in every instance, far-side shoulder belt peak forces were higher than equivalent near-side shoulder belt forces, where the shoulder belt was retained throughout the event, in almost half of the observations. There was no apparent relationship between shoulder belt forces and any vehicle parameters, which is not surprising since shoulder belt forces are controlled by load limiters in all of the present vehicles with the exception of the Forester.

To examine whether the high shoulder belt load seen in the Forester was anomalous or the result of a malfunction, the shoulder belt loads from a frontal rigid barrier test of the 2014 Forester were reviewed (NHTSA vehicle database test number 8313) and found to be similarly high at 6,640 N. Thus, the Forester may have a higher load limit for the driver-side seating position than the other vehicles in this group. The second-highest shoulder belt force occurred in the Honda Fit far-side occupant location, but a similar 50<sup>th</sup> percentile male test is not available for comparison.

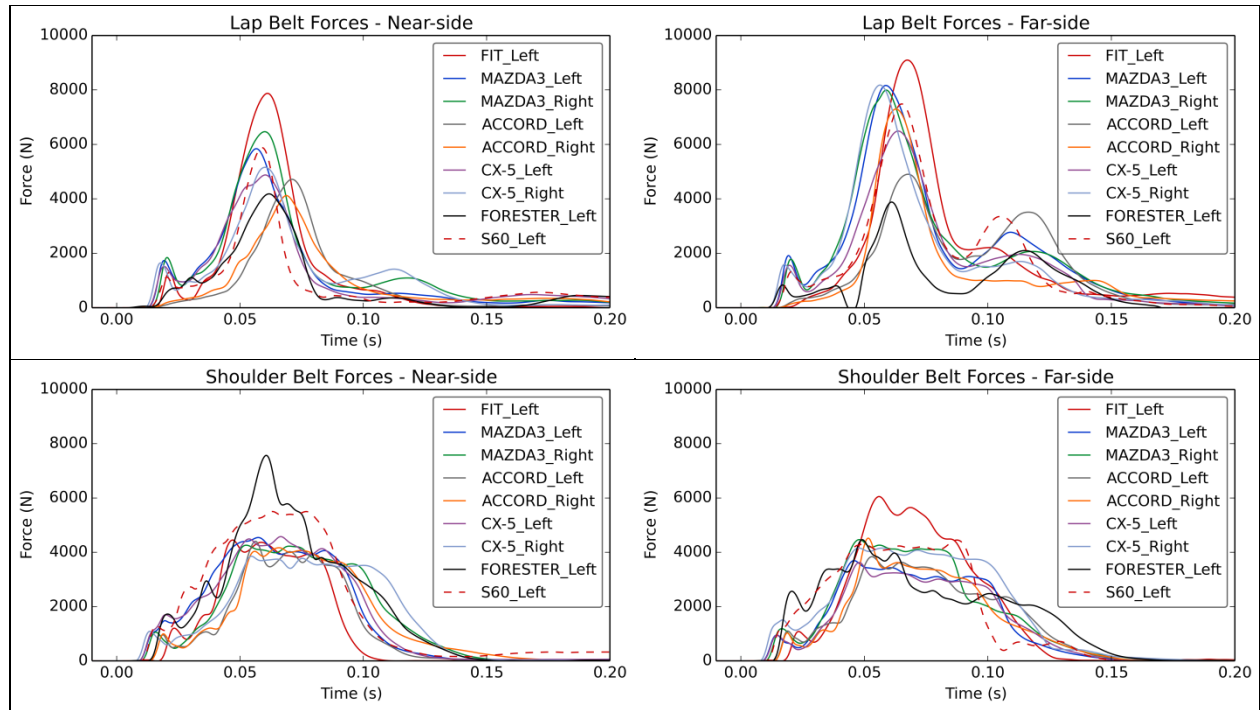


Figure 6. Lap and shoulder belt forces for the near- and far-side occupants.

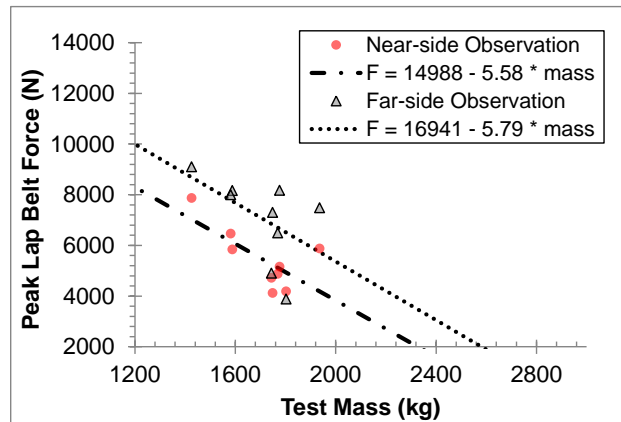


Figure 7. Relationship between lap belt load and vehicle mass.

**Near-side Occupant Kinematics.** In the LSI condition, the occupant in the driver’s seat began moving directly forward with a gradually-increasing outboard translation. The frontal air bag was typically fully-deployed by the

time head contact was made, usually in the center or left-center of the bag. As the head contacted the frontal air bag, it continued to translate in an outboard direction, often having a rotational velocity about the local Z-axis induced as the face interacted with the frontal air bag. Contact with the side curtain varied greatly based on the vehicle and side curtain air bag design (Figure 25, APPENDIX H). In general, the head translated into the gap between the frontal air bag and the side curtain air bag and rotated about the local Y-axis. Depending on the extent of deployment and stiffness of the side curtain air bag, the head was either protected from contact (Accord, CX-5, and S60) or translated and rotated past the air bag and contacted the door panel (Fit, Mazda 3, and Forester).

In the RSI condition, the overall occupant kinematics were essentially a mirror-image of the kinematics in the LSI condition. As the occupant moved forward and to the right, the head interacted with the frontal air bag and translated to the right towards the gap between the frontal and side curtain air bags. However, in the case of the Accord, the side curtain air bag contacted the head before it interacted with the frontal air bag and imparted an outboard rotation about its local Z-axis (Figure 8). The other RSI-P occupants showed similar kinematics to their LSI-D counterparts.

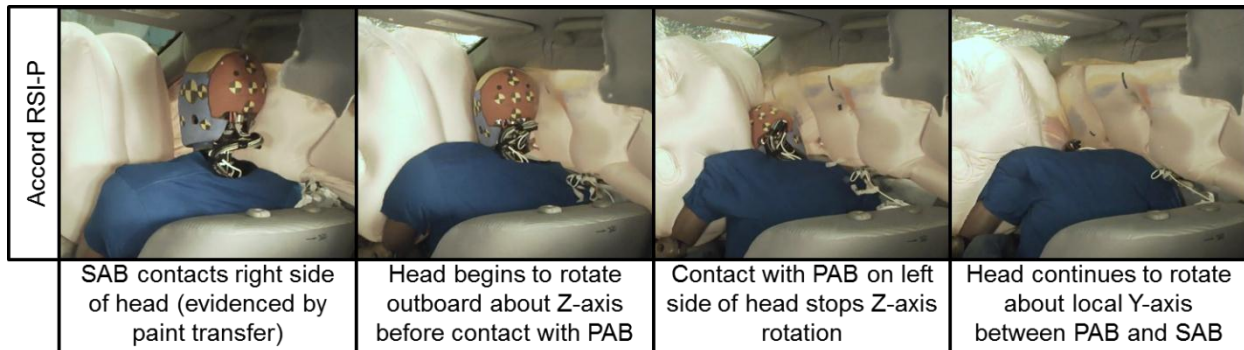


Figure 8. Kinematics of near-side occupant (RSI-P) in right-side impact test.

**Far-side Occupant Kinematics.** In the LSI condition, the far-side occupant was seated in the right front passenger seat. Like the near-side occupant location, the ATD began moving forward with an increasingly left lateral trajectory, inboard in this case. In all of the LSI vehicles, the frontal air bag appeared to be fully deployed by the time of head contact, and the head of the occupant contacted the left-hand side of the frontal passenger air bag. This contact initiated a positive Z-axis rotation of the head, and in all six of the LSI-P observations, the left side of the head contacted the center instrument panel (IP). In three of these six observations, contact was not evidenced by paint transfer but was apparent from high-speed video and head acceleration time-history (Figure 9). The peak head acceleration occurs in the Y-axis since it results from an impact to the side of the head, and occurs slightly after the peak head angular velocity since contact with the IP slows or stops the motion of the head. The earliest and most severe contact occurred in the Fit, where the head contacted the corner of a relatively narrow and visually stiff passenger air bag and rotated abruptly in the positive Z-axis direction to contact the center IP. On the other end of the spectrum was the CX-5, which had a wider and visually softer passenger air bag, which yielded under contact with the passenger's head until the point of maximum forward head excursion (Figure 10). Accordingly, out of all far-side occupants in this study, the Fit showed the highest head Z-axis angular velocity (4883 deg/s) while the CX-5 showed the lowest (1643 deg/s).

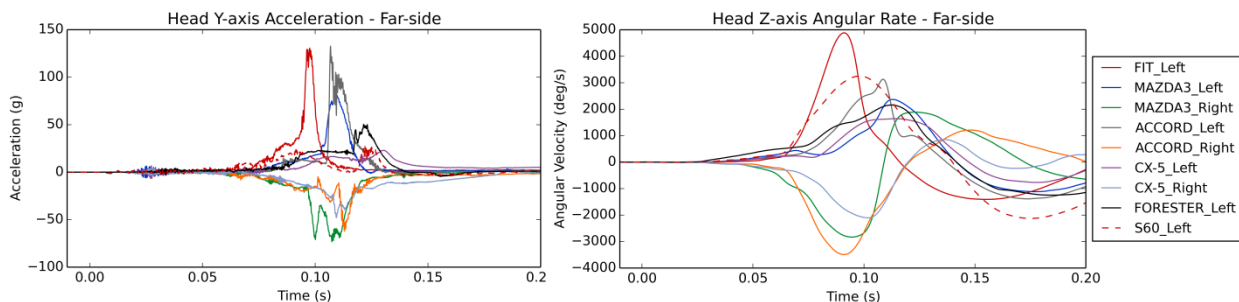
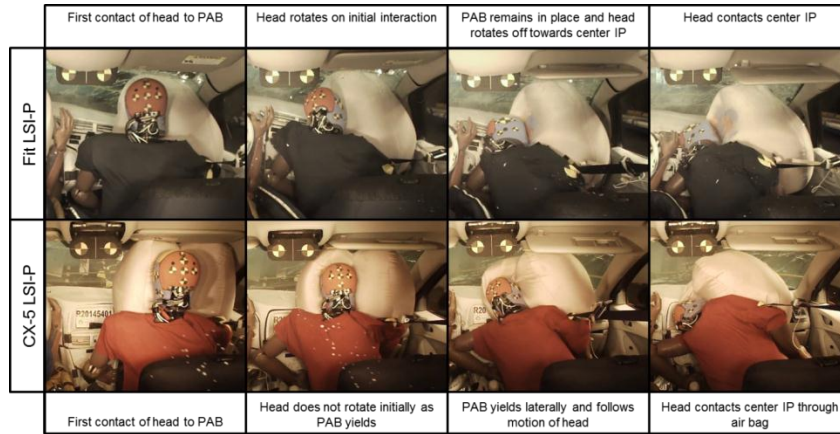
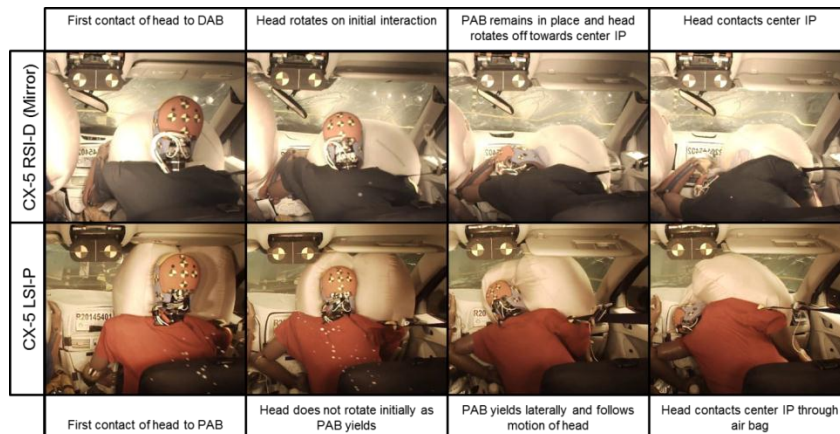


Figure 9. Y-axis head accelerations (left) and Z-axis angular velocities (right) of the far-side occupants.



**Figure 10. Kinematics of far-side occupant in left side impact test (LSI-P), comparing head rotation and center IP contact with different passenger air bag (PAB) designs.**

In the RSI far-side condition, while the overall kinematics were a mirror-image of the LSI far-side condition, there were some localized changes due to differences in the driver-side and passenger-side restraints and interior features. The frontal air bag on the driver side was initially closer to the occupant but generally smaller and stiffer, so the initial interaction with the head may have differed from the passenger far-side condition. Also, since the hands of the driver were initially placed on the steering wheel, the right hand contacted the center IP and was subsequently impacted by the head in two of the three RSI-D observations. This did not occur for the passenger in the LSI far-side condition, as the hands of the passenger were initially placed on his lap. The differences in kinematics are shown in Figure 11 by presenting the LSI-P condition as-is and the RSI-D observation as a horizontal mirror-image at the same point in time during the crash. The head of the occupant in the RSI-D condition began rotating about the local Z-axis earlier and at a greater magnitude. This comparison is not too different from that shown in Figure 10, as the interaction of the RSI-D occupant with a stiffer, unyielding frontal air bag resulted in greater head rotational velocity and, visually at least, more forward and downward head excursion.



**Figure 11. Comparison of the far-side driver and far-side passenger observations, taken at identical time steps during the test. Note that the RSI-D images are mirrored horizontally.**

### Occupant Injury Assessment.

For the purposes of this effort, occupant injury risk was assessed using the probability of an AIS  $\geq 3$  (or AIS  $\geq 2$  for the lower extremities) based on the injury criteria and underlying injury risk functions that can be applied to the THOR ATD. For the vehicles presented in Table 1 and Table 2, the body regions that showed the highest probability of injury include the brain (as predicted by BrIC), the chest (as predicted by the multipoint thoracic injury criterion), and the ankles (as predicted by ankle moment). These metrics show good agreement with the field injury exposure presented by Rudd et al. 2011 [6], where the body regions with the highest incidence of injury were the knee/thigh/hip, chest, lower extremity, and head. Summaries of the injury risk calculated by each criterion are

shown for the near-side (Table 5, APPENDIX D) and far-side (Table 6, APPENDIX E) occupants in the Appendix. This section will focus on the head, chest, knee/thigh/hip, and lower extremity. In the following bar charts, the shading of the bar represents the impact side (dark gray for left-side impact, light gray for right-side impact) while the fill pattern represents the occupant position (solid for near-side, cross-hatched far-side). RSI testing was not conducted for the Fit, Forester, and S60.

**Head.** Head injury predicted by the HIC<sub>15</sub> and BrIC injury criteria are shown in Figure 12. The highest injury risk predicted by HIC<sub>15</sub> occurs in the far-side condition, and three of the four observations above a 10 percent risk of AIS ≥ 3 injury occur in left-side impacts. Injury risk predicted by BrIC is notably higher, with a minimum of 23 percent risk AIS ≥ 3 injury in the Accord LSI-D observation. The average predicted BrIC injury risk for near-side occupants was 53 percent with five of the nine observations below a 50 percent risk of injury, while the far-side occupant average risk was 87 percent with all nine of the observations above a 50 percent risk of injury. The lowest-mass vehicles showed a higher injury risk as predicted by HIC<sub>15</sub>, but there was no apparent relationship between BrIC and any vehicle structural response parameters. The measured BrIC value appears to be more sensitive to local interactions with the frontal air bags (as shown in **Figure 10**) and side curtain air bags than the differences in vehicle kinematics within the range of the current set of vehicles. Considering the three paired left-side to right-side comparisons, injury risk predicted by BrIC was higher in right-side impacts for all of the far-side occupants, while not consistently different for the near-side occupants.

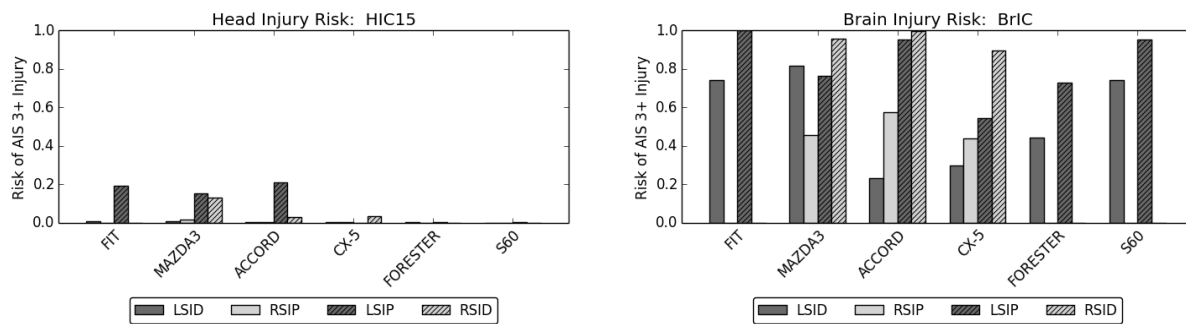


Figure 12. Risk of AIS ≥ 3 injury as predicted by HIC<sub>15</sub> (left) and BrIC (right).

**Chest.** Chest injury risk presented in Figure 13 represent the injury risk predicted by the peak resultant chest deflection measured at any of the four rib deflection measurement locations on the THOR ATD at any point in time. This deflection is calculated as spatial resultant representing the length of the vector between the initial rib location and the current rib location, as measured in a coordinate system on the local spine segment. In all but one of the tests in this series (Fit LSI), chest deflection was higher for the near-side occupant than for the far-side occupant. Comparing left-side impacts to right-side impacts, all three near-side conditions showed a higher risk of chest injury in the right-side impact than the left-side impact, while the difference was not consistent for the far-side occupants.

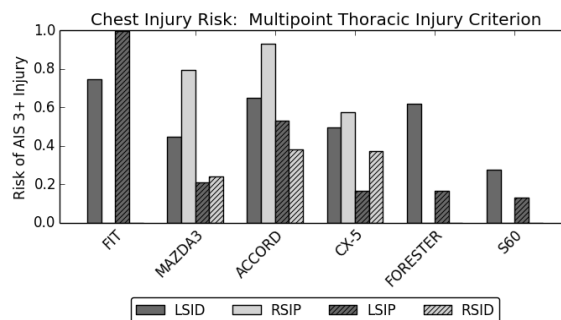


Figure 13. Risk of AIS ≥ 3 injury as predicted by multipoint thoracic injury criterion.

**Knee/Thigh/Hip.** While the axial load measured by the distal femur and the load measured at the acetabulum are intrinsically related due to the shared load path, the injury risk to the body regions in question is not necessarily linearly related. This has been observed in field data, as only 50 percent of the occupants in oblique crashes who sustained pelvis and/or hip injury also sustained femur shaft fracture [6]. Femur fracture risk was generally low, with

only one observation predicting greater than a 10 percent risk of injury (S60 LSI-D) which resulted from compressive loading of the right femur. The risk of acetabulum fracture in the same observation was greater than 50 percent, also occurring in the occupant's right leg. Three out of the four highest acetabulum injury risks were predicted to the far-side occupant in a left-side impact (Figure 14).

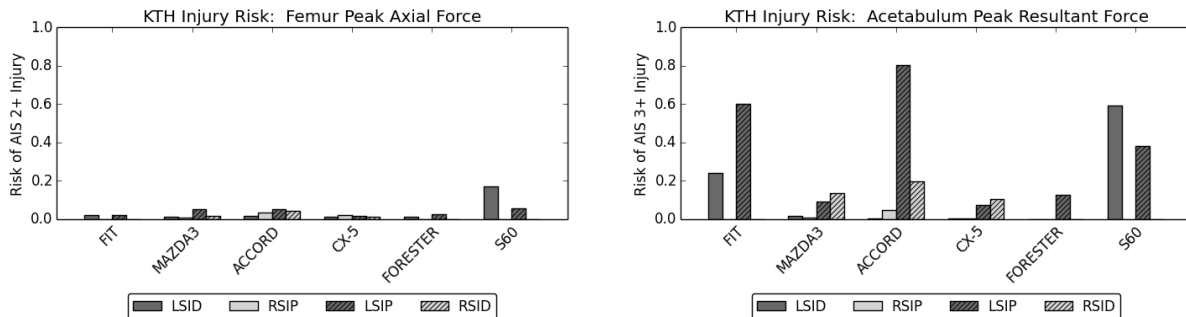


Figure 14. Risk of AIS  $\geq 2/3$  injury as predicted by femur axial force (left) and acetabulum force (right).

**Lower Extremity.** Risk of lower extremity injury was assessed using the Revised Tibia Index (RTI), which is summarized in Figure 15 as the maximum risk predicted using RTI for either the upper or lower tibia and either left or right leg. Injury risk predicted by RTI was generally low, with all but one observation predicting less than 25 percent risk of AIS  $\geq 2$  injury to the lower leg, specifically a tibia or fibula shaft fracture. The highest injury risk occurred again in the S60 LSI-D observation, again in the right leg which also saw a high risk of femur and acetabulum fracture. The S60 did have the highest right IP intrusion (see Figure 3), though this intrusion was only 22 millimeters. As shown in the past [5], the near-side occupant was expected to see a higher injury risk than the far-side due to intrusion into the occupant compartment. However, only five out of nine near-side occupants saw a higher injury risk than their far-side counterparts as predicted by RTI.

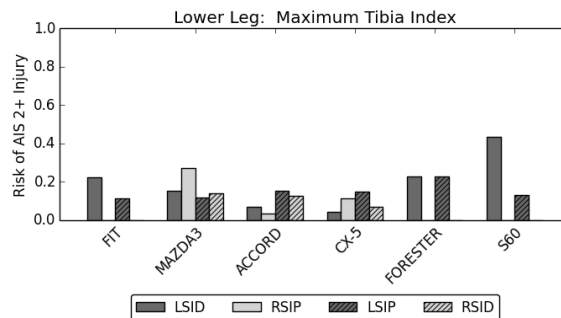


Figure 15. Risk of AIS  $\geq 2$  injury as predicted by Revised Tibia Index.

The prediction of ankle injury based on ankle moment was prevalent across all vehicles and occupant positions included in this study (Figure 16), especially due to ankle inversion/eversion. The average risk of ankle injury due to dorsiflexion moment was roughly 25 percent, while the average risk of ankle injury due to inversion/eversion moment was nearly 90 percent. Risk to near-side and far-side occupants were generally similar, as were risk of left and right ankle injury. Ankle inversion/eversion moment is generally induced by intrusion of the toe pan for the near-side occupant, as can be seen in high-speed video (Figure 26). However, high-speed video was not recorded in the far-side occupant seat position, so ankle kinematics can only be speculated based on occupant measurements. Another limitation in this assessment is that the tibia accelerations and lower tibia shear forces (FX, FY) were not measured in these tests due to channel count restrictions. However, based on the data presented by Kuppa et al. [16], the ankle moment measured at the lower tibia load cell may be an under-prediction of the peak ankle joint moment.

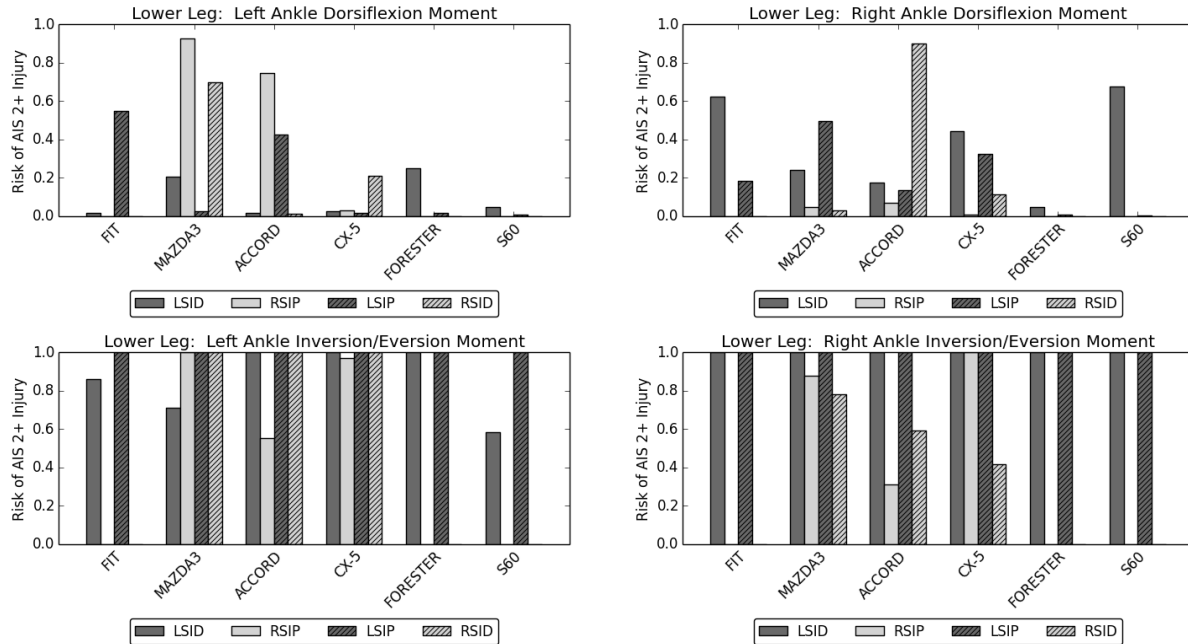


Figure 16. Risk of AIS  $\geq 2$  left and right ankle injury as predicted by ankle dorsiflexion (top) and inversion/eversion moment (bottom).

## DISCUSSION

### Vehicle Response

When comparing the intrusions of an LSI and RSI vehicle, the Accord had the greatest difference between left and right side (Figure 17). Figure 18 shows the post-test picture of the underbody for the Accord. The RSI picture was flipped in the figure to be able to make a better comparison. Figure 18 shows the Accord underbody had three different locations with different bending or pieces breaking off. The differences in this deformation may be due to the stack up of vehicle components on each side of the vehicle.

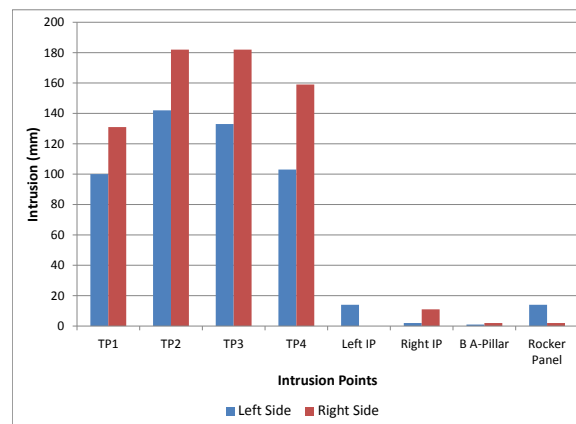


Figure 17 - Honda Accord interior intrusions

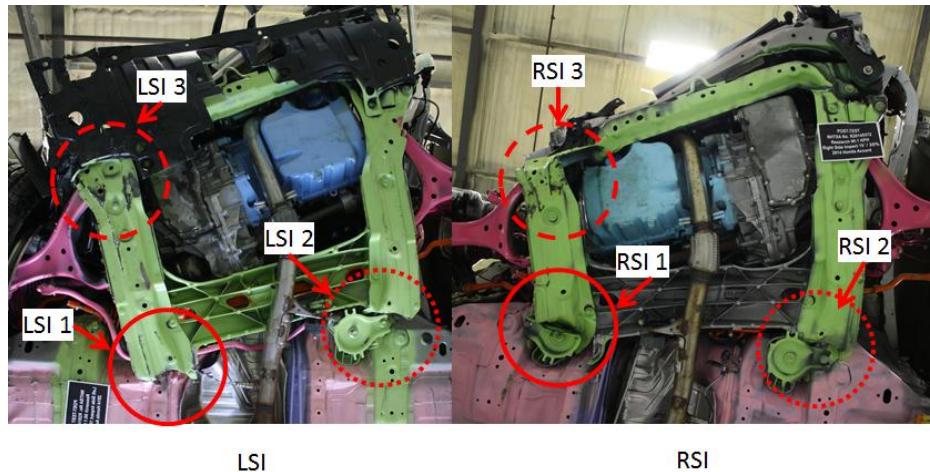


Figure 18 - Underbody of Honda Accord LSI and RSI

### Occupant Response

**Injury Risk.** The current study implemented THOR ATDs to predict injury risk in a simulated frontal oblique impact for a group of nine vehicles. Overall, the highest probability of injury for both occupants in these nine vehicles was predicted to occur in the head, chest, and ankle. Correspondingly, the most frequently injured body regions in oblique crashes were the knee/thigh/hip, chest, leg/foot, and head, as presented by Rudd et al. [6]. While knee/thigh/hip injuries were not shown to have a proportionally high injury risk in the current set of tested vehicles, high acetabulum and femur forces consistent with a high risk of injury have been measured in previously-tested vehicles [5].

**Ankle Injury.** This test mode indicated a high risk of ankle injury, primarily due to ankle inversion and/or eversion as predicted by the ankle moment measured by the THOR ATD. These high ankle moments were induced by intrusion into the toe pan coupled with interaction with the pedals for the occupants in the driver's seat. However, there was no clear disadvantage to the driver seat location compared to the passenger seat location, nor to the inboard limb compared to the outboard limb. There was also no distinct correlation between peak intrusion and ankle injury risk, as highlighted by the fact that the Accord RSI-P seating location showed the largest toe pan intrusion (Figure 4), yet measured the lowest ankle inversion/eversion moment for both the left and right ankles (Figure 16).

**Near-side versus Far-side.** Visually, one of the key differences between the near-side and the far-side occupant kinematics is that the far-side occupant appears to slip out of the shoulder belt before the point of peak head excursion. One would expect to see a difference in the measured shoulder belt forces between the near-side and far-side occupants at the point that the shoulder appears to escape the shoulder belt, roughly 100 milliseconds after impact. However, the timing of shoulder belt unloading is similar between the near-side and far-side observations (Figure 6), which suggests that the shoulder escaping the shoulder belt does not mean that the shoulder belt is not still restraining the occupant. Instead, the shoulder belt loads the lower torso, evidenced by the lower left being the quadrant of peak chest deflection in 5 of the 6 LSI observations. Interestingly, the quadrant of peak chest deflection for the three RSI far-side observations is the upper right, perhaps a result of the arms being initially positioned with the hands on the steering wheel.

Another notable difference between the near-side and far-side occupant kinematics is the rotation of the head. This can be demonstrated by calculating the individual components of BrIC by dividing the peak angular velocity about each axis of the head by its respective critical value. In six of the nine near-side observations, the Y-axis angular rate is the peak axis of rotation (Figure 19, left), similar to what would be expected in a full-frontal impact. Peak angular rates for the far-side occupant are noticeably higher than those of the near-side occupant, and dominated by Z-axis angular rate for all far-side observations (Figure 19, right).

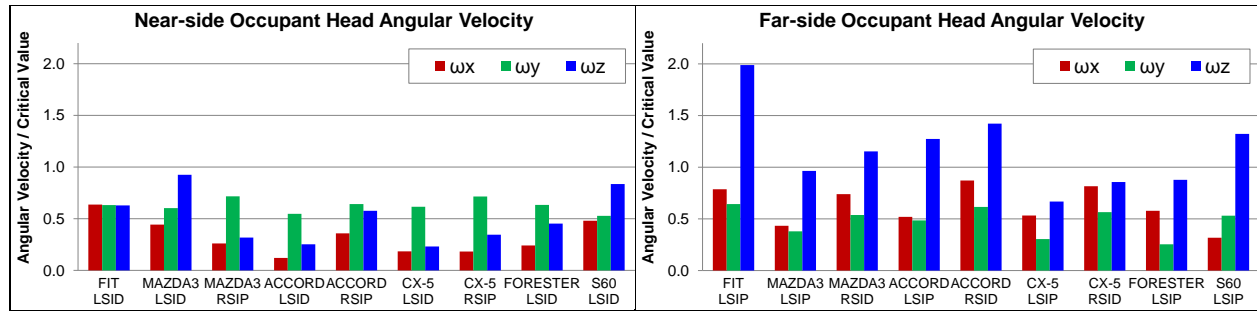


Figure 19. Components of head angular velocity for the near-side (left) and far-side (right) occupants.

**LSI versus RSI.** While the left-side and right-side impacts resulted in similar magnitudes of vehicle response, there were some differences in the occupant response that highlight important restraint system considerations. Comparing the three paired test conditions (Mazda 3, Accord, and CX-5 were all tested in both the LSI and RSI condition), the differences were more pronounced in the near-side occupant location than the far-side location. The far-side kinematics were generally a mirror image for the left- and right-side impacts, which can be seen in the head rotational velocity about the Z-axis (Figure 20, left). As the head interacted with the frontal air bag, it rotated outboard about its local Z-axis, resulting in positive angular velocity for the far-side passengers and negative angular velocity for the far-side drivers. However, the responses were not quite mirrored since the driver began to interact with the frontal air bag earlier than the passenger, with peak angular rates for the driver occurring earlier than their passenger counterparts in all three paired observations. The differences were less apparent for the near-side occupants (Figure 20, right), as the peak local Z-axis rotation was not consistently positive or negative for either group. Unlike the far-side occupant whose head interacted with only the frontal air bag, the head of the near-side occupant interacted with both the frontal air bag and the side curtain air bag. The driver-side frontal air bag and the passenger-side frontal air bag may have interacted with the side curtain air bag differently. Thus, it may be important to consider both left- and right-side oblique impacts in restraint system design.

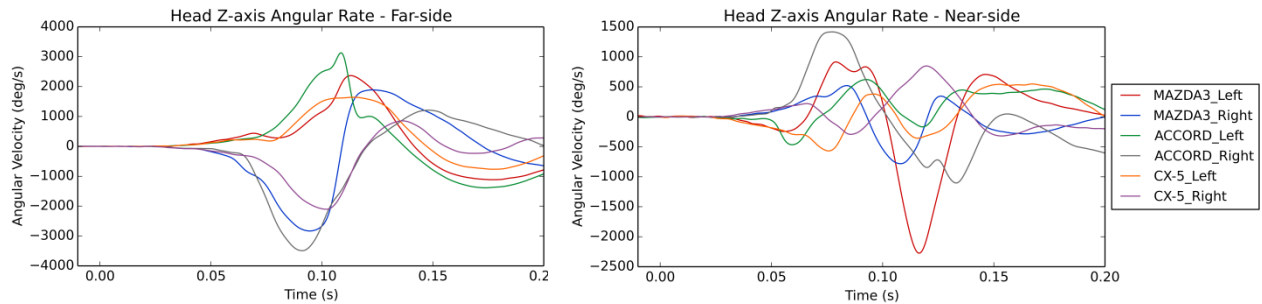


Figure 20. Comparison of head angular velocity in paired left- and right-side impact tests.

## CONCLUSIONS

The interior intrusions on the toe pan increased moving toward the center of the vehicle and the highest point of intrusion on the toe pan was TP3. The deformation on the LSI and RSI can be different due to the stack up of non-symmetrical vehicle component layouts.

The current set of vehicles tested in the NHTSA Oblique condition suggest that additional countermeasures to reduce injury risk may be needed, despite these vehicles being rated “Good” or “Acceptable” in the IIHS Small Overlap Impact test condition and including side curtain air bags meeting the requirements set forth by FMVSS No. 226. The body regions for which the highest risks of injury were predicted were the head, chest, and lower extremity, consistent with injury incidence found in previously-published reviews of NASS and CIREN data. This study reviewed the differences between left-side and right-side impacts and found that neither was of notably higher risk, though there were localized differences in the interaction of the occupants with the frontal air bag. These differences were more pronounced in the near-side occupant location, where the interaction with the frontal air bag and side curtain air bag differed noticeably between left- and right-side impacts of the same vehicle design.

## REFERENCES

1. Bean, J.D., et al., "Fatalities in Frontal Crashes Despite Seat Belts and Air Bags – Review of All CDS Cases – Model and Calendar Years 2000-2007 – 122 Fatalities," NHTSA Technical Report, Report No. DOT HS 811 202, September 2009.
2. Saunders, J., Craig, M. and Parent, D., "Moving Deformable Barrier Test Procedure for Evaluating Small Overlap/Oblique Crashes," SAE World Congress, paper no. 2012-01-0577, 2012.
3. Saunders, J., Craig, M. and Suway, J., "NHTSA's Test Procedure Evaluations for Small Overlap/Oblique Crashes," 22nd ESV Conference, Paper No. 11-0343, 2011.
4. Saunders, J. and Parent, D., "Repeatability of a Small Overlap and an Oblique Moving Deformable Barrier Test Procedure," SAE World Congress, paper no. 2013-01-0762, 2013.
5. Saunders, J. and Parent, D., "Assessment of an Oblique Moving Deformable Barrier Test Procedure," 23<sup>rd</sup> ESV Conference, Paper No. 13-0402, 2013.
6. Rudd, R., Scarboro, M., Saunders, J., "Injury Analysis of Real-World Small Overlap and Oblique Frontal Crashes," 22nd ESV Conference, Paper No. 11-0384, 2011
7. Ridella, S., Parent, D., "Modifications to Improve the Durability, Usability, and Biofidelity of the THOR-NT Dummy," 22nd ESV Conference, Paper No. 11-0312, 2011.
8. Lemmen, P., Been, B., Carroll, J., Hynd, D., Davidsson, J., Song, E., Lecuyer, E., "Development of an advanced frontal dummy thorax demonstrator," Proceedings of the 2012 IRCOBI Conference, 2012.
9. Törnvall, Fredrik. A New Shoulder for the THOR Dummy Intended for Oblique Collisions. Chalmers University of Technology, 2008.
10. AAAM: The Abbreviated Injury Scale – 1990, Update 1998. Des Plaines, IL. 2008.
11. AAAM: The Abbreviated Injury Scale – 2005, Update 2008. Des Plaines, IL. 2008.
12. Takhounts, E.G., Hasija, V., Moorhouse, K., McFadden, J., Craig, M., "Development of Brain Injury Criteria (BrIC)", Proceedings of the 57<sup>th</sup> Stapp Car Crash Conference, Orlando, FL, November 2013.
13. Crandall, J., "Injury Criteria Development: THOR Metric SD-3 Shoulder Advanced Frontal Crash Test Dummy," NHTSA Biomechanics Database, Report b11117-1, September 2013.
14. Parent, D., Craig, M., Ridella, S., McFadden, J., "Thoracic Biofidelity Assessment of the THOR Mod Kit ATD," 23rd Enhanced Safety of Vehicles Conference, Paper No. 13-0327, 2013.
15. Kuppa, S., Wang, J., Haffner, M., Eppinger, R., "Lower Extremity Injuries and Associated Injury Criteria," 17<sup>th</sup> ESV Conference, Paper No. 457, 2001.
16. Kuppa, S., Haffner, M., Eppinger, R., Saunders, J., "Lower Extremity Response And Trauma Assessment Using The THOR-Lx/HIIIr And The Denton Leg In Frontal Offset Vehicle Crashes," 17<sup>th</sup> ESV Conference, Paper No. 456, 2001.

APPENDIX A.

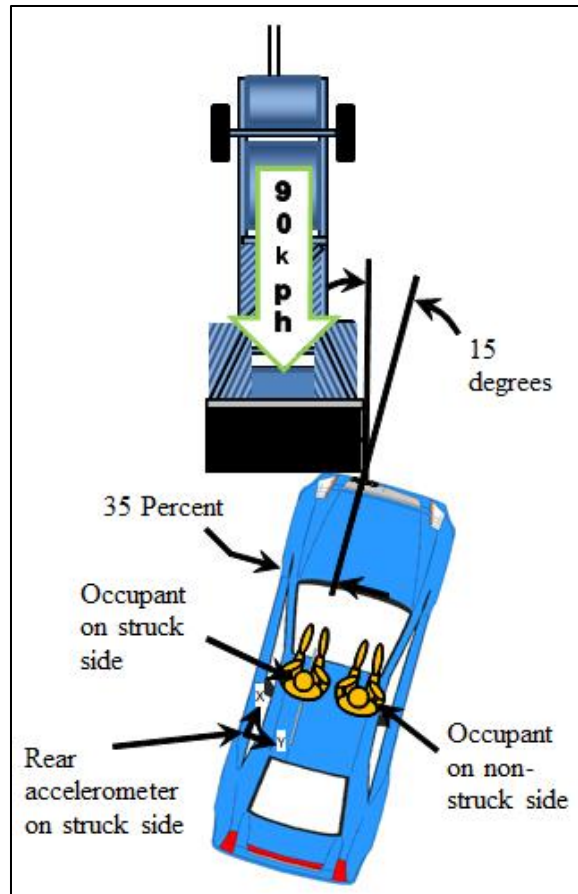


Figure 21. Test setup for Left Side Impact (LSI)

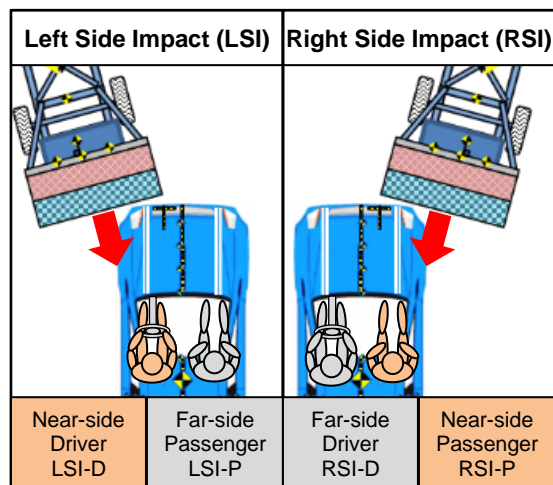
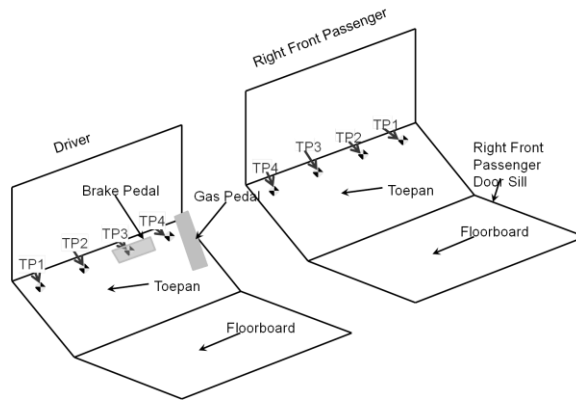


Figure 22. Occupant location terminology.

**APPENDIX B.**

**Table 3. Intrusion Points**

Description	Abbreviation	Figure
Left Footrest	TP1	Figure 23
Left Toe Pan	TP2	Figure 23
Center Toe Pan	TP3	Figure 23
Right Toe Pan	TP4	Figure 23
Left Instrument Panel	Left IP	
Right Instrument Panel	Right IP	
Center Steering Wheel	SW	
Bottom A-pillar	B A-pillar	Figure 24
Rocker Panel		Figure 24



*Figure 23: Interior intrusion measurements*

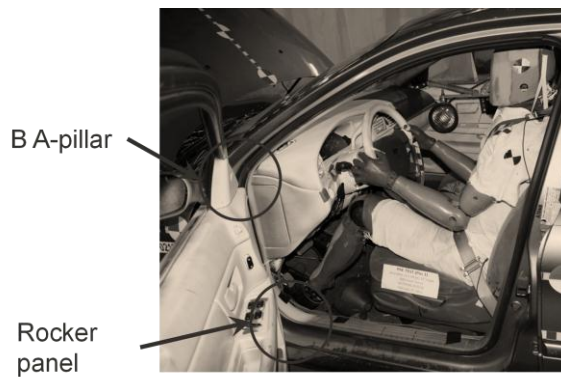


*Figure 24: Location of B A-pillar and rocker panel intrusion points*

APPENDIX C.

Table 4. Head contact locations and restraint deployment timing.

Mode	Vehicle	Contact Location (Evidence)	Frontal Air Bag Deployment	Side Curtain Air Bag Deployment	HIC15	Safety Belt Pretensioner
<b>Left Front Driver</b>						
LSI Oblique	Fit	AB (V, PT), SAB (V, PT), DP (V, PT)	AD (21)	AD (35)	264	AD (21)
	3	AB (V, PT), SAB (V, PT), DP (V, TAB)	AD (14)	AD (42)	268	AD (14)
	Accord	AB (V, PT), SAB (V, PT)	AD (16)	AD (46)	191	AD (18)
	CX-5	AB (V, PT), SAB (V, PT)	AD (13)	AD (43)	219	AD (13)
	Forester	AB (V, PT), SAB (V, PT), DP (V, PT)	AD (17)	AD (25)	193	AD (17)
	S60	AB (V, PT), SAB (V, PT)	AD (12)	AD (18)	152	AD (14)
RSI Oblique	3	AB (V, PT), IP (V, PT, TH)	AD (14)		750	AD (14)
	Accord	AB (V, PT), IP (V, PT)	AD (18)		419	AD (18)
	CX-5	AB (V, PT), IP (V, TH)	AD (12)		453	AD (12)
<b>Right Front Passenger</b>						
LSI Oblique	Fit	AB (V, PT), IP (V, PT)	AD (22)		910	AD (22)
	3	AB (V, PT), IP (V, TAB)	AD (16)		806	AD (13)
	Accord	AB (V, PT), IP (V, PT)	AD (18)		947	AD (18)
	CX-5	AB (V, PT), IP (V, TAB)	AD (15)		113	AD (15)
	Forester	AB (V, PT), IP (V, TAB)	AD (22)		200	AD (17)
	S60	AB (V, PT), IP (V, PT)	AD (14)		227	AD (15)
RSI Oblique	3	AB (V, PT), SAB (V, PT)	AD (14)	AD (42)	356	AD (14)
	Accord	AB (V, PT), SAB (V, PT), DP (V, PT)	AD (19)	AD (42)	190	AD (18)
	CX-5	AB (V, PT), SAB (V, PT)	AD (16)	AD (44)	247	AD (12)
		<b>AB</b> Air Bag	<b>AD ( )</b>	Available and Deployed (time deployed in ms)		
		<b>SAB</b> Side Curtain Air Bag				
		<b>RR</b> Roof Rail	<b>AN</b>	Available and Not Deployed		
		<b>IP</b> Instrument Panel	<b>N</b>	Not Available		
		<b>DP</b> Door Panel				
		<b>V</b> Video				
		<b>PT</b> Paint Transfer				
		<b>TAB</b> Contact Through Air Bag				
		<b>TH</b> Contact Through Hand				

APPENDIX D.

*Table 5. Summary of injury risk for near-side occupants in LSI and RSI Oblique crash tests*

		Test Number	9043	8787	8999	8789	9042	8788	8998	8478	8488
		Vehicle Model	Fit	Mazda3	Mazda3	Accord	Accord	CX-5	CX-5	Forester	S60
		Impact Side	Left	Left	Right	Left	Right	Left	Right	Left	Left
		Occupant Location	D	D	P	D	P	D	P	D	D
Body Region	Metric	AIS ≥ n									
<b>Head</b>	HIC15	3	0.006	0.006	0.016	0.001	0.001	0.003	0.004	0.002	0.001
	BrIC	3	0.740	0.818	0.454	0.230	0.576	0.297	0.440	0.442	0.743
<b>Neck</b>	Nij	3	0.463	0.374	0.463	0.251	0.545	0.342	0.499	0.351	0.492
<b>Chest</b>	Multipoint Deflection	3	0.747	0.448	0.793	0.650	0.929	0.497	0.572	0.617	0.277
<b>Abdomen</b>	Peak Deflection	3	0.198	0.049	0.127	0.143	0.259	0.076	0.189	0.000	0.000
<b>Left Leg</b>	Acetabulum Force	2/3	0.241	0.000	0.005	0.000	0.049	0.000	0.001	0.000	0.003
	Femur Force	2	0.019	0.010	0.009	0.017	0.023	0.014	0.019	0.012	0.019
	Tibia Index, Proximal	2	0.026	0.008	0.223	0.029	0.030	0.030	0.113	0.046	0.006
	Tibia Index, Distal	2	0.028	0.021	0.273	0.035	0.032	0.035	0.035	0.115	0.017
	Tibia Proximal Force	2	0.005	0.004	0.001	0.005	0.003	0.004	0.001	0.002	0.006
	Tibia Distal Force	2	0.000	0.000	0.000	0.000	0.002	0.000	0.001	0.000	0.001
	Ankle Dorsiflexion Moment	2	0.858	0.711	1.000	0.999	0.555	1.000	0.970	1.000	0.584
	Ankle [in/e]version Moment	2	0.016	0.204	0.924	0.018	0.745	0.025	0.028	0.251	0.048
<b>Right Leg</b>	Acetabulum Force	2	0.001	0.016	0.006	0.001	0.033	0.003	0.003	0.000	0.590
	Femur Force	2	0.020	0.009	0.008	0.009	0.036	0.007	0.010	0.012	0.168
	Tibia Index, Proximal	2	0.144	0.075	0.069	0.015	0.010	0.032	0.016	0.041	0.143
	Tibia Index, Distal	2	0.221	0.153	0.020	0.069	0.006	0.044	0.022	0.226	0.433
	Tibia Proximal Force	2	0.010	0.002	0.001	0.004	0.003	0.003	0.002	0.003	0.003
	Tibia Distal Force	2	0.000	0.000	0.001	0.000	0.002	0.000	0.001	0.000	0.000
	Ankle Dorsiflexion Moment	2	1.000	1.000	0.876	1.000	0.309	1.000	1.000	1.000	1.000
Ankle [in/e]version Moment	2	0.622	0.240	0.048	0.176	0.067	0.441	0.008	0.048	0.676	

APPENDIX E.

Table 6. Summary of injury risk for far-side occupants in LSI and RSI Oblique crash tests

		Test Number	9043	8787	8999	8789	9042	8788	8998	8478	8488
		Vehicle Model	Fit	Mazda3	Mazda3	Accord	Accord	CX-5	CX-5	Forester	S60
		Impact Side	Left	Left	Right	Left	Right	Left	Right	Left	Left
		Occupant Location	P	P	D	P	D	P	D	P	P
Body Region	Metric	AIS ≥ n									
Head	HIC15	3	0.194	0.152	0.130	0.209	0.028	0.000	0.035	0.002	0.003
	BriC	3	1.000	0.764	0.955	0.952	0.995	0.545	0.894	0.727	0.952
Neck	Nij	3	0.585	0.296	0.468	0.308	0.441	0.223	0.544	0.125	0.230
Chest	Multipoint Deflection	3	0.998	0.211	0.240	0.529	0.380	0.164	0.374	0.166	0.131
Abdomen	Peak Deflection	3	0.100	0.127	0.268	0.205	0.201	0.110	0.086	0.000	0.000
Left Leg	Acetabulum Force	2/3	0.271	0.014	0.136	0.804	0.000	0.001	0.106	0.125	0.382
	Femur Force	2	0.013	0.050	0.009	0.043	0.042	0.017	0.005	0.024	0.054
	Tibia Index, Proximal	2	0.114	0.117	0.140	0.010	0.128	0.146	0.035	0.228	0.092
	Tibia Index, Distal	2	0.103	0.036	0.105	0.153	0.050	0.114	0.000	0.084	0.128
	Tibia Proximal Force	2	0.001	0.001	0.002	0.003	0.006	0.001	0.004	0.003	0.002
	Tibia Distal Force	2	0.001	0.001	0.000	0.001	0.001	0.001	0.001	0.000	0.000
	Ankle Dorsiflexion Moment	2	1.000	1.000	1.000	1.000	1.000	1.000	0.000	1.000	1.000
	Ankle [in/e]version Moment	2	0.547	0.024	0.699	0.426	0.011	0.017	0.005	0.017	0.006
Right Leg	Acetabulum Force	2	0.600	0.090	0.005	0.024	0.198	0.072	0.006	0.009	0.364
	Femur Force	2	0.022	0.008	0.014	0.051	0.044	0.007	0.012	0.017	0.006
	Tibia Index, Proximal	2	0.028	0.062	0.038	0.002	0.045	0.090	0.014	0.048	0.098
	Tibia Index, Distal	2	0.027	0.045	0.014	0.010	0.023	0.114	0.000	0.138	0.115
	Tibia Proximal Force	2	0.002	0.001	0.003	0.004	0.003	0.001	0.004	0.002	0.004
	Tibia Distal Force	2	0.001	0.001	0.000	0.002	0.001	0.001	0.003	0.000	0.001
	Ankle Dorsiflexion Moment	2	1.000	1.000	0.782	1.000	0.593	1.000	0.414	1.000	1.000
Ankle [in/e]version Moment	2	0.181	0.496	0.028	0.136	0.898	0.324	0.115	0.009	0.002	

**APPENDIX F.**

*Table 7. THOR-PMHS paired tests used in development of multipoint thoracic injury criterion.*

Occupant Position	Environment	Restraint	Delta-V (km/h)	Age	Sex	Mass (kg)	Height (cm)	AIS 3+	PMHS BioDB	THOR BioDB	THOR Peak Res Defl (mm)
Front Driver	Gold Standard	3-point standard belt	10	59	F	80	167	No		11125	12.62
				69	M	84	178	No	11126		
				60	M	81	191	No			
Front Driver	Gold Standard	3-point standard belt	40	59	F	80	167	Yes		11123	49.4
				69	M	84	178	Yes	11124		
				60	M	81	191	Yes			
Front Passenger	1997 Ford Taurus	3-point force-limited belt plus air bag	48	57	M	70	174	No	8371	11129	51.3
				69	F	53	155	Yes	8372	11130	
				72	F	59	156	Yes	8373		
				57	M	57	177	No	8374		
Front Passenger	1997 Ford Taurus	Lap belt with air bag	48	40	M	47	150	Yes*	8377	11131	30.08
				70	M	70	176	No	8378	11132	
				46	M	74	175	No	8379		
Front Passenger	1997 Ford Taurus	3-point standard belt with air bag	48	55	M	85	176	Yes	8382	11127	54.83
				69	M	84	176	Yes	8383	11128	
				59	F	79	161	Yes	8384		
Front Passenger	1997 Ford Taurus	3-point standard belt	29	49	M	58	178	No		11133	42.75
				44	M	77	172	No	11134		
				39	M	79	184	No			
Front Passenger	1997 Ford Taurus	3-point standard belt	38	44	M	77	172	No		11135	51.17
										11136	
Front Passenger	Gold Standard 1	3-point standard belt	40	76	M	70	178	Yes	9546	11117	47.73
				47	M	68	177	Yes	9547	11118	
				54	M	79	177	Yes		11119	
				49	M	76	184	Yes			
				57	M	64	175	Yes			
				72	M	81	184	Yes	11014		
				40	M	88	179	Yes	11015		
37	M	78	180	No	11016						
Front Passenger	Gold Standard 2	3-point force-limited belt	30	59	M	68	178	No		11120	26.78
				66	M	70	179	No		11121	
										11122	
Rear Passenger	2004 Ford Taurus	3-point standard belt	48	51	M	55	175	Yes	9337	11143	57.96
				57	F	109	165	Yes	9338	11144	
				57	M	59	179	Yes	9339	11145	
Rear Passenger	2004 Ford Taurus	3-point force-limited belt with pretensioner	48	67	M	71	175	Yes		11140	46.66
				69	M	60	171	No		11141	
				72	M	73	175	Yes		11142	
Rear Passenger	2004 Ford Taurus	3-point inflatable force-limited belt with pretensioner	48	72	M	88	173	Yes		11137	29.66
				69	M	69	175	No		11138	
				40	M	83	186	No		11139	

APPENDIX G.

Table 8. Summary of injury criteria and associated injury risk functions used to assess injury risk using THOR test results.

Criterion [ref]	Calculation	Vars	Variable Definition	Risk Function
$HIC_{15}$	$HIC_{15} = \left  (t_2 - t_1) \left[ \frac{1}{(t_2 - t_1)} \int_{t_1}^{t_2} a(t) dt \right]^{2.5} \right _{max}$	$t_1$ $t_2$ $a(t)$	Beginning of time window in s End of time window in s Head CG resultant acceleration in Beginning of time window in g	$p(AIS \geq 3) = \Phi \left[ \frac{\ln(HIC_{15}) - 7.45231}{0.73998} \right]$
$BrIC$	$BrIC = \sqrt{\left( \frac{\max( \omega_x )}{\omega_{xc}} \right)^2 + \left( \frac{\max( \omega_y )}{\omega_{yc}} \right)^2 + \left( \frac{\max( \omega_z )}{\omega_{zc}} \right)^2}$	$\omega_{[x,y,z]}$ $\omega_{[x,y,z]C}$ $\omega_{xc}$ $\omega_{yc}$ $\omega_{zc}$	Angular velocity of the head about the local [x, y, or z] axis, in rad/s, filtered at CFC60 Critical angular velocities in rad/s 66.25 rad/s 56.45 rad/s 42.87 rad/s	$p(AIS \geq 3) = 1 - e^{-\left(\frac{BrIC}{0.987}\right)^{2.84}}$
$N_{ij}$	$N_{ij} = \frac{F_z}{F_{zc}} + \frac{M_y}{M_{yc}}$	$F_z$ $F_{zc}$ $M_y$ $M_{yc}$	Z-axis force measured at upper neck load cell in N Critical force (tension or compression) in N [2520/-3640] Y-axis moment measured at upper neck load cell Nm Critical moment (flexion or extension) in Nm [48/-72]	$p(AIS \geq 3) = \frac{1}{1 + e^{3.227 - 1.969N_{ij}}}$
Multi-point Thoracic Injury Criterion	$R_{max} = \max(UL_{max}, UR_{max}, LL_{max}, LR_{max})$ where $[U/L R/L]_{max} = \max\left(\sqrt{[L/R]X^2_{[U/L]S} + [L/R]Y^2_{[U/L]S} + [L/R]Z^2_{[U/L]S}}\right)$	$R_{max}$ $[U/L R/L]_{max}$ $[L/R][X/Y/Z]^2_{[U/L]S}$	Overall peak resultant deflection in mm Peak resultant deflection of the [upper/lower   left/right] quadrant in mm Time-history of the [left/right] chest deflection along the [X/Y/Z] axis relative to the [upper/lower] spine segment in mm	$P(AIS \geq 3   age, R_{max}) = 1 - \exp\left(-\left[\frac{R_{max}}{\exp(4.4853 - 0.0113age)}\right]^{5.03896}\right)$
Compression	$A_{max} = \frac{\max(\delta L, \delta R)}{d_{abd}}$	$\delta[L, R]$ $d_{abd}$	Peak X-axis deflection of the left or right abdomen in mm Undeformed depth of the abdomen [238.4 mm]	$p(AIS \geq 3) = 1 - e^{-\left(\frac{A_{max}}{0.4247}\right)^{3.6719}}$
Acetabulum Load	$F_R = \sqrt{F_x^2 + F_y^2 + F_z^2}$	$F_{[x,y,z]}$	X-, Y-, and Z- axis force measured at the acetabulum load cell in kN	$p(AIS \geq 3) = \Phi \left[ \frac{\ln(F_R/0.72) - 1.6526}{0.1991} \right]$
Femur Axial Load		$F_z$	Z-axis femur load in kN, filtered at CFC600	$p(AIS \geq 2) = \frac{1}{1 + e^{5.7949 - 0.5196F_z}}$
Revised Tibia Index	$RTI = \frac{F}{F_c} + \frac{M}{M_c}$	$F$ $F_c$ $M$ $M_c$	Measured compressive axial force in kN Critical compressive axial force [12 kN] Measured bending moment in Nm (resultant of medial-lateral and anterior-posterior directions) Critical bending moment [240 Nm]	$p(AIS \geq 2) = 1 - \exp\left(-\exp\left[\frac{\ln(RTI) - 0.2468}{0.2728}\right]\right)$
Proximal Tibia Axial Force		$F_z$	Z-axis upper tibia load in kN, filtered at CFC600	$p(AIS \geq 2) = \frac{1}{1 + e^{5.6654 - 0.8189F_z}}$
Distal Tibia Axial Force		$F_z$	Z-axis lower tibia load in kN, filtered at CFC600	$p(AIS \geq 2) = \frac{1}{1 + e^{4.572 - 0.670F_z}}$
Dorsiflexion Moment	$M_{yankle} = M_y - F_x D - \frac{m a_x D}{2}$	$M_y$ $F_x$ $D$ $m$ $a_x$	Y-axis moment measured at lower tibia load cell in Nm X-axis force measured at lower tibia load cell in N Distance between ankle joint and lower tibia load cell [0.0907m] Mass between ankle joint and lower tibia load cell [0.72kg] X-axis acceleration of the tibia in m/s <sup>2</sup>	$p(AIS \geq 2) = \frac{1}{1 + e^{6.535 - 0.1085M_y}}$
Inversion/Eversion Moment	$M_{xankle} = M_x - F_y D - \frac{m a_y D}{2}$	$M_x$ $F_y$ $D$ $m$ $a_y$	X-axis moment measured at lower tibia load cell in Nm Y-axis force measured at lower tibia load cell in N Distance between ankle joint and lower tibia load cell [0.0907m] Mass between ankle joint and lower tibia load cell [0.72kg] Y-axis acceleration of the tibia in m/s <sup>2</sup>	$p(AIS \geq 2) = \Phi \left[ \frac{M_x - 40Nm}{10Nm} \right]$

APPENDIX H.



Figure 25. Interaction of LSI-D occupants with driver air bag (DAB) and side curtain air bag (SAB).

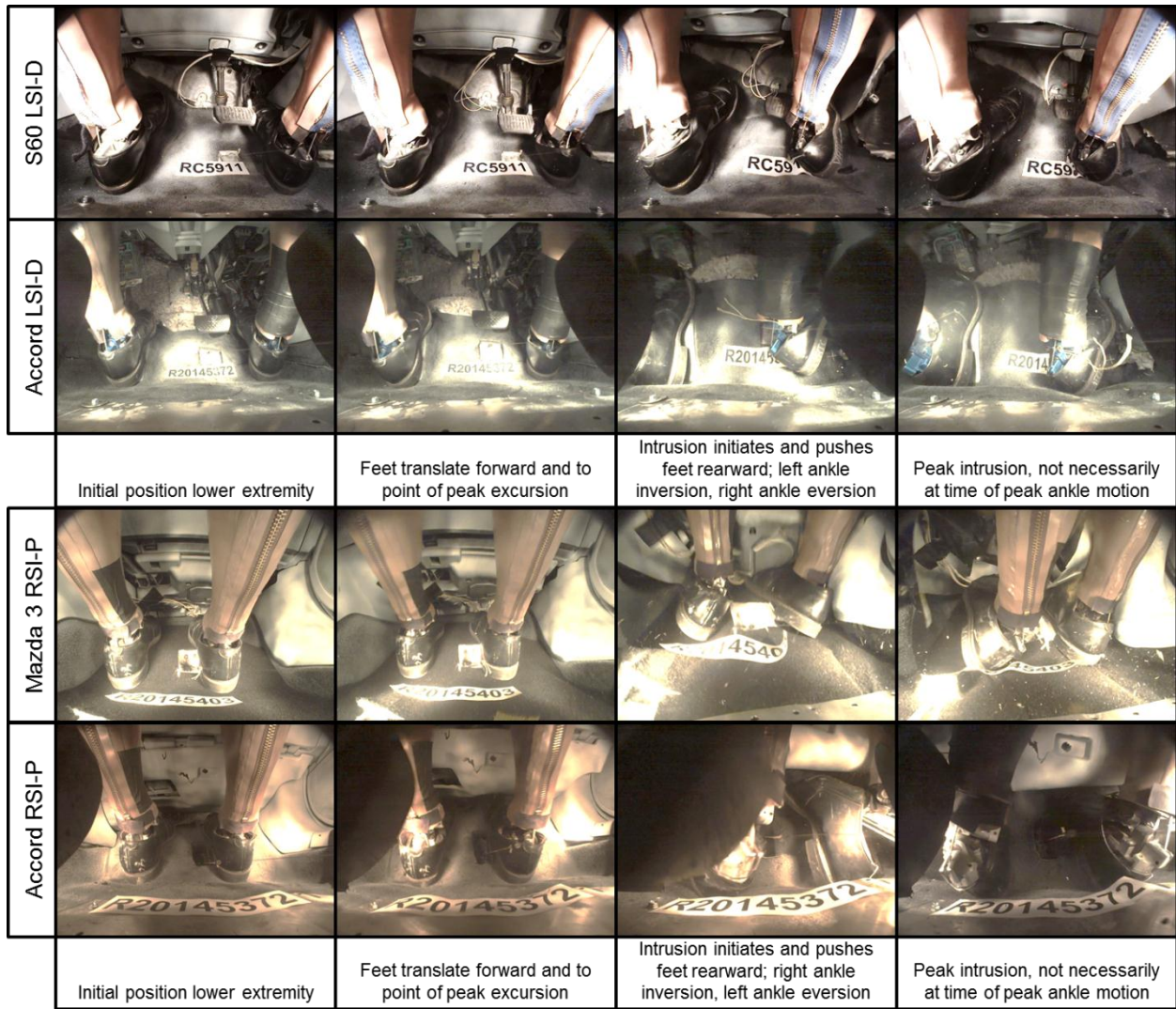


Figure 26. Lower extremity interaction with toe pan for vehicles with least (top of each pair) and most (bottom of each pair) toe pan intrusion.

# THE INCIDENCE AND SEVERITY OF SMALL OVERLAP FRONTAL CRASHES IN NASS-CDS

**Priya Prasad**

Prasad Engg, LLC

USA

**Dainius Dalmotas**

**Alan German**

D.J. Dalmotas Consulting, Inc.

Canada

Paper Number 15-0182

## ABSTRACT

The Insurance Institute for Highway Safety has recently introduced a small overlap frontal crash test in its frontal rating scheme. Another small overlap frontal crash test is under development by the National Highway Traffic Safety Administration (NHTSA). Whereas the IIHS test is conducted against a fixed rigid barrier, the NHTSA test is conducted with a moving deformable barrier that overlaps 35% of the vehicle being tested and the angle between the longitudinal axis of the barrier and the longitudinal axis of the test vehicle is 15 degrees. The field relevance of the IIHS test and the NHTSA test has been the subject of papers by Prasad et al. (2014a,b). The current study is aimed at examining the combined relevance of the two tests as representing frontal corner impacts involving small overlap. The field relevance is indicated by the frequency of occurrence of real world crashes that are simulated by the test conditions, the proportion of serious-to-fatal real world injuries explained by the test conditions, and rates of serious injury to the head, chest and other body regions in the real world crashes resembling the test condition. The database examined for real world crashes is NASS-CDS. The frontal corner impacts as represented by the 25% Small overlap frontal and the NHTSA tests together address slightly less than 9% of all frontal crashes and 6% to 12% of all MAIS3+F injuries to the drivers in these crashes. The IIHS test has a somewhat higher contribution in both the incidence and severity. The two crash modes together address 4.6% to 8.2% of all MAIS3+F head injuries. Similarly, the proportion of all frontal MAIS3+F chest injuries addressed by the two crash modes or corner tests is estimated to be 6% to 10.6%.

The available data for the passenger involved in driver-side frontal corner crashes indicate that elderly female occupants predominantly experience serious head and chest injuries. All, except one, injured passengers were females. The average age of injured females who had chest injuries was slightly over 65 years. Injury rates of the head and the chest are substantially lowered in far-side than in near-side frontal impacts. Crash test ATD rotational responses of the head in the tests substantially over predict the real world risk of serious-to-fatal brain injuries.

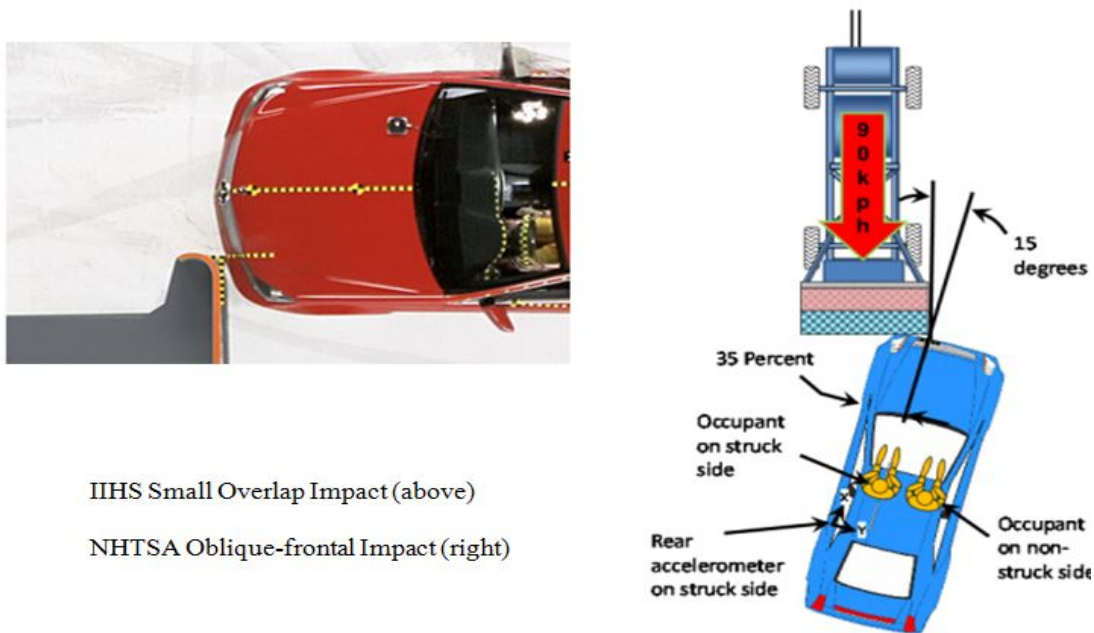
## INTRODUCTION

Light vehicles are currently designed to meet or exceed the requirements of the FMVSS 208 in frontal impacts. This regulation includes perpendicular and angular tests against a rigid barrier and a 40% offset test against a deformable barrier. The rigid barrier tests are conducted at 25 mph with unbelted dummies, and at 35 mph with belted dummies. Whereas the offset, deformable barrier test is conducted at 25 mph for the FMVSS 208, vehicles are also designed to perform well in the IIHS 40% offset, deformable barrier tests. Over the years, most vehicles had achieved the highest ratings in the IIHS frontal tests, and also good ratings in NHTSA's frontal NCAP. This prompted the IIHS and NHTSA to investigate additional test configurations for frontal impacts. The IIHS has adopted a 64 kph frontal crash test in which 25% of the front-end of a vehicle is engaged by a rigid barrier, generally referred to as a Small Overlap Impact (SOI) test, and is shown in Figure 1. The structural and dummy responses are used to rate the vehicle as Good, Acceptable, Marginal or Poor. To get the highest rating, Top Safety Pick+ (TSP+), the vehicle has to achieve at least an acceptable rating in the new test. Mueller et al. of the IIHS have reported on various structural design strategies adopted in vehicles redesigned to perform well in the SOI mode.

Simultaneously, NHTSA conducted a meeting of NHTSA experts to examine the reasons why vehicle occupants are killed despite being belted and protected by airbags in frontal impacts (Bean et al. and Rudd et al. (2009)). A detailed study of 122 fatal frontal crashes in NASS was performed in which primary and secondary causes were subject to group consensus. 49 of the 122 crashes (40%) were considered to be exceedingly severe or had anomalies. 29 of the 122 (24%) were **corner and/or oblique impacts** in which it was judged that the primary factor affecting fatalities was limited structural engagement of the front longitudinal rails of vehicles that are designed for energy absorption. The frequency of occurrence of the corner and/or oblique crashes in the NASS database was not estimated. This study led to a research program of crash testing by NHTSA and some of the test results have been reported by Saunders et al. (2011, 2012, 2013 and 2014).

After conducting a large number of developmental frontal crash tests, NHTSA has selected a movable deformable barrier crash test, shown in Figure 1, in which a Research Moving Deformable Barrier (RMDB) impacts the test vehicle on its left or on its right front corner a vehicle. The test vehicle is stationary and positioned at a target angle of 15° and at a target overlap of 35% to the forward line of motion of the RMDB. The RMDB is towed down the test track in a full forward direction, without any crabbing, and at the targeted impact velocity of 90.12 kph (56.0 mph) into the test vehicle. Regardless of the test vehicle’s mass, RMDB’s mass is 2490.7 kg (5491 lbs.). At the time of writing of this paper, results of eighteen (18) crash tests conducted by NHTSA have been placed in the public domain. Test reports of 6 RMDB tests of vehicles rated “Good” in the IIHS SOI test have also been added to the website. NHTSA’s rationale for selecting the Oblique RMDB test has been outlined in several papers by Saunders et al referenced earlier.

It is worth noting that both tests shown in figure 1 could be classified as corner impacts. In the IIHS SOI test the stationary barrier overlaps the front end of the tested vehicle by 25% leading to missing the front rail entirely in virtually all vehicles in the US fleet. This test comes close to the definition of a corner crash not involving the front rails as in Bean et al. In the RMDB test, the barrier overlaps the front-end of the impacted vehicle by 35%. This initial impact geometry ensures that the barrier impacts the front-rail in the vast majority of light vehicles, but at an angle. Both test conditions are also referred to as “small overlap” frontal tests.



IIHS Small Overlap Impact (above)  
 NHTSA Oblique-frontal Impact (right)

Figure 1. Small Overlap Crash Tests

Saunders and Parent (2014) summarized the status of NHTSA's research in January 2014 and have placed their analysis on NHTSA's website. Their analysis of existing data indicates that the Oblique RMDB test is representative of vehicle-to-vehicle crashes and the test procedure is repeatable. Testing of newer, high sales volume vehicles show injury risk trends similar to previous older vehicles. Far-side dummy occupant responses in these tests show head rotational velocities associated with high risk of brain injury.

Saunders and Parent (2014) also tested six vehicles that had achieved the IIHS Top Safety Pick+ (TSP+) rating utilizing the Oblique RMDB test procedure and compared their results with those of non-TSP+ vehicles. In general, the five TSP+ vehicles in the NHTSA Oblique RMDB tests yielded lower passenger compartment intrusions than the fourteen non-TSP+ vehicles, however injury risks as determined from the THOR dummy responses were similar in the two groups of vehicles. A particularly important finding was that the provisional Injury Assessment Reference Value (IARV) for rotational velocity of the head, BrIC, was exceeded in both the TSP+ and the non-TSP+ group of vehicles. Additionally, the average BrIC was higher for the far-side occupants than near side occupants, i.e. front seat passenger involved in a left corner impact as in figure 1.

## **FIELD RELEVANCE OF THE CORNER TESTS**

The relative importance of the two tests in Figure 1 has been covered by several studies aimed at identifying the real world distribution of frontal crashes, in terms of frontal engagement and the proportion of all serious-to-fatal occupant injuries addressed in frontal crashes. A brief review of these studies follows.

The earliest study somewhat addressing small overlap frontal crashes in Sweden was reported by Planath et al. In 1993, Planath et al. reported the results of a study of frontal crashes in Sweden. A class of frontal crashes labeled as Severe Partial Overlap Crash (SPOC) occurred 3% of the time, but accounted for 14% of AIS2+ injuries to occupants of vehicles involved in frontal crashes. In a subsequent paper, Planath and Nilsson compared several frontal crash tests in regulations and mentioned that Volvo had developed an additional test procedure for SPOC that consisted of a 35% overlap, frontal test against a rigid barrier at 64 km/h. It was also stated "Exclusive use of SPOC in the development process would however be detrimental." This test did not gain too much attention, perhaps due to the introduction of the European 40% overlap against a fixed deformable barrier in the European regulation and by the IIHS in the USA and by NCAPs around the world. The results of further crash studies in Sweden performed by Lindquist et al. in 2003 and 2004 once again focused the attention of researchers to Small Overlap Impacts (SOI). Lindquist claimed that nearly half of all frontal crash fatalities in Sweden were in these SOI's. In these crashes the front longitudinal members were not engaged resulting in substantially greater passenger compartment intrusions than in frontal crashes in which the rails were engaged. The 2003 and 2004 studies kicked off similar studies in US and Europe. The IIHS conducted a study of frontal crashes of vehicles that were rated "Good" in their frontal crash program and at least one front-outboard occupant had an AIS $\geq$ 3 injury unless the only such injury was to the extremities. Brumbelow and Zuby reported results of the study in 2009. They defined small overlap as being when the major load path was outboard of all major longitudinal members. The small overlap accounted for nearly 25% of all the cases included in the study. The IIHS followed up by conducting several frontal crash tests to help them develop the test shown in Figure 1.

Kuehn et al. (2013) from the German Insurers Accident Research Group conducted a retrospective analysis of 3242 accidents involving passenger cars- 1930 of these were frontal collisions and 485 of which involved collisions in which the frontal engagement was considered to be small overlap. Unlike the results from Sweden, their conclusion was that "In terms of fatalities, the relevance of small-overlap car accidents is low. In terms of serious injuries (AIS2+) to the lower extremities, the relevance of small-overlap car accidents is high."

A Frontal Impact Taxonomy study was conducted by Sullivan et al. (2008), in which all NASS frontal crashes were distributed in eight different bins. The proportional contribution of each bin was determined in terms of frequency of occurrence and injury severity. Sullivan et al. reported that nearly two-thirds of all frontal crashes were full-engagement and offset with a nearly even split. A bin classified as SS/Corner

accounted for slightly less than 14% of all frontal crashes, slightly less than 12% of all vehicles in which at least one occupant had an MAIS3+ injury and slightly over 10.5% of all vehicles in which at least one occupant was fatally injured. This bin would contain the IIHS 25% offset and NHTSA's Oblique RMDB test conditions and vehicle deformations, and would give an upper limit of the incidence of the two crash types combined and injuries associated with them.

Scullion et al. (2010) modified the Frontal Impact Taxonomy study of Sullivan et al. into seven bins and concentrated on identifying the frequency of occurrence of and injury rate in small overlap frontal crashes in NASS. They defined small offset as a case in which the frame rail was not engaged and the center of damage was located entirely outside the frame rails. This case would fit the conditions produced in the IIHS SOI tests. In this study, slightly over 69% of all frontal crashes could be described by offset plus full engagement and 7.5% could be classified as small offset. The MAIS3+ injury risk was slightly lower than that in full-engagement crashes. Although the relative contribution of the small offset crashes as a proportion of all MAIS3+ frontal crashes was not reported, it had to be much less than that of offset plus full engagement crashes. In subsequent papers by Scullion et al. and Morgan et al. the small offset crashes continued to show up as relatively much smaller proportion of frontal crash modes than the full engagement and offset crashes.

Samaha et al. have reported the results of a more detailed FIT study of the NASS CDS cases for MY 1985-2011 vehicles involving belted drivers in vehicles equipped with airbags. In this study, the light vehicle fleet was partitioned into four weight classes and the FIT of individual weight classes was determined. In their crash classification the corner impact bin was separated into two classes- "small offset front" and "small offset side." The combined corner bin accounted for 7% of all crashes and 10% of all MAIS3+ driver injuries. The vehicle fleet was also divided in two groups of MY's- 1985 to 1999 and 2000+. Two driver age groups were also studied- 16 – 50 years and 50+ years. For both age groups, the involvement and injury rates were estimated as a function of FIT classification. The distribution of various body regions with moderate- and serious-to-fatal injuries by FIT classification was also determined for the two MY groups and age groups. For example, in the 16-to-50 yr. age group, full engagement and offset crashes accounted for approximately 79% of all serious-to-fatal head injuries and the corner crashes accounted for approximately 10% of all serious-to-fatal head injuries. Similar results were observed for lower extremity injuries- the corner crashes accounted for approximately 8% of all serious-to-fatal lower extremity injuries.

During the course of the Samaha et al. study, random check of photographs of case vehicles binned in the "small offset side" category, showed that some of them would not fit the damage patterns produced in either the IIHS SOI tests or in the Oblique RMDB tests conducted by NHTSA. Subsequently, a NASS case review process was used by Prasad et al. (2014a,b) that relied on hard copy reviews of frontal crashes in NASS-CDS. This involved binning potential corner crashes in either the IIHS like crashes or in NHTSA's Oblique RMDB like crashes.

## **Objective**

The objective of this paper is to consolidate the main results of the two studies as they relate to frontal corner impacts and add further observations not covered in the earlier studies.

To establish the field relevance, the frequency of occurrence of the crash types and the resulting rates of serious-to-fatal injuries in real world frontal crashes were estimated from the publicly available database, NASS.

**Collision Deformation Classification (CDC):** Since these studies utilize the Collision Deformation Classification (CDC) as the first filter of the frontal crash data in NASS for comparison with test data, a brief introduction of the CDC is deemed appropriate in this section. A simplified description of the CDC is shown in Figure 2. It is important to note that a CDC code for any given vehicle is based solely on contact damage; any damage that is induced to the vehicle structure as a result of an impact is specifically excluded from consideration. Essentially, the front end of a vehicle is divided into three sections- L, C and R. L covers the left one-third of the vehicle, R covers the right one-third of the vehicle and C covers the center one-third of the vehicle. By the definition of the IIHS test with only 25% overlap of the barrier all IIHS

test like deformations should be in the L section (or R for right-front impacts). Since the overlap of the front-end of a test vehicle with NHTSA's barrier is 35%, the deformation of the front-end should be in the Y (or Z) section by definition. Therefore, all crashes that have CDC classification FY or FZ would contain the CDC observed in NHTSA's tests, and similarly all FL or FR crashes would contain the CDC observed in the SOI crashes conducted by the IIHS. Based on the definitions of FY and FL, given any error in the direct damage estimate, it is quite possible that some of the FY's could be FL's and some of the FL's could be FY's.

**METHODOLOGY**

Two crash test databases maintained by the IIHS and the NHTSA were interrogated. In the IIHS database there were results of 65 vehicle crashed in the SOI crash mode. In the NHTSA database results of 18 vehicles crashed in the Oblique RMDB mode were available. The damage patterns of the vehicles were assigned CDC classifications. The IIHS CDC classifications were 12FLXXXX and the NHTSA test vehicles 11FYXXXX. As shown in Figure 3, NASS frontal crash database was interrogated with the following restrictions: 3-point belted front-outboard occupants involved in planar impacts (i.e. no rollovers), airbags fitted on driver and passenger sides, direction of force 11, 12, 01, and all CDC extents. NASS calendar years were restricted to 1988 to 2010. The age of the front-outboard occupants was restricted to 15 years or older. This Subset of frontal crashes was referred to as Subset 03 in the two Prasad et al. papers. It contained 21,433 cases representing 9,793,461 cases when weighted. Hard copy reviews of all FL and FR crashes (not restricted by the PDOF) identified by the search in which a front outboard occupant had an MAIS3+F injury were conducted. Damage patterns of the involved vehicles were compared to those observed in the IIHS SOI tests and binned as “Good”, “Moderate” or “poor” match with those observed in the SOI tests. The “Poor” matched cases were further examined to see if they could be classified in the Oblique RMDB crash bin. A similar process was followed for the FY and FZ classification of crashes as shown in Figure 3. Once again, the cases rated as “Poor” match with damage patterns observed in the Oblique RMDB were reviewed to verify if they could be classified in the IIHS bin. Details of the process can be found in the Prasad et al. papers. In this paper only the main results will be presented.

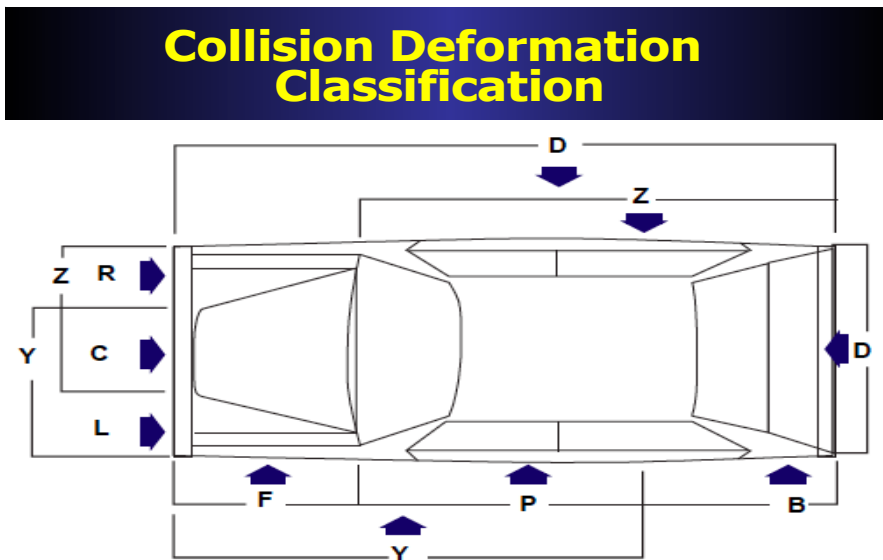


*Figure 2. Schematic Of the Collision Deformation Classification*

Prasad et al.(2014a) have reported the results of the CDC-FL branch shown in Figure 3 for all MY vehicles, MY2000+ vehicles and the 2000+ MY vehicles that were rated “Good” in the IIHS Moderate Offset tests to be consistent with the Brumbelow and Zubly study. Both the FIT analysis and hard copy reviews of the NASS cases were performed. The FIT analysis indicated that 7.5% of all frontal crashes

could be represented by the IIHS SOI tests. The frequency of occurrence of the NHTSA test like deformations was estimated by Prasad et al (2014b) as 1.24%. Therefore, the two small overlap corner crashes account for approximately 9% of all frontal crashes. The IIHS test condition also accounted for 6.1% of all MAIS3+F injuries to the front outboard occupants. These proportions were similar for the 2000+ MY vehicles as shown in Table 1. Note that Table 1 contains data for paired driver and passenger, i.e. driver side and passenger side crashes with occupants on the side impacted. Considering that the Samaha et al. study included “small offset side” also, the results of the FIT analysis in the two studies are similar. Samaha et al. also found little difference in injury distribution between all MY vehicles and 2000+ MY vehicles. Based on the above, hard copy reviews of the NASS cases in FY or FZ branch in Figure 3 was limited to the 2000+ MY vehicles. The results of the hard copy analysis are shown in Figure 4.

**Table 1. Summary of Estimated Contribution of IIHS SOI- like Crashes**

	All MY	MY2000+	MY2000+ & Good
SOI % MAIS3+F	2.9% to 6.8%	3.9% to 7.1%	3.0% to 7.5%
SOI %MAIS3+F	6.1% FIT Analysis 5.2% to 9.3%	4.5% to 8.8%	4.7% to 9.2%

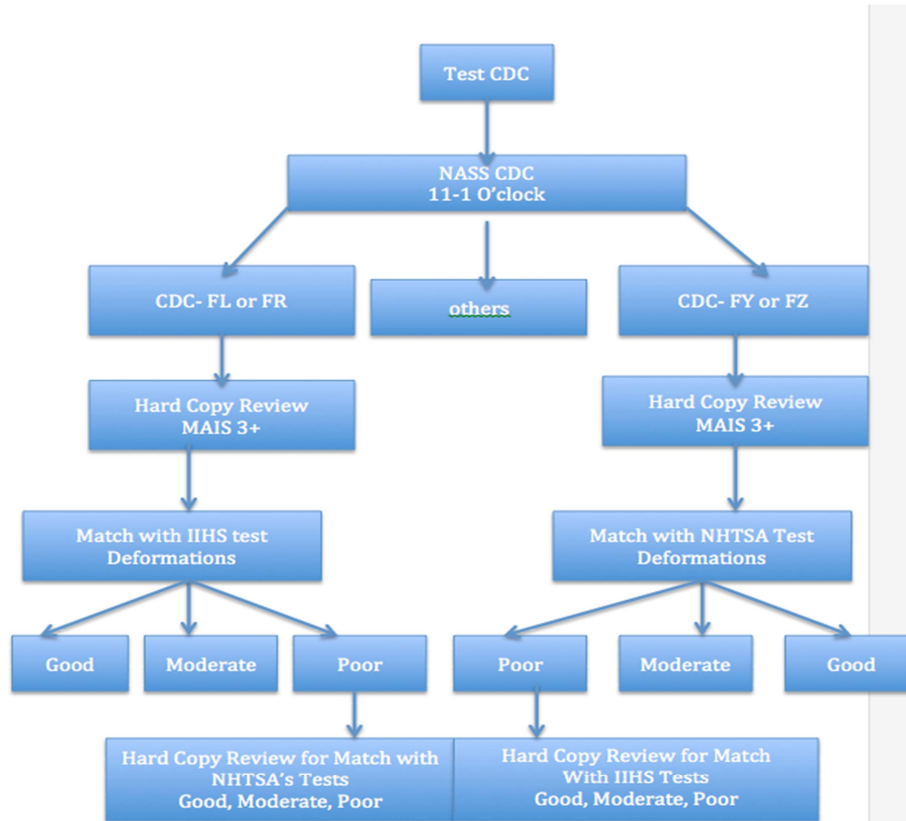


**Figure 3:** Schematic of the process used to identify NASS Frontal crashes that could be represented by NHTSA's Oblique RMDB Tests or by the IIHS SOI

NASS cases involving MY 2000 and newer vehicle and MAIS  $\geq 3$  or fatal belted driver reviewed for similarity to NHTSA 35% overlap, 15° angled frontal RMDB Impact and the IIHS SOI Tests

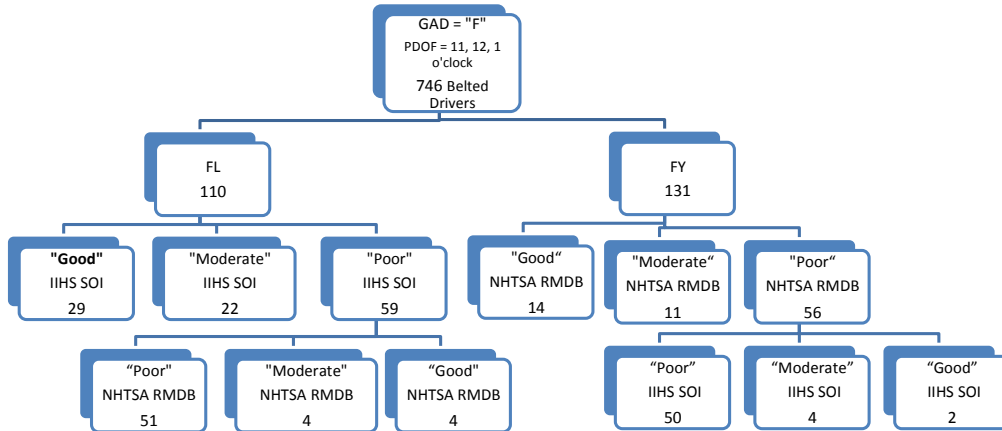


Figure 4: Distribution of Driver MAIS3+F Injuries by FL and FY Damage Locations

Figure 4 shows that there were 746 drivers with MAIS3+F injuries in 2000+ MY vehicles that were involved in frontal crashes. Of these, 110 were in crashes with frontal damage classified as FL. Hard copy analysis of these 110 cases showed that 29 had a “good” match with the IIHS tests and 22 had “moderate” match with the IIHS tests. Out of the 59 cases with poor match with the IIHS tests, 4 were considered to be a “Good” match with NHTSA’s Oblique RMDB tests. There were 131 cases with FY classification. Out of these, 14 were considered to be “Good” match with the RMDB tests and 11 had a “moderate” match. Out of the 56 with “Poor” match with the RMDB test, 2 were considered to have “Good” match with the IIHS test and 4 had “Moderate” match with the IIHS tests. Adding up, there are 31 “Good” matches with the IIHS tests and 18 “Good” matches with the Oblique RMDB tests. The total number of “Good” matches is assumed to indicate the lower bound of the estimated proportion of all frontal crash MAIS3+F injuries. There are 31 “Good” matches with the IIHS SOI test yielding 31/746 or 3.9% of all frontal MAIS3+F injuries. Similarly there are 18 “Good” matches with the NHTSA RMDB test yielding 2.4% of all frontal injuries considered. The two tests together address 6.3% of all MAIS3+F frontal injuries to belted drivers. If the sum of the “Good” and “Moderate” matches is assumed to be the upper bound of injuries addressed by either test, the IIHS test represents approximately 7.6% and the RMDB test represents approximately 4.4% all MAIS3+F driver injuries in frontal crashes. Therefore, an upper-bound of approximately 12% is estimated as being addressed by the two small overlap corner tests discussed in this paper. Therefore the two small overlap corner tests address 6.3% to 12% of all driver frontal MAIS3+F injuries. The authors believe that a point estimate closer to the lower bound is more likely outcome of the current analysis described in the paper, since the upper estimates contain cases with “Moderate” match with the test data several of which have extent 9 with massive damage not seen in the IIHS tests. The estimates made by Sullivan et al. and Samaha et al. are within the range of estimates in this analysis.

#### Distribution of injuries by damage location

With insights gained from the hard copy reviews, further interrogation of the Subset 03 reported in Prasad

et al. was conducted to estimate MAIS3+ injury rates by damage locations for belted Front Outboard Occupants (FOO). Particularly, AIS3+ head/face and chest injuries were investigated as a function of seating position, Direction of Force and Damage Extent.

**RESULTS of NASS Data Analysis:**

The overall composition of frontal crashes being considered in this paper is shown in Tables 2. In Tables 2, numbers in parentheses give the percentage of the total of the individual cell, e.g. 12.8% of the drivers are involved in crashes whose damage location is coded as FL. Table 3 contains the injury rates for the drivers and passengers based on weighted data. The raw counts are also shown. Note that in order to have increased raw sample size, all MY’s counts were used. In spite of that, the raw numbers for the passenger side are relatively small.

Table 2: Involved Driver and Passenger By Damage Location (All MY) Subset 03 Prasad et al.

Subset 03 Drivers GAD/SHL1	Driver Raw count	Driver weighted	Passenger Raw count	Passenger weighted
FL	2154	1,066,113 (12.8%)	448	200,952 (13.7%)
FY	2586	1,137,490 (13.7%)	499	173,508 (11.8%)
FD	8873	3,929,359 (47.2%)	1798	708,527 (48.2%)
FC	273	91,581 (1.1%)	60	18701 (1.3%)
FZ	2187	1,122,328 (13.5%)	455	173,517 (11.8%)
FR	1739	976,964 (11.7%)	361	194,421 (13.2%)
All	17,812	8,323,834 (100%)	3621	1,469,626 (100%)

Table 3: MAIS3+F Injury rates by Damage Location (All MY)

Subset 03 Drivers GAD/SHL1	Driver Raw count	Driver weighted (%)	Passenger Raw count	Passenger weighted (%)
FL	224	2.0	28	0.9
FY	285	2.0	34	4.1
FD	832	1.6	160	1.6
FC	48	2.3	8	11.4
FZ	148	1.0	42	1.2
FR	83	1.0	38	0.8
All	1620	1.6	310	1.7

Examination of table 3 indicates that the driver injury rates in the near-side frontal impacts, i.e. in the FL and FY damage locations, are nearly two times those in far-side damage locations, i.e. in FR and FZ locations. This trend does not appear to be true for the passenger, especially when the far-side is the FY location. The FY location is slightly over three times more injurious than the FZ location for the passenger. The passenger injuries in the FY damage location were examined further in terms of the demographics of those injured.

**Passenger Head and Chest injuries in FY damage location crashes**

There were only six passengers with MAIS3+ head injuries and all were females. Three of the six were in multiple impact crashes. One had a head contact coded as Center IP and below, one contacted the right B-pillar, one the right Grab Handle, one had contact with the passenger airbag and one showed only belt contact, one had an unknown contact. Based on the small numbers other more detailed analysis was not conducted.

There were 18 cases of MAIS3+F chest injuries. All except one were female occupants whose average age was slightly over 65 years. The source of injury for all except one was coded as the belt restraint and hardware. One injury source was coded as Floor or console. Based on the chest injuries and source, there is no evidence of passenger occupant slipping out of the shoulder belt in the far-side crashes.

**Driver Head and Chest Injuries by Damage Location:**

The distribution of driver head and chest injuries by frontal damage location was studied next and is shown in Table 4. Nearly half of all MAIS3+F head injuries occur in crashes with damage location coded FD, i.e. both rails were engaged. The corner impacts would include a subset of the FL and FY damage locations that account for nearly 27% of all head injuries. However, not all FL crashes are represented by the IIHS test and not all FY crashes are represented by the Oblique RMDB test. Based on Figure 4, approximately 26.4% to 46% of MAIS3+F injury producing FL crashes are like the IIHS SOI, and 10.7% to 19% of all FY crashes are like the Oblique RMDB crash. Applying these to the numbers in Table 4, one would estimate that the two crash modes together address 4.6% to 8.2% of all MAIS3+F head injuries. Similarly, the proportion of all frontal MAIS3+F chest injuries addressed by the two small overlap or corner tests is estimated to be 6% to 10.6%.

Table 4. Composition of Frontal Sample by Damage Location (Drivers Only)

(From Prasad et al. 2014b)

Subset #03	Sample Counts		% Composition by GAD1/SHL1					
			Head/Face AIS>=3		Chest AIS>=3		Fatality or MAIS>=3	
Drivers	Unweighted	Weighted	Unweighted	Weighted	Unweighted	Weighted	Unweighted	Weighted
GAD/SHL1	Unweighted	Weighted	Unweighted	Weighted	Unweighted	Weighted	Unweighted	Weighted
FC	273	91,581	2.4%	3.4%	3.3%	1.7%	3.0%	1.6%
FD	8,873	3,929,359	48.1%	49.9%	53.7%	49.7%	51.2%	48.3%
FL	2154	1,066,113	17.4%	11.0%	12.7%	15.1%	13.8%	16.4%
FR	1739	976,964	6.1%	12.9%	5.0%	6.9%	5.4%	7.5%
FY	2586	1,137,490	20.5%	15.9%	16.3%	19.4%	17.5%	17.6%
FZ	2187	1,122,328	5.5%	7.0%	9.0%	7.3%	9.1%	8.6%
<b>All</b>	<b>17,812</b>	<b>8,323,834</b>	<b>100.0%</b>	<b>100.0%</b>	<b>100.0%</b>	<b>100.0%</b>	<b>100.0%</b>	<b>100.0%</b>

The MAIS3+F head, chest and overall are shown in Table 5 for the driver. These rates are for frontal crashes in which the damage extent is between 3 to 6 which is the range of extent of frontal damage produced in the regulatory and public domain tests (IIHS 40% and 25% Overlap, the NCAP and RMDB Small Overlap tests). Examination of Table 5 shows that the head injury rate is highest in FD crashes and lowest in the FR and FL crashes. Similarly, the chest injury rate is highest in the FD crashes and lowest in the FR and FL crashes.

Table 5. Frontal Injury Rates by Damage Location Drivers only/ CDC Damage Extents: 3 to 6  
(From Prasad et al, 2014b)

Subset #03 Drivers CDC Exts: 3-6	Sample Counts		Injury Rates ( % )					
			Head/Face AIS $\geq$ 3		Chest AIS $\geq$ 3		Fatality or MAIS $\geq$ 3	
GAD/SHL1	Unweighted	Weighted	Unweighted	Weighted	Unweighted	Weighted	Unweighted	Weighted
FC	82	11,538	4.88%	1.08%	15.85%	4.14%	32.93%	8.22%
FD	1,528	262,248	5.82%	2.09%	13.74%	5.32%	32.79%	14.36%
FL	872	350,921	1.83%	0.19%	3.44%	1.15%	12.50%	2.97%
FR	732	397,919	0.96%	0.12%	1.91%	0.41%	6.56%	1.13%
FY	595	139,669	7.90%	1.86%	11.76%	2.53%	33.61%	10.53%
FZ	367	110,873	1.91%	0.44%	8.17%	1.33%	22.62%	5.56%
<b>All</b>	<b>4,176</b>	<b>1,273,167</b>	<b>4.07%</b>	<b>0.77%</b>	<b>8.79%</b>	<b>1.97%</b>	<b>23.18%</b>	<b>5.84%</b>

## DISCUSSION

A historical review of various studies aimed at examining the real world relevance of frontal corner crashes as represented by the IIHS 25% overlap and the NHTSA RMDB test conditions has been presented. The estimated proportion of serious-to-fatal injuries addressed by the corner impacts varies substantially depending on the sampling scheme of the different datasets studied and reported. Some studies in Europe show high proportions of fatal frontal crashes that could be explained by the small overlap tests and some show very little if any. In the US, NASS-CDS is a nationally representative accident sampling scheme from which the field relevance of these crashes can be estimated for the US. Towards this end, the authors of this paper have estimated the frequency of occurrence and the proportion of frontal crash injuries addressed by the tests simulating frontal corner impacts. The estimates are similar to those by other authors who have attempted to estimate the frequency of occurrence of these crashes and the population affected by them using the NASS-CDS database.

### Comparison of the Results With Current Test Data

The results shown in Table 5 indicate good correlation with the results of the IIHS 25% overlap tests. Prasad et al. (2014a) have reported their analysis of the 25% overlap IIHS crash test data that indicate head and chest injury risks predicted by dummy responses to be low but lower extremity injury responses to be higher than those observed in the 40% overlap tests. The NHTSA tests also indicate lower extremity injuries in the RMDB tests to be important. However, very little data with the THOR dummy exist in other frontal crash modes to evaluate the relative importance of the RMDB tests conducted so far. Based on the analysis of Samaha et al. the corner tests (IIHS and the RMDB tests together) potentially address slightly less than 10% of all AIS3+ lower extremity injuries. When the limited existing test data from the RMDB tests are examined, the projections from the tests do not agree with the field data as analyzed in this report or others by Prasad et al. (2014b), Samaha et al., Sullivan et al. and Scullion et al.. The serious head injury risks predicted by the dummy responses are substantially higher than those observed in the field. This prediction is traced to be due to the utilization of the new rotational injury criteria, BrIC (Takhounts et al.), to predict head injury risk in the tests. The brain injury risk

predicted by the dummy head responses for the passenger in driver-side RMDB tests are substantially over-predicting head injury risks. As discussed earlier in this paper, only six serious head injuries were identified in all serious injury producing FY crashes and all were to females and some were in multiple event crashes. Similarly, chest injury of passengers in FY type of corner crash appears to be an issue with elderly females (average age 65+ years) with injury source identified as the belt system. In the RMDB tests, the dummy kinematics is such that it slips out of the belt. This slipping out of the shoulder belt is not supported by the field data. It is not clear if the passenger dummy kinematics is due to artifacts of the dummy design, the RMDB or the initial test conditions.

## CONCLUSIONS

1. The frontal corner impacts as represented by the 25% Small overlap frontal and the Oblique RMDB tests together address slightly less than 9% of all frontal crashes and 6% to 12% of all MAIS3+F injuries to the drivers in these crashes.
2. The two crash modes together address 4.6% to 8.2% of all MAIS3+F head injuries. Similarly, the proportion of all frontal MAIS3+F chest injuries addressed by the two crash modes or corner tests is estimated to be 6% to 10.6%.
3. The available data for the passenger involved in driver-side frontal corner crashes indicate that female occupants predominantly incur serious head and chest injuries. All, except one, injured passengers were females. The average age of injured females who had chest injuries was slightly over 65 years.
4. Injury risks in far-side frontal corner crashes are lower than those in near-side frontal corner crashes.
5. The field data do not support the RMDB test data in terms of predicted head injury risks and observed kinematics of the passenger dummy in far-side frontal crashes.

## REFERENCES

- Bean, J., Kahane, C. K., Mynatt, M., Rudd, R. W., Rush, C. J. and Wiacek, C. (2009), Fatalities in Frontal Crashes Despite Seat Belts and Air Bags- Review of All CDS Cases- Model and Calendar Years 2000-2007 – 122 Fatalities. Report No. DOT HS 811 102. US DOT, Sept. 2009.
- Kuehn, M., Hummel, T. and Bende, J., Small-Overlap Frontal Impacts Involving Passenger Cars, Paper No. 13-0370, ESV Conference, 2013.
- Lindquist, M., Hall, A., and Björnstig, U. (2003), Real world car crash investigations — A new approach. *IJCrash*. (4) 375-384. 2003.
- Lindquist, M., Hall, A. and Björnstig (2004), Car Structural Characteristics of fatal frontal crashes in Sweden, *IJCrash*, 2004 Vol 9.
- Morgan, R. M., Cui, C., Marzougi, D., Digges, K. H., Cao, L. and Kan, C-D (2012), Frontal Pole Impacts, Proc. IRCOBI Conf., 2012.
- Morgan, R. M., Cui, C., Digges, K. H., Cao, L. and Kan, C-D. (2012), Impact and Injury Patterns in Between-Rails Frontal Crashes of Vehicles with Good Ratings for Frontal Crash Protection, Proc. 56<sup>th</sup> AAAM Conference, 2012.
- Becky C. Mueller, Andrew S. Brethwaite, David S. Zuby, Joseph M. Nolan (2014), Structural Design Strategies for Improved Small Overlap Crashworthiness Performance, *Stapp Car Crash Journal*, Vol. 58, 2014.
- Planath, I., Norin, H., and Nilsson, S., Severe Frontal Collisions with Partial Overlap - Significance, Test Methods and Car Design, SAE Technical Paper 930636, 1993.
- Planath-Skogsmo, I. and Nilsson, R., Frontal Crash Tests – A Comparison of Methods,” SAE Technical Paper 942228, 1994,
- Prasad, P., Dalmotas, D., and German, A. (2014b), The Field Relevance of NHTSA’s Oblique Research Moving Deformable Barrier Tests, *Stapp Car Crash Journal*, Vol. 58, 2014.

Prasad, P., Dalmotas, D., and German, A. (2014a), An Examination of Crash and NASS Data to evaluate the Field Relevance of IIHS Small Offset Tests, SAE 2014-01-1989, SAE International Journal of Transportation Safety, July 2014.

Rudd, R. W., Bean, J., Cuentas, C., Kahane, C. J., Mynatt, M. and Wiacek, C. (2009), A Study of the Factors Affecting Fatalities of Airbag and Belt Restrained Occupants in Frontal Crashes, Proc. ESV Conference, 2009.

Rudd, R. W., Scarboro, M., Saunders, J. (2011), Injury Analysis of Real-World Small Overlap and Oblique Frontal Crashes, Proc. ESV Conference, 2011.

Samaha, R. R., Prasad, P., and Nix, L. (2013), Opportunities for Injury Reduction in US Frontal Crashes: An Overview by Structural Engagement, Vehicle Class, and Occupant Age, Stapp Car Crash Journal, Vol. 57, 2013.

Saunders, J. and Parent, D. (2014), Update on NHTSA's Oblique Research Program, SAE 2014 Government Industry Meeting, NHTSA Website, Public Meeting, <http://www.nhtsa.gov/Research/Public+Meetings/SAE+2014+Government+Industry+Meeting>.

Saunders, J., Craig, M. J. and Suway, J. (2011), NHTSA's Test Procedure Evaluations for Small Overlap/Oblique Crashes, Proc. ESV Conference, 2011.

Saunders, J., Craig, M. and Parent, D. (2012), Moving Deformable Barrier Test Procedure for Evaluating Small Overlap/Oblique Crashes, SAE World Congress, Paper No. 2012-01-0577, 2012.

Saunders, J. and Parent, D. (2013), Repeatability of a Small Overlap and an Oblique Moving Barrier Test Procedure, SAE World Congress, Paper No. 2013-01-0762, 2013.

Saunders, J. and Parent, D. (2013), Assessment of an Oblique Moving Deformable Barrier Test Procedure, Paper No.: 13-0402, 23<sup>rd</sup> ESV Conference, Seoul, Korea, 2013.

Scullion, P., Morgan, R. M., Mohan, P., Kan, C-D, Shanks, K., Jin, W. and Tangirala, R. (2010), A Reexamination of the Small Overlap Frontal Crash, Proc. 54<sup>th</sup> AAAM, 2010.

Scullion, P., Morgan, R. M., Digges, K. H. and Kan, C-D (2011), Frontal Crashes Between the Logitudinal Rails, Proc. ESV Conference, 2011.

Sullivan, K., Henry, S. and Laituri, T. R. (2008), A Frontal Impact Taxonomy for USA Field Data, SAE 2008-01-0526.

## **ACKNOWLEDGEMENTS**

The authors would also like to acknowledge the support of the Alliance of Automobile Manufacturers who funded this study.

# A SEMI-ANALYTICAL APPROACH TO IDENTIFY SOLUTION SPACES FOR CRASHWORTHINESS IN VEHICLE ARCHITECTURES

**Lailong Song**

**Johannes Fender**

BMW Group, Research and Innovation Center  
Germany

**Fabian Duddeck**

Technische Universität München  
Germany

Paper Number 15-0183

## ABSTRACT

In an early design phase for vehicle crashworthiness, the use of classical optimization is limited. One reason for this is that development of structural components is distributed over different departments. Additionally, crash performance depends on several components and their interaction. Common components in vehicle architectures are subject to various load cases in multiple vehicles. Thus, the entire vehicle architecture has to be considered during optimization. In order to enable distributed development the system needs to be decoupled, which means that a variation in one component does not require modifications of other components in order to reach the global structural performance goal.

The objective of this paper is to introduce a method to define the component-wise force-deformation requirements of vehicle architectures for front crash structure design. The force-deformation properties of the components are subject to constraints, from which an analytical description of the design space of the vehicle architecture is derived. The optimal orthogonal solution space within this design space is identified via optimization process. This results in maximal intervals for variations of the component forces over their deformations under the given boundary conditions. The validity of the solution space is proven through explicit FE simulation.

## INTRODUCTION

### 1.1 Load Case (USNCAP)

In 1978, the U.S. National Highway Traffic Safety Administration (NHTSA) introduced the crash test to evaluate the crashworthiness of the vehicles on market. This result is published in the U.S. New Car Assessment Program (USNCAP). One of the test scenarios is a vehicle impact against a fixed rigid barrier with 56km/h. Two dummies, which are protected by the restraint system, are seated in the front seats. The injury criteria are assessed based on the data collected during the crash by the dummies.

In vehicle crashworthiness design, the system is decomposed into two main sub-systems: vehicle structure system and restraint system. The analyse on the vehicle structure response, which is fundamental to the occupant protection, is the primary focus in this paper.

### 1.2 Structure Design

The crash relevant components are designed to absorb the kinetic energy of the vehicle by plastic deformation. These components usually form several parallel load paths going through the front structure of the vehicle in driving direction. During the deformation of the load paths, the **acceleration at the B-pillar** must not exceed the critical value. The B-pillar acceleration is correlated with the dummy acceleration, which is restricted by the injury criteria (Huang, 2002). Furthermore, the compartment deformation is constrained to prevent the occupants from crushing and penetration injury. The **firewall intrusion** is considered as a measurement of the severity of the compartment deformation in front crash. In addition to the dummy protection, the **number of the affected components** depending on the crash velocity is considered due to the structural reparability and reusability.

### 1.3 The Vehicle Cluster within Architecture

For economical reasons, the vehicle are desired to share as many components as possible. The vehicles are grouped into one cluster if they are coupled in the following ways:

**Direct coupling:** When several vehicles share common components, they are directly coupled. (shown in Figure 1)

**Indirect coupling:** The indirect coupling denotes the situation, in which several vehicles don't have common components. Nevertheless they have common components with the same vehicle(s) as shown in Figure 1.

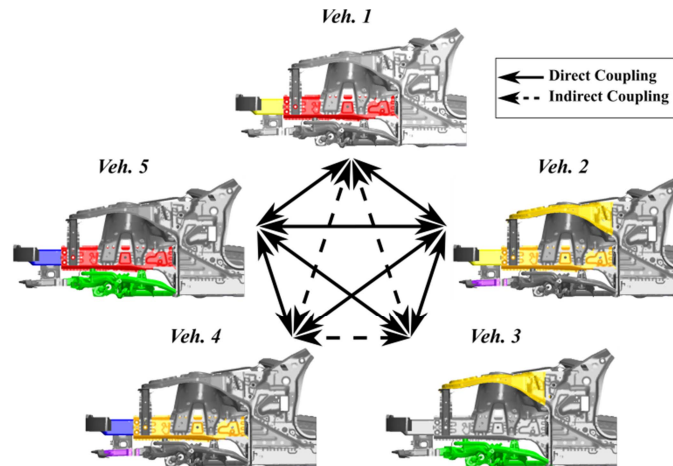


Figure 1. The coupling relation of a cluster with five vehicles.

The common components, which are assembled in different vehicles, must fulfill the functional requirements of each vehicle respectively. The design of common components is difficult if the mass distribution and feasible deformable lengths of the vehicles vary. Therefore, an approach to coordinate the local requirements from all the individual vehicle structures into one requirement for the component design should be established. These requirements defined in early phase can guide the later component design.

### 1.4 Simplified Modeling

The simplified model can be used to derive the functional requirement of the original structure effectively in the whole vehicle design process.

One prominent approach to simplify the structure is the lumped mass-spring (LMS) model. It was introduced by Kamal in the early 1970s. The frontal structure of the vehicle is represented one-dimensionally by masses and springs. This model delivers acceptable results seeing that the main features of the structure behavior in the crash are captured (Kamal, 1970). However, the characteristics of the springs must be collected from experiment, which limits the applicable field of the approach. Based on this, Ni and Song built a new model, in which the springs are substituted by shell and beam. This frame structure is analyzed by the finite element simulation to identify its behavior in the crash, based on which a study is conducted to define appropriate force-deformation curves for all the components (Ni & Song, 1986). Lust established a two-phase approach to study the connection between component property and the response of the overall vehicle structure in crash. In the first phase, the force-deformation curve of the component is individually analyzed. The identified force-deformation curve is considered to be scalable regarding the wall thickness of the component. In the second phase, the mass-spring model is built to obtain the overall structural response (Lust, 1992). Due to the increasing demand on the accuracy of the simplified model in prediction, the deviation between static crush test and real dynamic crash load case was put into consideration. Kim developed a mass-spring model for a quasi-static load case (Kim, Mijar, & Arora, 2001).

For the simplified model stated above, if the force-deformation curves of the component are calibrated to achieve the overall structural performance goal in crash, in the further component design process, optimizing the component to match the predefined force-deformation curve is not plausible. On this account, the concept of solution space was

developed by Zimmermann (Zimmermann & von Hoessle, 2013). The simplified model provides intervals for the force-deformation curves. The intervals calculated for all the components form the solution space of component design. This solution space is applied during component design: if the force-deformation curve of the component lies inside the solution space, the entire structure fulfills the expected functional goal. The solution space is identified with two approaches: the stochastic approach requires an FE model for the calibration of a load path model, which has its limitations in the early phase (Zimmermann & von Hoessle, 2013); the analytical approach includes a two-level solution procedure which sometimes over constrains the solution space. When calculating the solution space for vehicle architecture with common components in different vehicles, the analytical approach confronts an over determined system and thus delivers no solution space (Fender J. , 2013).

## 1.5 Vehicle Architectures

In order to minimize the development cost of the vehicle, the concept of the vehicle platform is introduced. A platform denotes a technical basis, on which various vehicle models can be constructed. The platform is also called vehicle architecture. In practice, besides the economical reason, the producers can take more advantage of the concept, e.g. less variant in components, efficient innovation, stronger global standardization and diversity in product (Gonçalves & Ferreira, 2005).

The common parts that make up an automotive platform are: chassis, suspension, steering mechanism and drive train components (WhyHighEnd.com, 2010). Analogously the platform concept is also applied for the corresponding components in Crash. The vehicles, which share the common components in the passive safety design, are grouped in one cluster. The solution spaces for the different vehicles with common components are identified by the stochastic approach based on a simplified load path model. The common components obtain a single functional requirement which fulfills the structural goal in different vehicles respectively.

## ANALYTICAL SOLUTION SPACE

### 2.1 Analytical Solution Space for Single Vehicle

**2.1.1 Basic Concepts** The process of the vehicle structure design is divided into several phases. The V-model shown in Figure 1 illustrates the detailed division of the phases. In the early phase, the package and platform of the new vehicle are decided. Thereby the rough mass distribution and topology are available. The structural parameters are thus extracted.

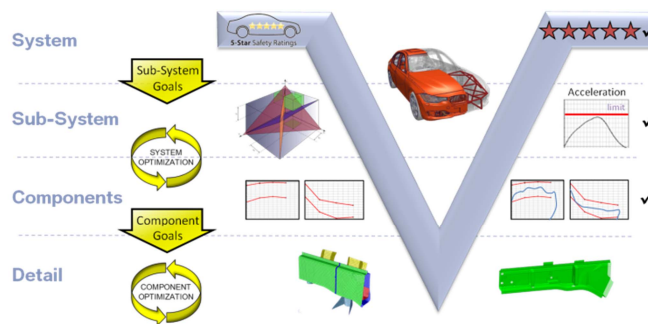


Figure 2. The process of structure crashworthiness design. (Fender J. , 2013)

**Available deformation length:** The available deformation of the front structure is the primary factor for the energy absorption. The total deformation length can be derived from the length of the frontal structure, the drive type, predefined topology and the firewall intrusion. This information is available and used for crashworthiness design in the early phase.

**Mass:** In the USNCAP front crash test, the impact velocity is predefined. Hence the mass of the vehicle determines the kinetic energy of the system to be dissipated. For the design of frontal structures, the total mass is divided into

two parts. The mass of the rear part of vehicle is concentrated at one point behind the firewall. The mass of the front end is distributed over the structure. Each component is attached with a concentrated mass, this simplification is proved to maintain the sufficient accuracy (Fender, Duddeck, & Zimmermann, 2014).

**The geometry space and deformation space:** The vehicle structure can be modeled using surrogate elements and concentrated mass points. In the symmetric front-crash, since the dominant momentum change happens in the driving direction (x direct), only the resistance forces in this direction are taken into consideration. The deformation conjugated to the force regarding energy is thus the deformation in x-direction. The maximal deformable length of the component is estimated in the early design phase. When integrated into the structure, the components are blocked often by rigid devices in between. In order to predict the actual available deformation of each component, a geometry space is first built up. The deformation space, which is significant for kinetics and energy absorption, is constructed by trimming the geometry space. Sections are inserted where a mass point or an ending of the component are met. The shortest load path is the bottle neck of the feasible deformation of the structure as shown in Figure 3.

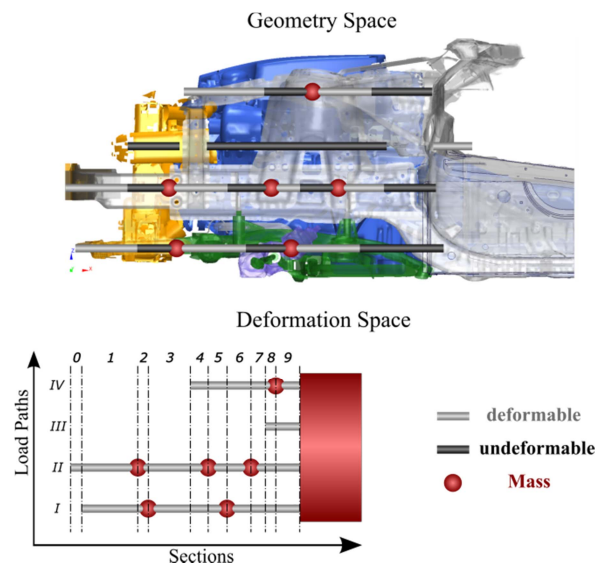


**Figure 3. Geometry space vs. deformation space.**

**2.1.2 Constraints** As discussed in section 1.2, three criteria are defined, in order to describe the performance of the structure in crash. In this section, the functional constraints are discussed based on information included in the deformation space.

**Critical acceleration:** The acceleration of the vehicle compartment is evaluated section wise in the deformation space. Therefore, the critical acceleration gives out the criteria on the force levels in components:

$$a_i = \frac{F_i}{M_{act,i}} \leq a_{crt,i} \quad (1).$$

In which  $F_i$  is the sum of the axial resistant forces of all parallel load paths in section  $i$ .  $M_{act,i}$  is the sum of the masses whose velocities are bigger than zero. This results in a system with  $N$  inequalities.  $N$  is the number of the sections of the system. If the acceleration in each section is smaller than the critical value, the structure fulfills the acceleration criterion.

**Firewall intrusion:** The criterion on the maximal firewall intrusion is satisfied if the velocities of all the mass point are null, before the feasible deformation is totally used up. In the deformation space, this condition can be described thusly:

In section  $i$ :

$$\int F_i(u)du \geq \frac{1}{2}M_{act,i}v_i^2 - \frac{1}{2}M_{act,i}v_{i+1}^2 \quad (2).$$

In which,

$F_i(u)$  : is the sum of the axial force from all the components in section  $i$  over  $u$

$u$  : is the deformed length of section  $i$

$M_{act,i}$ : is the active mass of section  $i$

$v_i$ : is the velocity of the structure when the section  $i$  starts to deform

The final velocity of the previous section and the initial velocity of the subsequent section are the same. And the velocity of the compartment should be zero after the last section in front structure deforms. In consequence, when the inequalities are summed up section wise, the terms with the intermediate velocities are eliminated, which yields the inequality:

$$\sum_{i=0}^N \frac{\int F_i(u)du}{M_{act,i}} \geq \frac{v_0^2}{2} \quad (3).$$

If Eq. (3) is fulfilled, the firewall intrusion is restricted.

**The order of deformation:** If the impact velocity is relatively low, it is not necessary to absorb energy by collapsing all the components. Moreover, the successive deformation behavior mitigates the dependencies of the components. On this account, the order of deformation criterion requires that:

$$F_1(u_1) - M_1 a(u_1) \leq F_2(u_2 = 0) \quad (4).$$

The indices represent the component 2 locates after component 1 in the same load path.

Up to here, the three constraints for the force-deformation curve of each component are introduced based on the information in deformation space.

**2.1.3 The Concept of Solution Space** One of the basic goals for the passive safety design in the early phase is to set up the expected force-deformation characteristic for the components. However this goal is ambitious because of the limited available information.

Zimmermann established an approach to find out a robust, compatible and flexible guideline for the component design. The fundamental concept can be explained in an example with a primitive deformation space, shown in Figure 4. The three boundary conditions are applied onto the axial resistance force of the components. The feasible field of designs is the triangle, in which the optimal design  $A$  is located. The optimum offers not only the lowest acceleration but fulfills the firewall intrusion and order of deformation constraints as well. However, this design is neither robust nor independent, i.e. If  $F_1$  is changed, the design may violate the constraints.  $F_2$  must be adjusted correspondingly to bring the design back to the feasible field.

The solution space approach creates in this situation a suitable rectangle (a hypercube in high dimensional space) inside the design space. All the designs inside this solution space fulfill the three constraints. In each dimension, the level of the resistance forces is restricted by an interval. For a component with several sections, the intervals form a corridor for the force-deformation curve of the component.

Inside the solution space, the change of the resistance force level in one dimension doesn't lead to constraint violations in other dimensions, which means that the change of force level in one component doesn't require the adaption of the others to fulfill the overall structural requirements.

With the solution space concept, the passive safety design in early phase can be transformed into the problem: calculate the solution space of the structure; i.e. identify the corridors for the force-deformation curves of the components. In the component design phase, if the force-deformation curve of individual component locates inside the corridor, the total structure fulfills the three constraints.

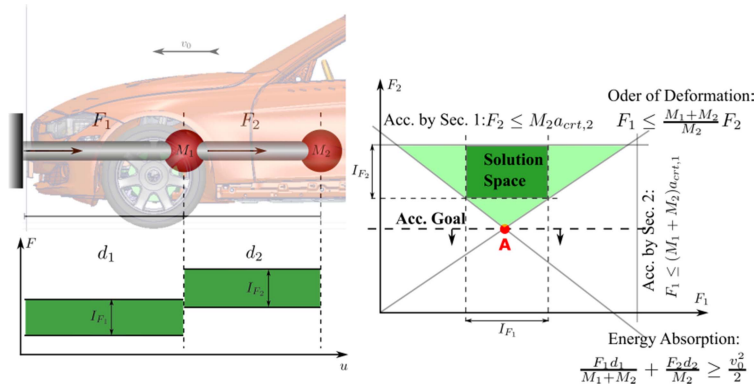


Figure 4. Solution space of a structure with two components. (Zimmermann & von Hoessle, 2013)

## 2.2 Solution Space for One Cluster within Vehicle Architecture

If the components have identical length and concentrated mass in the geometry space, these components can in principle be defined as common components. However, the commonality is in reality based on more criteria from other disciplines. Therefore, the common components are manually pre-defined.

**2.2.1 Construction of the Coupled Deformation Spaces** The common components are marked with the same name in the deformation space. The relationships are managed using a mapping. The structure of the mapping is shown in Figure 5.

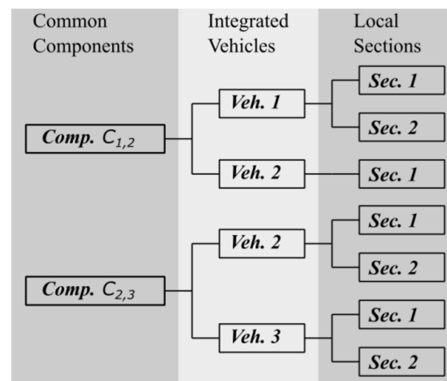


Figure 5. Mapping list of the vehicle relationship in cluster.

The force-deformation curve of the component is discretized by sections. As a consequence, the common components, which share the same corridor, must have the same section discretization. In another words, the section division of common components should have identical distances and count. For this reason, the artificial sections are inserted into the deformation spaces to synchronize the section division of the common components. For instance, three deformation spaces with common components are synchronized in the following way:

### a. Independent construction of the deformation space

As shown in Figure 6 in step I, the three deformation spaces are built independently for each structure. The building process is the same as for single structure – sections are inserted where a mass point or an ending of the component are met.

### b. Consecutive synchronization of sections for each component

The new artificial sections are inserted, so that the common components have the identical section division as shown in Figure 6 in step II and III. Since the sections are transversely through all parallel load paths, the parallel components are affected as well. This synchronization leads to a finer discretization for the deformation space. When the common components have comparable relative spatial positions among structures, the section count for the common components converges. Important positions (mass point and ending of component) within the spatial range of the common components are eventually marked with section bounds. In the case of a cluster with  $N$

vehicles, each has  $p_i$  components and  $q_i$  mass points, the synchronization converges before maximal  $\sum_{i=0}^N (p_i + q_i)$  iterations.

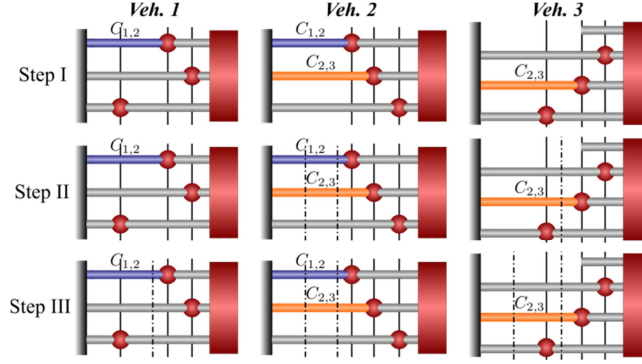


Figure 6. Artificial sections are inserted to synchronize the deformation spaces.

## 2.3 Solution Space Identification

The goal of this solution process is to find the largest possible solution space in the design space, which is described by the three constraints. The notations used in the solution process are the following:

$F_{u(pper),ij}/F_{l(ower),ij}$  : the upper and lower boundaries of the force interval in section  $i$ , load path  $j$ .

$M_{ij}$  : the value of the mass point at section  $i$ , on load path  $j$ .

$M_{act,i}$  : the active mass when the system deforms till section  $i$ .

$d_i$  : the length of the section  $i$ .

$a_{crt,i}$  : the critical acceleration of the section  $i$ .

$v_0$  : the initial velocity of the vehicle

**2.3.1 Constraints** The upper and lower boundaries of the intervals are the unknowns to be identified in the solution process. Suppose that the system has  $N$  sections and  $M$  load paths. The constraints for an optimization problem can be formulated as follows:

The upper boundaries of force-deformation curves in each component should satisfy the inequalities for critical acceleration:

$$\sum_{j=1}^M F_{u,ij} \leq M_{act,i} \cdot a_{act,i} \quad (5).$$

The lower boundaries of force-deformation curves in each component should satisfy the equalities Eq. (6) w.r.t. the energy absorption criterion:

$$\sum_{i=1}^N \left( \sum_{j=1}^M F_{l,ij} \right) \frac{d_i}{M_{act,i}} = \frac{v_0^2}{2} \quad (6).$$

The order of deformation between components in the same load path applies constraints between the upper and lower boundaries of the intervals. If a component ends at section  $i$ , the constraint is:

$$F_{u,ij} - \frac{M_{ij}}{M_{act,i}} \sum_{j=1}^M F_{u,ij} \leq F_{l,(i+1)j} \quad (7).$$

These constraints are applied to the intervals of the force-deformation curves for each vehicle structure in the cluster. Among the vehicles, extra equalities are needed to ensure the identical corridors for common components. For instance, components  $C_A$  and  $C_B$  are common in deformation spaces  $D_A$  and  $D_B$ , which are built from the structure of vehicle  $A$  and  $B$  respectively.  $F_{u,ij}^A, F_{l,ij}^A$  are the upper and lower boundaries of the force intervals for  $C_A$  in  $D_A$  with the section set  $I_A$  while  $F_{u,mn}^B, F_{l,mn}^B$  are the boundaries of the force interval for  $C_B$  in  $D_B$  with the section set  $M_B$ . The section set  $I_A$  and  $M_B$  have an offset  $\delta$ , i.e.  $I_A = M_B + \delta$ . The commonality requires that:

$$F_{u,ij}^A \equiv F_{u,(i+\delta)n}^B, F_{l,ij}^A \equiv F_{l,(i+\delta)n}^B \quad \forall i \in I_A \cap \{M_B + \delta\} \quad (8).$$

**2.3.2 Objective Functions** Under these constraints, the optimal values of the upper and lower boundaries are calculated by quadratic programming. The objective function is defined as follows:

**Width of the corridor:** In the application, it is more flexible to design the component with wider corridor for the force-deformation curve. Thus, the largest solution space is desired within the design space. The closer the corridor boundaries approach to the constraints, the wider the corridors are. In order to maintain the convexity of the optimization problem, the objective function is formulated with sum of squares (SoS).

The widths of the corridor for different components are controlled by a weighting factor. This is practical, when the force-deformation behavior of one component is easier to control (e.g. crushing component) than that of another component (e.g. buckling component). Thus, the widest corridor is achieved by finding the minimum of Eq. (9).

$$\min. \quad \Psi = \sum_{i=0}^N \left[ \left( \sum_{j=0}^M \omega_{ij} \right) \left( \sum_{j=0}^M F_{u,ij} - M_{act,i} \cdot a_{crt,i} \right)^2 \right] \quad (9).$$

In which  $\omega_{ij}$  denotes the weighting factor of the corridor segment at section  $i$  and load path  $j$ .

**Smoothness of the corridor:** If dramatic overshootings exist in the corridor, it is difficult to design the force-deformation curve of the component to fulfill the corridor. Therefore, the smoothness of the corridor should be tuned to reduce the complexity of the engineering work. For component  $C_k$  with  $S$  corridor segments, the objective function for corridor smoothness is written as:

$$\min. \quad \phi_k = \frac{1}{S-1} \sum_{i=1}^S (F_{m,ij} - \bar{F}_M)^2 \quad (10).$$

In which  $\bar{F}_M = \frac{1}{S} \sum_{i=1}^S (F_{u,ij} + F_{l,ij})/2$ .  $\Phi$  is the sum over the objective functions of each corridor.

**Uniform distribution of the corridor widths:** The force-deformation curve to be designed may not fulfill an extreme narrow corridor. Therefore, the widths of the corridors should be as uniform as possible. If the influence of the pre-defined weighting factors is eliminated, the objective function is formulated to minimize the variation of the corridor widths:

$$\min. \quad \Theta = \frac{1}{D-1} \sum_{i=1}^N \sum_{j=1}^M \left( \frac{F_{u,ij} - F_{l,ij}}{\omega_{ij}} - \bar{\Delta F} \right)^2 \quad (11).$$

In which  $\bar{\Delta F} = \frac{1}{D} \sum_{i=1}^N \sum_{j=1}^M (F_{u,ij} - F_{l,ij})/\omega_{ij}$ , and  $D$  is the number of corridor segments.

As a consequence, the solution process is transferred into a multi-objective optimization problem. The overall objective function is built by weighted sum of the sub-objective functions Eq. (9-11):

$$\min. \quad \Sigma = \Omega_{w(idth)} \cdot \Psi + \Omega_{s(smoothness)} \cdot \Phi + \Omega_{d(istribution)} \cdot \Theta \quad (12).$$

The objective function is formed by SoS and therefore semi-positive definit. The equality and inequality constraints are linear. As a result, a unique optimum of this convex problem can be found by interior point method (IPM) (Nocedal & Wright, 2006) (Vandenbergh, 2010).

## RESULTS

### 3.1 Solution Space Calculation

The upper and lower boundaries of the force interval in each section and load path are packed into the solution vector  $\vec{x} = [F_{l,ij}, F_{u,ij}]^T, i \in [0, N], j \in [0, M]$ . This solution vector is obtained by solving the quadratic optimization problem:

$$\min. \quad \vec{x}^T H \vec{x} + b^T \vec{x} \quad (13).$$

under the equality and inequality constraints. In which  $H$  is the Hessian matrix of  $\Sigma$  and  $b$  is the first derivative of  $\Sigma$ . Tuning the weighting factor of the sub-objective functions leads to different optimal solution spaces as shown in Figure 7.

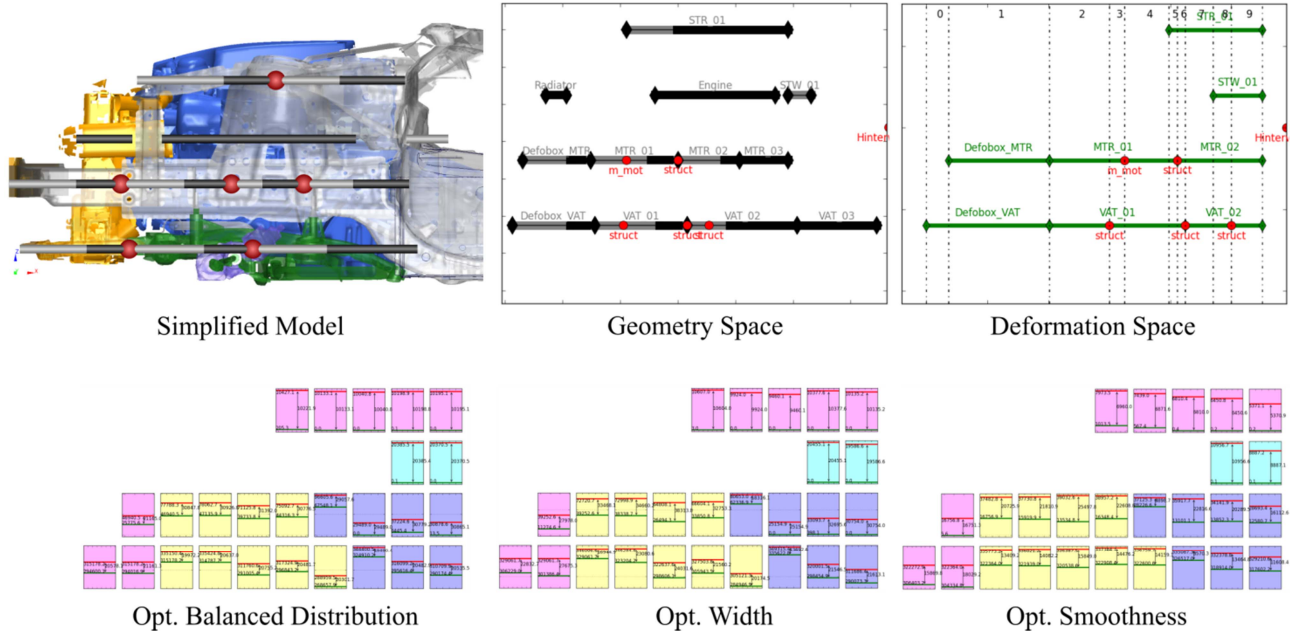


Figure 7. Calculation of the solution space concerning different applications.

A solution of the cluster is shown in Figure 8, which shows that the common components (marked with red and green respectively) integrated in different vehicles are constrained with the identical corridors. For each vehicle, the deformation spaces before and after synchronization are shown on the left in Figure 8.

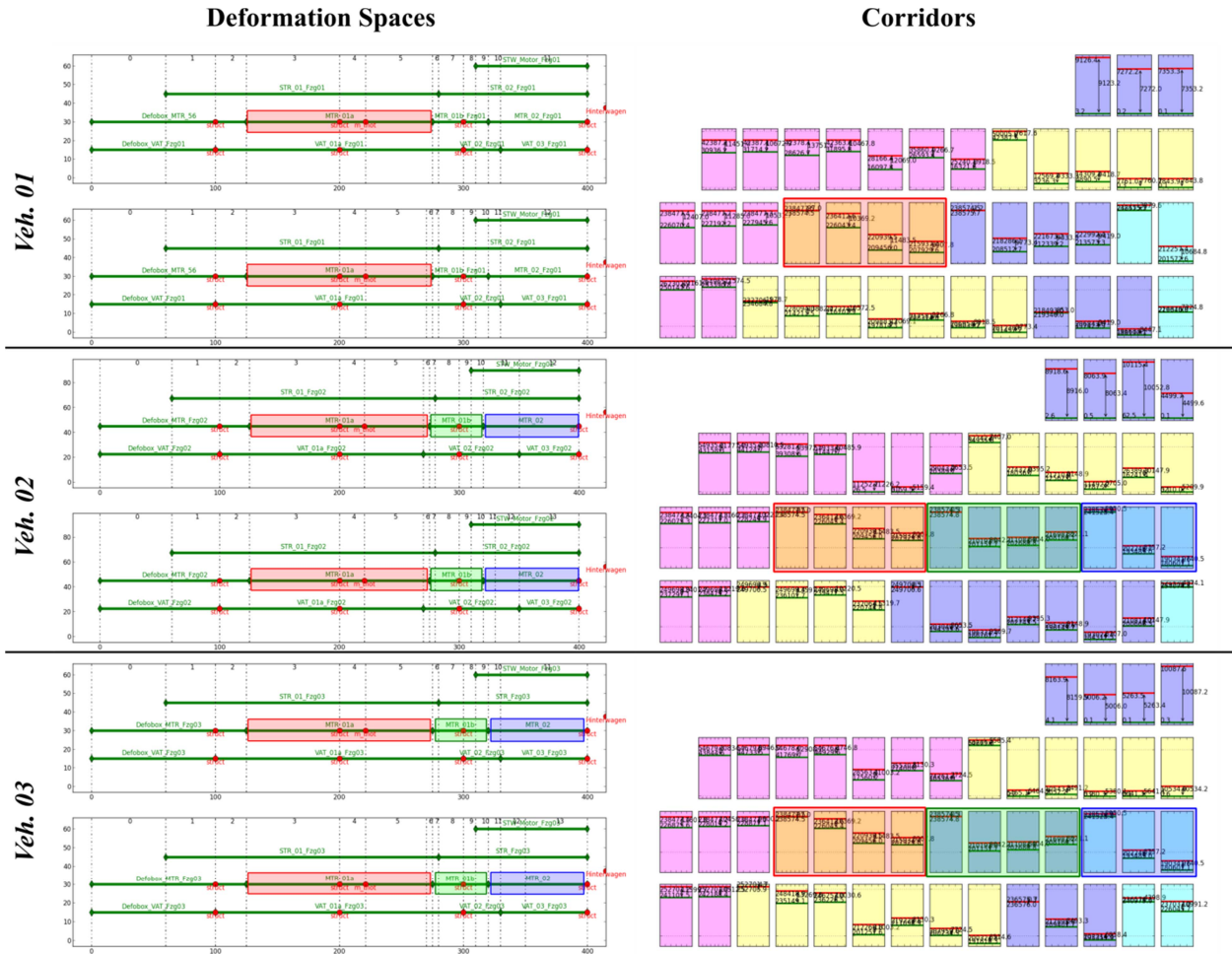


Figure 8. Corridor calculation for vehicle cluster.

### 3.2 Validations of the Component Functional Goals

In order to validate the method, a simplified FE model is constructed. The structure with four thin-wall components is crashed against a rigid barrier. The acceleration of the mass at the back of the structure is constrained. The solution space of the structure is calculated with the method stated above. In the initial design, the force-deformation curve of the last component violates its corridor; the acceleration of the mass exceeds the critical value as shown in Figure 9. In order to fulfill the goal of structural design, the component is modified (e.g. variation in wall thickness, introduction of beads and holes) to yield a force-deformation response which lies inside its corridor. The acceleration goal is subsequently achieved as shown in Figure 9.

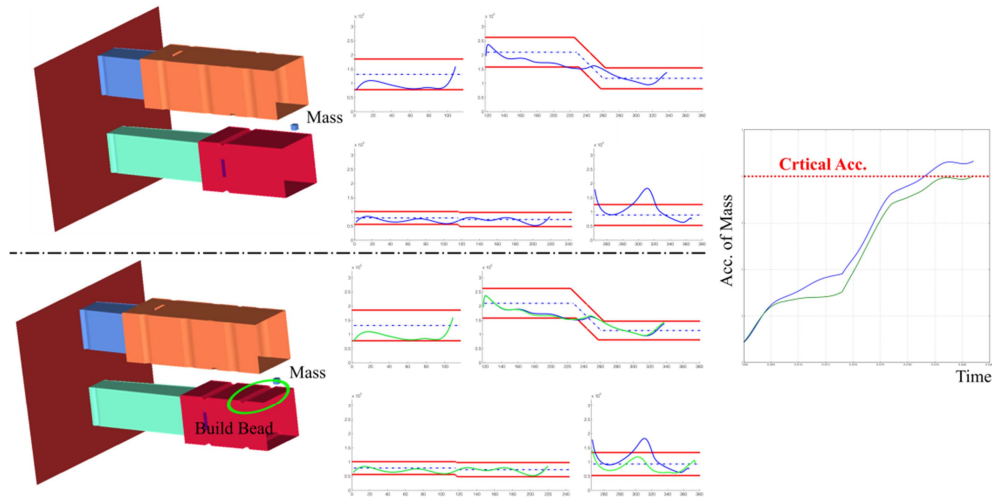


Figure 9. Component design based on corridors.

## CONCLUSIONS

The solution space of the vehicle cluster is described analytically and identified through the numerical optimization. The approach can be used to decouple the design of the components while maintaining the commonality of the vehicle architecture. This solution space provides each component an interval for force-deformation responses. These intervals as the functional goals, compared with a single curve, ensure more flexibility for the component design.

With the solution process established in this work, the features of the solution space can be adjusted by tuning the weighting factors in Eq. (12) in order to minimize the effort of the structural optimization in component design.

As a conclusion, this approach can serve the V-model design process by establishing the functional goals for individual components within vehicle architecture.

## REFERENCES

- Fender, J., Duddeck, F., & Zimmermann, M. (2014, Vol. 49 No. 3). On the Calibration of Simplified Vehicle Crash Models. *Structural and Multidisciplinary Optimization*, pp. 455-469.
- Gonçalves, A., & Ferreira, N. (2005). *Automobile Front-end Structure: Modularity and Product Platform*. Instituto Superior Técnico: tech. rep.
- Graff, L. (2013). *A Stochastic Algorithm for the Identification of Solution Spaces in High-dimensional Design Spaces*. Philosophisch-Naturwissenschaftlichen Fakultät der Universität Basel: Doctoral Dissertation.
- Huang, M. (2002). *Vehicle Crash Mechanics*. CRC Press LLC.
- Kamal, M. M. (1970, Feb.). Analysis and Simulation of Vehicle to Barrier Impact. *SAE Paper No. 700414*.
- Kim, C., Mijar, A., & Arora, J. (2001, vol. 22 no. 4). Development of Simplified Models for Design and Optimization of Automotive Structures for Crashworthiness. *Structural and Multidisciplinary Optimization*, pp. 307-321.
- Lust, R. (1992, vol. 4 no. 2). Structural Optimization with Crashworthiness Constraints. *Structure Optimization*, pp. 85-89.

- Ni, C. M., & Song, J. (1986, vol. 79). Computer-aided Design Analysis Methods for Vehicle Structural Crashworthiness. *Proc. of Symposium on Vehicle Crashworthiness Including Impact Biomechanics*, pp. 125-139.
- Nocedal, J., & Wright, J. (2006). *Numerical Optimization*. Springer.
- Vandenberghe, L. (2010). *The cvxopt Linear and Quadratic Cone Program Solvers*. UCLA Engineering Henry Samueli School of Engineering and Applied Science: tech. rep.
- WhyHighEnd.com. (2010). Retrieved from Automobile Platform and Platform Sharing:  
<http://www.whyhighend.com/automobile-platform.html>
- Zimmermann, M., & von Hoessle, J. E. (2013, vol. 94 no. 3). Computing Solution Spaces for Robust Design. *Numerical Methods in Engineering*, pp. 290-307.

# **SMALL OVERLAP FRONTAL IMPACT – EXPERIENCE AND PROPOSAL FOR A FUTURE APPROACH**

**Bengt Larsson**  
**Joerg Bakker**  
Daimler AG  
Germany

Paper Number 15-0244

## **ABSTRACT**

This paper examines the field relevance regarding frequency and severity of small overlap accidents by comparing accident data from GIDAS, NASS and Mercedes-Benz accident research and from this perspective shows a proposal of a more realistic small overlap test configuration. The result shows a field relevance of approx. 7% in relation to all frontal impact accidents. With respect to an occupant injury severity of MAIS3+ the field relevance is reduced to approx. 3%. Detailed investigations regarding vehicle deformations and occupant loadings on a Mercedes Benz C-Class (MJ 2013 and earlier) show significantly higher severity in the IIHS load case compared to a typically small overlap field accident. Furthermore, a better severity correlation between field accidents and a car-to-car small overlap or the NHTSA small overlap research load case has been observed. In case of the IIHS small overlap test mode some preferential vehicle concepts related to the results has been observed. Investigations show that front wheel drive vehicles with a “east-west” (lateral) engine mount design seem to have some advantage compared to rear wheel drive vehicles with a “north-south” (longitudinal) engine mount design. Accident data analysis confirms that small overlap accidents have field relevance, although the severity of the accidents is lower compared to the IIHS small overlap test mode. In order to obtain a more realistic test configuration the proposal is to use a deformable barrier in order to simulate this kind of accidents.

## **INTRODUCTION**

The IIHS Small Overlap test program is one of the latest challenges for the automotive development. This load case was implemented in order to simulate the severity of small overlap field accidents, and since the introduction there is a discussion if this load case accurately enough reflects real world accidents. In the first step a review of accident data from GIDAS(Germany), NASS (US) and Mercedes-Benz accident research and published studies was conducted in order to give an overview of the relevance of frontal impact collisions where a small overlap without engagement of the front longitudinal members and an injury severity of MAIS3+ occurred. In the second step a case-by-case study of the relevant small overlap accidents with involvement of Mercedes-Benz vehicles was done to compare with the results obtained in IIHS small overlap crashtests. The objects for the comparison were vehicle deformation paths and vehicle collision kinematics. In the third step a closer investigation of the specific IIHS load case was done in order to better understand and classify the test and to answer regarding questions robustness, what kind of field collisions are addressed and if certain vehicle concepts like front wheel drive or rear wheel drive are preferential. In the fourth step a closer look on the repeatability of the IIHS load case was taken: result comparison of two identical vehicle crash tests and simulations test setup variations. Finally in the fifth step different test configurations were investigated that first better reflect real world accidents and second show more robustness and repeatability regarding vehicle kinematics and deformations, because it is important that a test configuration is driven by the most typical types of crashes occurring in the field so that potential design changes will lead to benefits in real-world crashes.

### **1. Field relevance regarding frequency, severity and opponents of small overlap accidents**

#### **1.1 Frequency**

There have been many publications about the relevance of the IIHS small overlap test in real world accident scenarios, for example [1],[2],[3], and [4]. Especially, when the test was introduced in 2012, many numbers were quickly published in the press that assessed the relevance in the range 20 – 25% of all frontal collisions. However, there is a simple relation between overlap degree and the frequency of its occurrence in crashes. This relation is valid for the whole range of overlap degrees in frontal offset collisions and basically reflects the frequency

distribution of overlap degree in a random impact into the car front. Accident data shows this relation, which can be seen in figure 1-1 (left) where the cumulative frequency of frontal collisions up to a certain overlap degree with different injury severity levels (from uninjured MAIS 0+ to MAIS 2+) is shown. We can see a linear increase with the level of overlap, independent of the injury severity. According to this distribution, the relevance of a small offset crash with 25% overlap degree could be determined as 25%. The question is, can we derive a relevance of an offset crash from this relation? It seems like no particular overlap degree has a special relevance and one could argue that the bigger the overlap, the bigger the relevance. However, technical considerations come into play when considering the range of accidents one specific offset crash test should represent. In case of the small overlap crash, the crash structure, i.e. the longitudinal members should not be impacted so that they would have the ability to absorb energy. This is the specific characteristic of this crash, separating it from other possible offset configurations, and should be reflected in a corresponding accident analysis. Obviously, having 25% overlap as the only selection criterion for accident data is not enough, as many of these cases also overlap with the structure of the car, due to a bigger variance of impact situations and vehicles in real world accident data than in the crash test. Also, within the group of small overlaps that do not impact the longitudinal members, there are types of accidents with very different characteristics, such as super small overlaps (sideswipes) or impacts with a small oblique component resulting in deformations mostly more on the side than at the front of the vehicle.

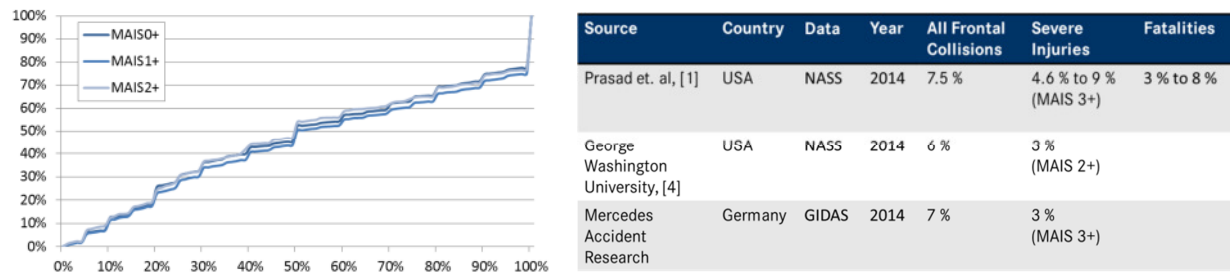


**Figure 1-1. Cumulative frequency of overlap degree in car frontal collisions at different injury levels (left) and different studies with in-depth analysis of small overlap crashes and their relevance (right).**

In order to filter out the cases with a small overlap and no impact on the longitudinal members, a detailed and manually conducted study of single accident cases is a reliable but costly method. Automatic selection is usually not very accurate with current accident databases in this situation as they lack the exact detail of deformation of the longitudinal members. Figure 1-1 (right) shows the results of several different and recent efforts to conduct such a manual analysis and it turns out that they are comparable, even when based on different datasets. With respect to all frontal collisions and independent of the injury severity, the small overlap represents about 7 %. These numbers also show that the overall relevance of small overlap impacts is comparable in the US and Germany.

In an analysis of GIDAS data (German In-Depth Accident Study as of 07.2013) from Germany, 2524 frontal car crashes were classified into different overlap characteristics shown in figure 1-2. Full overlap takes up to 41% of all impacts. Partial overlaps can roughly be divided into three big groups: large (50 – 75% overlap), moderate (30 – 50% overlap), and different types of small overlap (up to 30%). The rest is made up of central impacts and others. The variety of small overlap crashes ranges from super small overlaps, which are basically sideswipes, to impacts more into the side structure of the vehicle. Due to the nature of impacting the corner of the vehicle, there is a greater variety of different types of crashes in the group of small overlaps, than in the other partial overlaps. Some of these differences are shown in the following sections, when injuries and collision opponents are examined for each group.

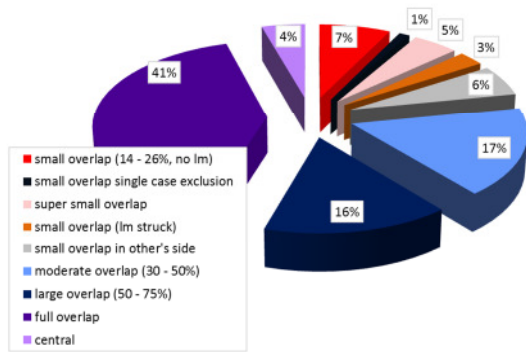


Figure 1-2. Distribution of severe frontal collisions with different overlap characteristics.

## 1.2 Injury severity

In the previous section, the relevance of small overlap has been discussed on the accident level. When it comes to injuries, the type of injuries sustained in small overlap crashes is different than in other frontal crashes which has an influence on the injury severity. Serious injuries (AIS 2+) in small overlap crashes are mostly located in lower and upper extremities (figure 1-3) opposed to head/neck and chest in other frontal crashes with the latter injury types are generally more serious than the former ones. Thus, the overall relevance is different and decreases at different injury levels to about 3% for MAIS 3+ injuries (and fatalities) in small overlap crashes (figure 1-3). This pattern is not only observed in accident data, but also in the crash test dummy loads of small overlap crashes vs. other frontal crashes, that have been conducted so far. Also, other studies on US accident data show similar results [4].

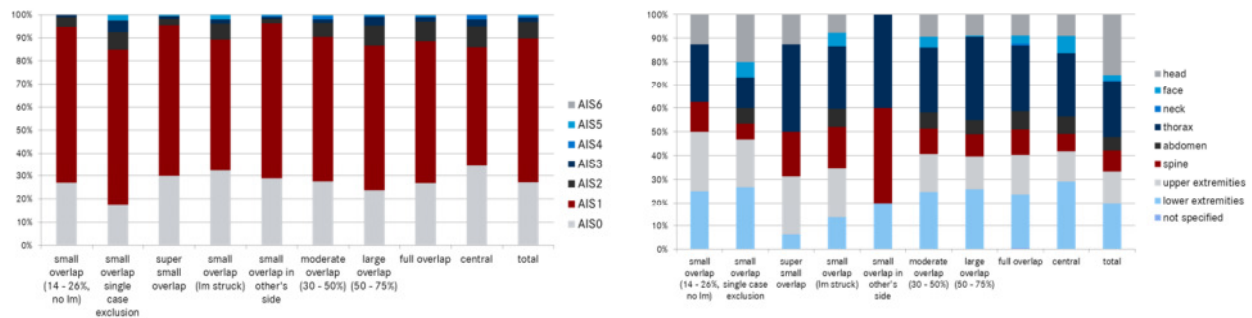
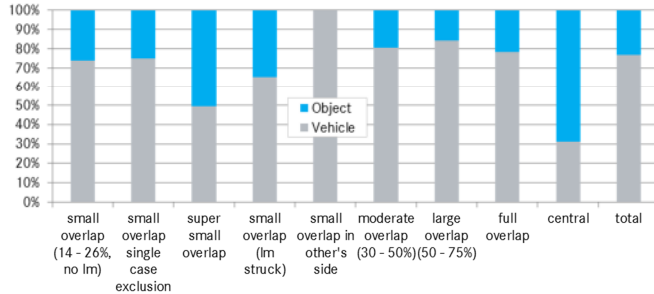


Figure 1-3. Injury severity and body regions of AIS2+ injuries in crashes with different overlap characteristics.

## 1.3 Collision opponent

The most striking difference between real world accidents and the small overlap crash test configuration gets obvious when looking closer to the impact opponent. In general, when looking at all types of frontal collisions, object collisions are not as frequent as vehicle collisions. This holds also true for small overlap crashes and is in the same order of magnitude as in all severe frontal impacts. Vehicle opponents occur four times as often as object collisions (figure 1-4). Looking at the small overlap object collisions only, it is not surprising that nearly all of them are collisions against a tree or pole. Out of the 49 object collisions, 28 hit a tree and another 9 a pole. In sum these are 76% tree/pole collisions of all small overlap object collisions, which is 20% of all small overlap impacts. To

summarize, the collision opponent in a small overlap accident is in most cases (94%) either a vehicle or a tree/pole where vehicles are clearly dominant with 74%. Similar results were found by [1], [2] where in 22 small overlap crashes, 19 were impacts with the front or side of another vehicle (86%) and 3 were impacts with a pole, post, or tree (14%).



**Figure 1-4. Collision opponent in crashes with different overlap characteristics.**

## 2. Small overlap field accidents versus IIHS small overlap crashtest results

To get a picture how IIHS small overlap test results match to known field accidents a comparison of the deformation patterns and kinematics between tested vehicles and real world collisions was investigated. In this case field accidents analyzed from the Mercedes-Benz accident research were compared to the same Mercedes-Benz carline tested in the IIHS crash test setup. As a representative example for this research a Mercedes-Benz C-Class (MJ 2013 and earlier) involved in a vehicle-to-vehicle accident to a mid-size car with an overlap of 23% for the C-Class is shown below (fig. 2-1 above). The C-Class had a calculated Energy Equivalent Speed (EES) of approx. 60 km/h at collision, which is comparable to the EES severeness of the IIHS small overlap test (58- 60 km/h). The occupant in the C-Class suffered no injuries.

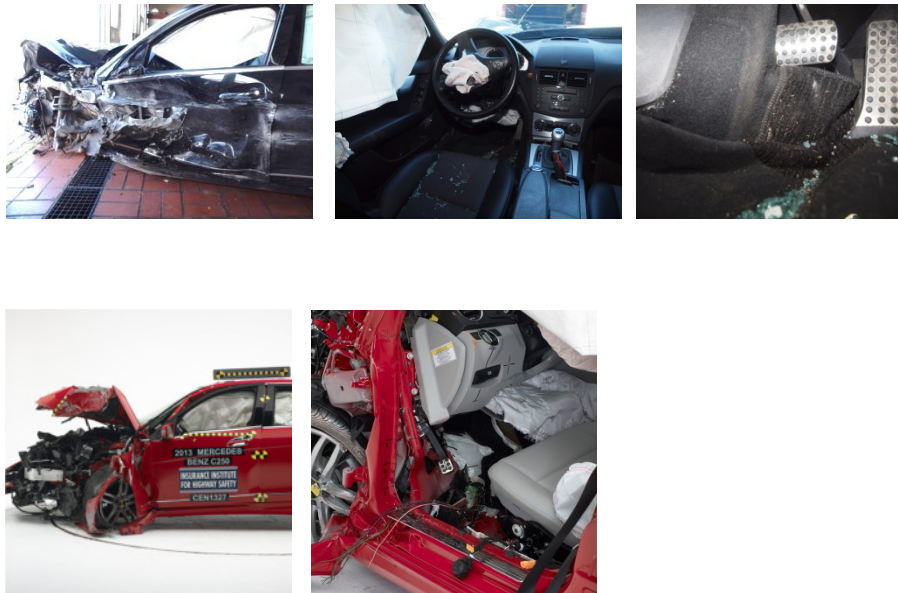


**Figure 2-1. Small overlap field accident, C-Class (MJ 2013 and earlier) vs. IIHS small overlap test result C-Class (MJ 2013 and earlier) [IIHS data]**

The occupants head, neck and chest was well protected by the seatbelt, driver airbag and side- and curtain airbag. Further the intrusion in the foot area was on a low and therefore acceptable level: no structural rupture and no trapping of the lower extremities. The C- Class (MJ 2013) was official tested in the IIHS small overlap and some test results, especially regarding the intrusion at the lower occupant compartment, were unfavorable (fig. 2-1 below).

Although the collision severeness between the field accident and the IIHS test is comparable, significant differences particularly at the lower compartment intrusions are observed. The explanation for these discrepancies is assumed to be the different collision partners: the rigid barrier in the IIHS test setup induces higher and compared to field accidents not representative intrusions.

### 3. IIHS small overlap crashtest - working range and limits

To better understand the IIHS small overlap crash configuration the published data from IIHS crash test during the development of the load case was investigated. Additional car-to-car tests with same and different vehicle test partners were conducted in order to examine the vehicle kinematics and how these fits to the IIHS test configuration. Furthermore vehicle tests in the IIHS setup with different vehicle design concepts, longitudinal (“north-south”) and lateral (“east-west”) engine mount were reflected, to find out possible differences in output and behavior.

For development of the IIHS small overlap crash configuration a Volvo S60 was often used as a test vehicle. The data from these tests is available on the home page of IIHS and tests were conducted both against barriers (rigid and deformable) and vehicle-to-vehicle configuration. At first car-to-car tests were studied in order to investigate the vehicle kinematics. As an example two car-to-car configurations are shown below (figure 3-1 above):

- Volvo S60 vs. Volvo S60 with 28% overlap,  $v = 64$  km/h [data from IIHS home-page]
- Volvo S60 vs. Volvo S60 with 22% overlap,  $v = 64$  km/h [data from IIHS home-page]

In both cases both vehicles more (28% overlap) or less (22% overlap) stuck to each other and rotated around the vertical axis. A fully glancing off behavior, which has been observed in the IIHS small overlap crash setup of the Volvo S60 (figure 3-1 below), did not occur

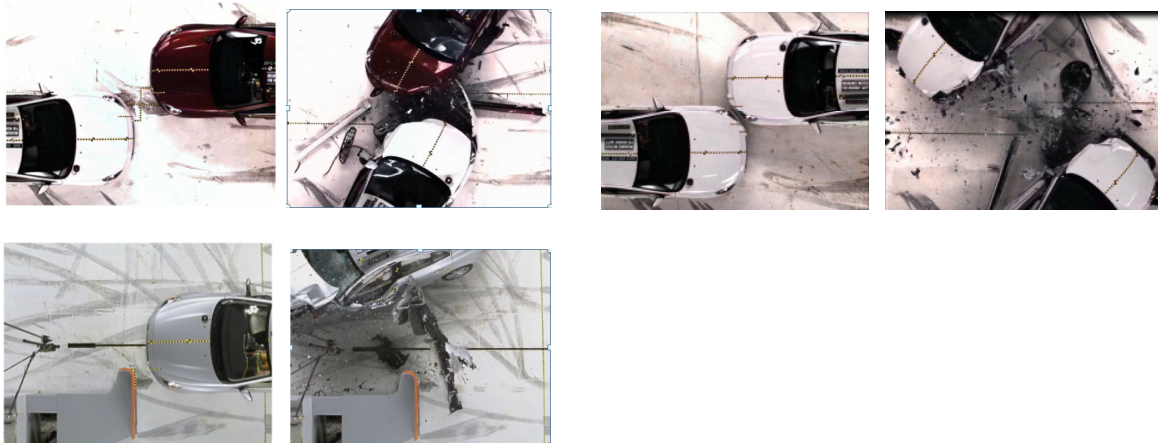


*Figure 3-1. Volvo S60 vs. Volvo S60, 28% overlap (above left), Volvo S60 vs. Volvo S60, 28% overlap (above right) and Volvo S60 tested in the IIHS small overlap test configuration (below) [IIHS data]*

The first conclusion is that the IIHS test setup more simulates a collision against a rigid object like a pole, post or tree prior to a deformable vehicle-to-vehicle collision. The second conclusion concerns the question of the repeatability (see also step 4 below): a minor variation of the overlap 25% +/-3%, seen in the vehicle-to-vehicle tests, causes a major change of the vehicle kinematics regarding the degree of glancing off.

During the development of the load case the IIHS tested different barrier types. The examples in figure 3-1 and figure 3-2 are showing the rigid barrier with two different radius of the barrier edge: 50 mm vs 150 mm. The test with the Volvo S60 shows a different kinematics between these two barriers: a glancing off with the 150 mm radius and a stuck behavior against the 50 mm radius barrier. Thus, a smaller change of the barrier geometry leads to major change of the vehicle kinematics. In fact, the kinematic result at the barrier with the smaller radius is fitting better to the vehicle-to-vehicle tests.



**Figure 3-2. Volvo S60 tested in the IIHS small overlap test configuration overlap 20% with a 50 mm radius edge (left) and delta-V characteristic of the Volvo S60 tested in the IIHS small overlap test configuration 25% overlap with a 150 mm barrier radius edge vs. 20% overlap with a 50 mm barrier radius edge (right) [IIHS data]**

A glancing off kinematic also leads to less reduction of the kinetic energy at the barrier, what firstly means that the vehicle moves uncontrolled forward with a residual amount of velocity, and secondly to less vehicle structural stress (figure 3-2 right: e.g. Volvo S60 approx. 20 km/h residual velocity after impact). Certainly a glancing off behavior obtains a higher amount of lateral velocity than a sticking behavior that could lead to higher injury risk for the occupants at head and chest, but on the other hand the intrusions and structural stress at the upper compartment area normally are lower compared to a sticking behavior.

The cars that up to now have been rated in IIHS small overlap impact have a vehicle architecture either with a longitudinal engine mount (normally rear wheel drive) or a lateral engine mount (normally front wheel drive).

Two characteristics are observed

- None of the vehicle concepts with a longitudinal engine mount (“north-south”) have a glancing off tendency at impact.
- For vehicle concepts with a lateral engine mount (“east-west”) every degree of glancing off seems to be possible, but a major part (81%) of the investigated vehicles have a clear glancing off tendency at impact

To get one explanation for the reason of these differences the two concepts below are compared with regard to the barrier impact.

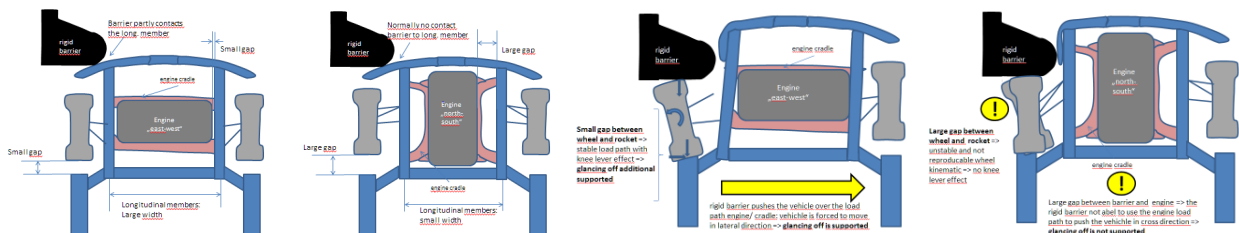


**Figure 3-3. Vehicle concept engine mount “east-west” (left) and “north-south” (right) Schematic results: vehicle concept engine mount “east-west” (left) and “north-south” (right)**

Viewed in figure 3-3 are two structures with the same vehicle width. The main differences between the two concepts that have an important impact on the degree of glancing off at the rigid barrier are:

- The width of the longitudinal members: a large width can allow a partly barrier impact to the longitudinal member
- The gap between the longitudinal member and engine: a small gap allows a lateral engine load path, that pushes the vehicle in lateral direction away from the rigid barrier during the impact
- The gap between wheel and rocket (side member): at the barrier wheel impact a small gap allows a stable and reproducible contact to the rocket and during the impact phase the wheel works like a knee lever to support a vehicle glancing off kinematic. A large gap results in an instable and non-reproducible wheel contact to the rocket.

Conclusion:

For this reasons vehicles with a lateral engine mount concept have benefits in the IIHS small overlap crash mode: the geometry of the rigid barrier allows a pushing effect away from the barrier and increase the degree of glancing off possibility.

In the same way vehicles with a longitudinal engine mount do not benefit from the glancing off effect: almost the whole input kinetic energy has to be managed by the vehicle structure.

#### 4. IIHS small overlap – repeatability

During the development of countermeasures and vehicle improvements it was observed that the results of identical vehicle tests didn't give a reasonable repeatability: abnormal large result deviation compared to deviations occurring in for example moderate frontal offset crash configurations. To investigate this, simulations of a large luxury vehicle with a) slightly different overlaps (30%, 20%) and b) different positions of the wheel rim at impact to the barrier were done. Another factor that in a major way influences the test result deviations is the wheel rim styling. In two IIHS small overlap configuration tests of a Mercedes-Benz vehicle with identical body structures and configurations except for the 5 spoke wheel rim styling (fig 4-1) indicate this. In these two cases the rim impact to the barrier for the both vehicles was similar: impact between two rim spokes. However, during the ongoing crash phase the deformation and kinematic of the wheels differs successively, which at the end leads to a complete different structural result especially with respect to the toepan intrusion. These results were also confirmed in numerical simulations with different rim designs and stylings.

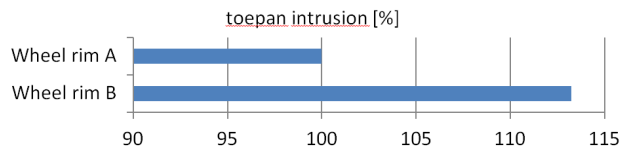


**Figure 4-1. Vehicle with wheel rim A (left) and rim B (right, [IIHS data]): rim impact at the rigid barrier, wheel kinematic during crash and structure response at the rocket (vehicle side member, front view)**

Numerical simulations of an identical wheel rim but with different rim positions at the rigid barrier impact shows large differences of the rim deformations and wheel kinematic, which causes a variation of body structure intrusions (fig 4-2 above). Depending on the rim deformation and rim impact to the body structure the vehicle intrusions differs up to 30 - 40%. In this case especially a wheel rim styling with fewer spokes seems to be more critical (rim strength distribution more inhomogeneous). Further, other parts like the size and thickness of the brake disc and its rupture behavior and the position of the brake caliper have an additional impact on variation of the wheel kinematic and crash results.

Next, a simulation reflects the influence of a smaller variation of the degree of overlap in the IIHS small overlap setup. The overlap was varied between 20% and 30% and compared to the basis setup 25% in all cases the longitudinal member was not struck (fig. 4-2 below). A slightly smaller overlap (20%) shows results with intrusion deviations up to >20% and a slightly higher overlap (30%) induce intrusion deviations even up to >30%. Thus, a smaller change of the vehicle overlap against the IIHS rigid barrier would significant change the vehicle intrusion values.

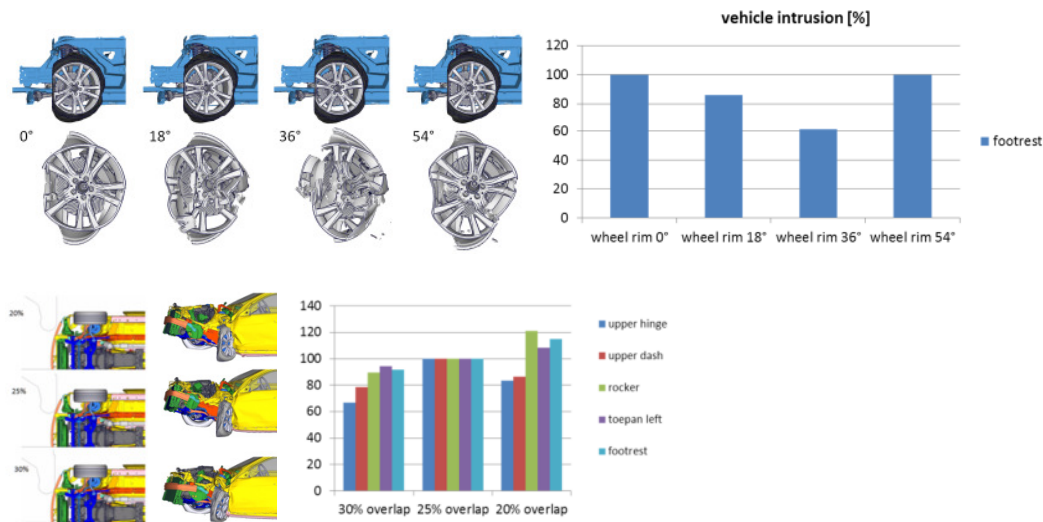


Figure 4-2. above: Wheel rim deformations at different wheel positions at impact to the rigid barrier (0° = 54°)  
below: overlap variation at impact and influence on the vehicle intrusions (large luxury vehicle)

#### Conclusions:

In the shown examples minor variations to the vehicle setup or test setup causes significant deviations to the test result output. Claiming the same high safety requirement for all vehicle configurations and options, for example wheel rim styling, this lack of repeatability and high deviations makes it hardly feasible to reach that claiming goal. On the other hand this means that the IIHS small overlap configuration with the chosen rigid barrier geometry and shape could lead to a point optimization of a certain vehicle setup.

### 5. Investigations of further small overlap crash test configurations

At the introduction of the IIHS small overlap one main intention was to address severe injuries (MAIS3+) at head and chest areas [Zuby paper 09-0257]. However, almost every tested vehicle since the introduction in 2012 has shown only minor occupants loadings of the 50% HIII in these areas. The major occupant loadings are located to the dummy extremities (femur, tibia and foot) often due to high vehicle body intrusion values in the foot / floor area. For this reason Mercedes-Benz has made further considerations and investigations towards a small overlap load case that could better cover both field accidents severity and also be a robust test

configuration with an acceptable repeatability for the vehicle development. The starting point for finding such a load case the objects were:

- no involvement of primary crash structure like longitudinal frame members
- test velocity that covers 90% of the relevant field accidents
- barrier configuration that covers the most common field accidents impact objects
- get a stable and reproducible behavior of the suspension and wheel kinematics with a insignificant impact of for example wheel rim stylings and wheel rim position at barrier contact
- better balancing of the occupant loadings: vehicle kinematic that for both glancing off and/or sticking behaviour stronger addresses the head/ neck / chest loadings prior to leg and lower extremities loadings

Relevant conclusions and evaluations that have been shown in the previous steps and could be considered for an optimization of a small overlap test configurations are:

- in the examined field accidents a 40 km/h Delta-V covers more than 90% of the real cases, or in other words
- an Energy Equivalent Speed (EES) of 46 km/h covers 90 % of the reviewed relevant accidents
  - ⇒ This gives a representative velocity of 56- 58 km/h against a rigid barrier or 64km/h against a deformable (ODB) barrier.  
(In comparison: EES for IIHS Small Overlap is approximately 55-60 km/h. In GIDAS, this value represents a cumulative frequency of approx. 98%)
- As shown in the first step above the most small overlap accidents two vehicles are involved. In GIDAS this represent approx. 75% of the cases. Only 25% are vehicle-to-object accidents. This means, that the most common real collision objects are prevalent deformable and not rigid.
- a rigid barrier causes issues regarding repeatability especially with respect to wheel kinematics for longitudinal engine mount vehicle concepts.
- the geometry of the rigid IIHS barrier seems to benefit lateral engine mount vehicle concepts where a glancing off effect reduces the needed energy absorbing capacity for the vehicle.

In order to match the requirements to the above conclusions Mercedes-Benz started a simulation and test evaluation program to find an adequate small overlap test configuration. The main result of that work was the recommendation to use a deformable element in front of a rigid barrier. In the investigation the common ODB deformable barrier (Euro-NCAP / IIHS) and the discussed NHTSA oblique/ small overlap deformable barrier were used. The tested configuration with the deformable ODB barrier is as follow

- ODB barrier in front of a rigid block
- Rigid block w/o edge rounding
- 25% overlap, 0° obliqueness
- Vehicle velocity  $v= 64$  km/h
- Vehicle weight and equipment in accordance to the IIHS test protocol

The first observation of the test result is that the use of the deformable barrier makes the reproducibility of the wheel kinematics much higher: due to the deformation of the barrier the wheel displacement is more defined guided towards the side member (rocket). Also the influence of different wheel rim designs and/or wheel rim positions at impact to the barrier is much lower and makes the evaluation of developed vehicle changes much more accurately and predictably (fig 5-1 above).

With this test vehicle (longitudinal engine mount) a sticking kinematic behavior at the barrier impact occurs. The wheel kinematic with a stable contact to the side member leads to a robustly load path on the axis barrier-wheel- side member. This load path increases the rotating velocity of the vehicle and induces a stronger occupant lateral movement towards the vehicle side structure (fig 5-1 mid, below).

The higher lateral excursion of the occupant in the test mode with the deformable barrier increases the injury risks for head and neck. On the other hand the floor intrusions and injury risks for the lower extremities are reduced. In the overall evaluation and comparison of the two test setups the use of the deformable barrier results in a more balanced injury risk distribution: higher injury risks for head/neck/chest and lower injury risks for feet and legs, which also shows a good alignment to the results from the real life accident analysis.



**Figure 5-1. above and mid: IIHS small overlap test mode (left), small overlap w. deformable barrier (right)  
below: Occupant at maximum excursion; IIHS small overlap test mode (left), small overlap w. deformable barrier (mid), vehicle lateral velocity (right), C-Class (MJ 2013 and earlier)**

To review the results above an additional study was done with the discussed crash mode NHTSA small overlap:

- Movable deformable barrier, mass 2500 kg, barrier velocity 90 km/h, vehicle velocity 0 km/h
- 20% overlap, 7° obliqueness

The result is similar to the outcome of the deformable ODB test: the deformable barrier guides the wheel to stable contact with the side member and a high lateral vehicle movement. The intrusions at upper and lower area are good balanced: compared to the IIHS small overlap configuration the upper area is more and the lower area less loaded. Thus, this configuration reflects the original target requirements in a good way (fig 5-2 above and mid).

The occupant kinematic in NHTSA small overlap setup also differs compared to the IIHS small overlap: the upper torso rotates more around the vertical axis, which could increase the injury risk to head/ neck and chest if the coverage of the driver- and curtain airbag is insufficient (fig 5-2 below)



**Figure 5-2.** above: NHTSA small overlap - wheel kinematic (left) and A-pillar deformation (right)  
 mid: NHTSA small overlap vs. IIHS small overlap - intrusions and lateral vehicle velocity  
 below: Dummy kinematic / torso rotation: IIHS small overlap (left) and NHTSA small overlap (right),  
 C-Class (MJ 2013 and earlier), HIII- dummy.

The two examples small overlap with the ODB barrier and the NHTSA small overlap configuration shows that it is reasonable to use a deformable barrier in front of a rigid or movable block. This configuration is able to address the most of previously formulated objects and would make the development more precise and robust. In the investigated setups with the deformable barrier reflects a sticking vehicle kinematic at the barrier impact. In order to also address lateral engine mount vehicle concepts, which have a higher tendency to glancing off, it could be discussed to combine a deformable barrier in front of a rigid block with rounded edge (similar to the IIHS rigid barrier). Such a combination could have the potential to fulfill the previously formulated objects even better.

## CONCLUSIONS

Field accident data shows that severe small overlap frontal impacts occurs but have comparatively a low relevance. Most of the cases are vehicle-to-vehicle impacts, so this should be the focus for a realistic near-to-real-world crash test setup. The experience and investigations of the IIHS small overlap test configuration shows that the load case only partly covers the real world accidents, emphasizing injury risks occurring at the lower extremities of the occupants. The chosen rigid barrier with a large rounded edge also gives a benefit for lateral engine mount vehicle concepts, where the barrier can be used to push the vehicle laterally away from the barrier. Further the rigid barrier has an influence on occurring test result deviation, inter alia, depending on wheel rim positions. To get a more general small overlap crash test configuration, which can cover a larger part of the field accidents and shows more robustness in vehicle development process, the use of a deformable barrier layer in front of the rigid block should be considered.

## REFERENCES

- [1] P. Prasad, D. Dalmotas and A. German, “An Examination of Crash and NASS Data to Evaluate the Field Relevance of IIHS Small Offset Tests.”, 2014 SAE International
- [2] M. L. Brumbelow and D. S. Zuby, “Impact and Injury Patterns in Frontal Crashes of Vehicles with Good Ratings for Frontal Crash Protection.”, 21st International Technical Conference on the Enhanced Safety of Vehicles, Stuttgart, Germany – June 2009
- [3] B. C. Mueller, A. S. Brethwaite, D. S. Zuby and J. M. Nolan “Structural Design Strategies for Improved Small Overlap Crashworthiness Performance.”, Stapp Car Crash Journal, Vol. 58 (November 2014)
- [4] P. Scullion, R. M. Morgan, P. Mohan, C.-D. Kan, K. Shanks, W. Jin, and R. Tangirala “A Reexamination of the Small Overlap Frontal Crash.”, 2010

## **What is the Benefit of the Frontal Mobile Barrier Test Procedure?**

**Thorsten Adolph**

**Julian Ott**

Federal Highway Research Institute (BASt)  
Germany

**Burkhard Eickhoff**

Autoliv B.V. & Co. KG Country  
Germany

**Heiko Johannsen**

Medical School Hannover  
Germany

Paper Number 15-0254

### **ABSTRACT**

Frontal impact is still the most relevant impact direction in terms of injury causation amongst car occupants. Especially for car-to-car frontal impacts the mass ratio between the involved vehicles has a significant impact on the injury risk (the heavier the opponent car the higher the injury risk). In order to address this issue frontal Mobile Deformable Barrier test procedures have been developed world-wide (for example the MPDB procedure that was fully described during the FIMCAR Project). The objective of this study was to investigate how vehicles of different weight classes perform in a mobile barrier test procedure compared to a fixed barrier test procedure (the full width rigid and offset deformable barrier test). Beyond that, the influence of vehicle mass and vehicle deformation on injuries was evaluated based on real world accident data.

Five vehicle types were selected and tested in a fixed offset test procedure (ODB), a full width rigid barrier test procedure (FWRB) and a mobile offset test procedure (MPDB). For the accident analyses data from the German In-Depth Accident Study (GIDAS) was evaluated with a focus on MAIS 2+ injured belted front row car (UN-R 94 compliant cars) occupants in frontal impact accidents.

Test data indicates higher dummy loadings, in particular for the head acceleration and chest acceleration, in the MPDB test for the vehicles with a mass lighter than the trolley (1,500 kg) compared to the FWRB test. The trend of increased vehicle stiffness (especially illustrated by tests with the MPDB and small cars) shows the need of a further improvement of passive restraint systems to reduce the occupant loading and with it the injury risk.

The analyzed GIDAS data confirm the higher injury risk for occupants in cars with an accident weight of less than 1,500 kg compared to those with a crash weight above 1,500 kg in car-to-car and car-to-object or car-to-HGV, respectively. Furthermore the injury risk increases with decreasing mass ratio (i.e., the opponent car is heavier) in car-to-car accidents. Independent from the higher injury risk, the risk for passenger compartment intrusion in frontal impact appears not to be independent on the crash weight of the car.

### **INTRODUCTION**

Frontal impact is still the most relevant impact direction in terms of injury causation [1]. While the stability of passenger compartments has been improved in Europe substantially in recent years, the performance of the restraint system becomes now even more important [2]. In the traditional restraint system test, the vehicle is crashed between 40 and 56 km/h against the rigid wall independent of the vehicle mass. This is a test procedure used in many countries all over the world. In real-world car-to-car impacts a light vehicle is more likely to be hit by a heavier vehicle and due to the principle of conservation of momentum, the lighter of the two vehicles has to withstand higher loading than the heavier vehicle. Higher loading not only affects cabin integrity, but also cabin acceleration as the lighter of the opponents suffer from a greater change of velocity ( $\Delta v$ ) due to the conservation of momentum. A test with a frontal mobile barrier would reflect these circumstances and was discussed several times in the past [3], [4] and [5]. For the present investigation the frontal mobile test procedure as defined by the FIMCAR

Project [5] was used, because the mass of the trolley and the stiffness of the barrier represents a European midsize car [6–8].

Current accident studies show that many injuries are caused by high vehicle acceleration in frontal impacts compared to injuries caused by intrusions into the passenger compartment [2]. It was also stated that the accidents with acceleration loading induced injuries had a high overlap. On the other hand crash tests with a low overlap at the corner of the vehicle are discussed in other consumer information programmes or regulatory bodies [3, 9–11]. However in Europe, crash tests with a high overlap seem to have a higher priority [12].

With the analyses of real world accident data the following questions should be answered. Have occupants in smaller vehicles (less than 1,500 kg) a higher injury probability in frontal impacts compared to occupants in vehicles heavier than the crash trolley? And if so, is this due to the passenger compartment stability (intrusions) or due to higher occupant loads as a result of the crash pulse and the restraint system?

The different loading in terms of vehicle deformation, vehicle acceleration and injury assessment values for vehicles with a mass lighter and heavier than the mobile barrier should be investigated with the help of crash test data. It is assumed that lighter vehicles have a higher loading with a frontal mobile offset barrier compared to a fixed barrier test (FW / ODB) and that heavier vehicles have a lower loading.

## **METHODS**

### **Methods Accident Data**

For the accident analyses, data from the German in-depth accident study (GIDAS) was evaluated with a focus on MAIS 2+ injured belted front row car occupants<sup>1</sup> in frontal impact accidents. To ensure that only UN-R 94 [13] compliant vehicles were included, only vehicles with a date of first registration in 2003 or later were considered. Furthermore only completely coded and reconstructed accidents up to 2013 were included in the study to guarantee that not only EES but also delta-v was available. The GIDAS sampling method is explicitly explained in [14]. The final data set consisted of 98 cases including 112 front seat occupants with MAIS 2+ injuries.

The accident severity was evaluated using the reconstructed delta-v and EES values. The deformation of the vehicle was classified using the overlap and the CDC classification. The overlap is in percentage and it is important to note that the overlap is coded independently from the involvement of the vehicle corners (e.g., a center pole impact with a pole having a diameter of 20% of the vehicle width is coded as 20% overlap). That distinction was necessary to separate between accidents with a small overlap at the edge of the vehicle and pole impacts. For the analysis it was estimated which kind of frontal impact test procedure would cover best the accident scenario. Here the four possibilities pole, small overlap, half overlap and full frontal were considered. The accident scenarios were identified by separating between offset crash (30 % to 50 %) and large overlap crash (80% to 100%), see also Figure 2. All cases were manually checked in regard to the deformation classification with the help of the accidents pictures.

The collision opponents were classified, on the one hand, as vehicles and, on the other hand, as fixed structures (e.g. road side barriers, walls), poles (trees, traffic lights, street lamps) and others.

The injury severity was coded for the whole person by the official police classification (not injured, slightly injured, severe injured (hospitalization for more than 24 hours) and fatally injured (fatality as a direct result of the accident within 30 days after the accident)). All injuries were separately analyzed using the AIS 2005 classification. The vehicle mass was described with the estimated crash weight of the specific vehicle at the time of the first impact.

### **Methods Crash Test Data**

Crash test data from different vehicle models were obtained in the test configurations: offset test according to the Euro NCAP test protocol (ODB), Full Width Rigid Barrier test (100% overlap, FWRB), and against a Mobile barrier with the Progressive Deformable Barrier attached (MPDB). To evaluate the injury risks Hybrid III

---

<sup>1</sup> MAIS = Maximum Abbreviated Injury Scale, injury severity classification according to AIS 2005

50% dummies on the driver seat were used. Table 1 is showing the vehicles used, including the acronyms, the test masses and the data source the test is obtained from.

**Table 1 Test vehicles, acronyms and data base used for the analyses**

Vehicle acronym	DS	VU	SI	VT	VX
Test mass	1164 kg	1050 kg	1181 kg	1900 kg	2400 kg
ODB	Euro NCAP	Euro NCAP	Euro NCAP	Euro NCAP	Euro NCAP
FWRB	BASt	BASt	BASt	n.a.	n.a.
MPDB	BASt	BASt	BASt	FIMCAR	FIMCAR
Description	Compact car, four doors, cheap	Super mini, two doors, new vehicle design	Compact car, two doors, popular	Midsize SUV	SUV

The ODB test was conducted with a test speed of 64 km/h and an overlap of 40% using a deformable barrier face as defined in [13]. The FWRB had a test speed of 50 km/h, with 100% overlap and without a deformable barrier face [15]. The MPDB test procedure is explained in detail in [7] including the specifications for the test trolley. The closing speed was 100 km/h and the mass of the trolley was 1,500 kg. These values were not changed for the different vehicles. The progressive deformable barrier used for the MPDB is bigger and significantly stiffer compared to the ODB barrier. This makes barrier bottoming out much more unlikely. The barrier is specified in [16].



**Figure 1 Crash trolley used of the test with mobile barrier specified in [7] using the PDB v8.0 XT**

To analyze the loading on the vehicle the maximum acceleration measured at the b-pillar driver side was measured. Additionally the OLC (Occupant Loading Criterion, [17]) was calculated based on that acceleration signal. OLC predicts the relative motion of the dummy and vehicle and calculates the average acceleration experienced by the dummy when its relative position is in the interval between 65 mm and 235 mm. The structure of the vehicle was evaluated based on the a-pillar displacement (at waist line) measured after the test.

The restraint performance was evaluated using the following indices: belt forces measured at the upper shoulder belt between shoulder and the upper anchorage point (B3) and - if available - measured at the lap belt between the hip and the lower anchorage point (B6). Furthermore the airbag deployment time<sup>2</sup>, the airbag contact time<sup>3</sup> and the seatbelt pretensioner time<sup>4</sup> was analysed. The time points were determined based on the high speed videos.

<sup>2</sup> Airbag deployment time = Timing correlating with first frame in the high speed film when the Airbag cover breaks

<sup>3</sup> Airbag contact time = Timing correlating with first frame in the high speed film when the dummy head contacts the airbag

<sup>4</sup> Seatbelt pretensioner time = Timing correlating with first frame in the high speed film when the seatbelt moves

For the analyses of the loading on the occupant the injury criteria from the HIII dummy were used. The focus was on the criteria which are sensitive to assess the loading from the vehicle acceleration: head acceleration (3ms value, HIC within 36ms), chest compression, chest acceleration (3ms value) and pelvis acceleration (peak). The injury criteria were scaled to the ratio of 100% injury assessment reference values (IARVs) to provide a better overview and to enable a better comparison according to UN-R 94 where possible [13, 18–20] [18]. For the chest and pelvis acceleration 60g as 100% were defined, see also Table 2.

**Table 2 Injury assessment reference values used for the analyses of the occupant loading**

Injury Criteria	Pelvis acceleration	Thorax Acceleration	Thorax deflection	Head acceleration	Head injury criterion
Acronym	Pelvis Acc	Thorax Acc	Thorax Defl	Head a3ms	HIC 36
IARV	60g	60g	42mm	80g	1000
Notes	peak value	3ms value	max. value	3ms value	within 36ms

## RESULTS AND DISCUSSIONS

### Accident Data

The following picture (Figure 2) shows the distribution of the overlap crash scenarios for the 98 cases. Almost half of the accidents had a very large or a full overlap. The other three crash scenarios (offset, small overlap edge, small overlap in the middle) were almost equally distributed with values between 15% and 20%.

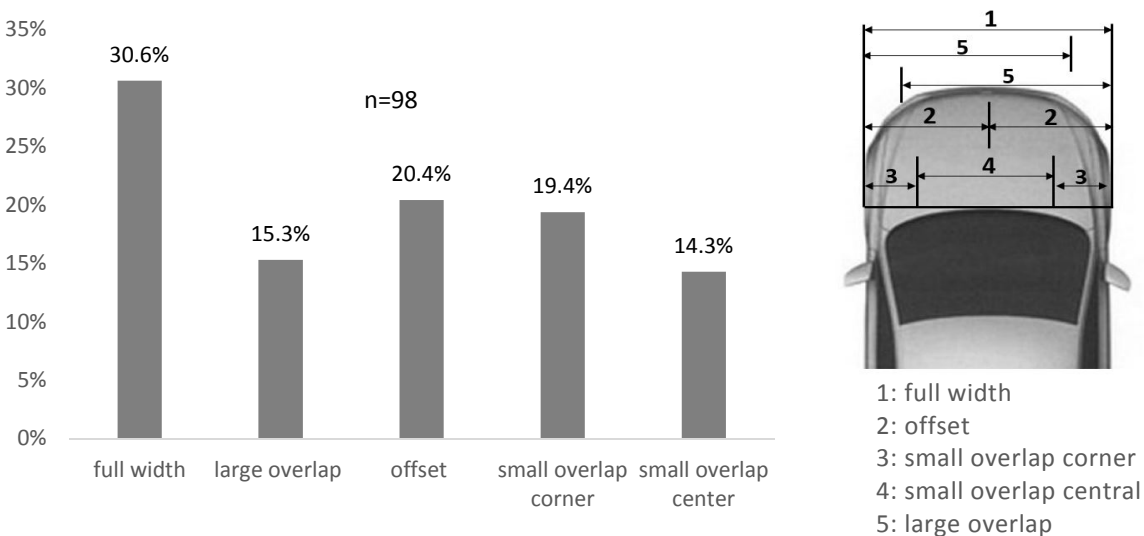


**Figure 2 Overlap crash scenarios for MAIS 2+**

Of the 98 cases, 52 accidents involved another vehicle and in the other cases the opponent was an object. Figure 3 shows the mass distribution (left) and mass ratio (right) of the vehicle opponents. The mass ratio was calculated by dividing the crash weight of the case vehicle by the crash weight of the opponent vehicle. Thus a mass ratio smaller than one indicates cases with the opponent being heavier than the case vehicle and vice versa. The mass was categorized in 300 kg steps starting with 800 kg. The mean value of the vehicle opponent mass was at 1,472 kg which is very close to the mass of the crash test trolley used (1,500 kg). With regard to the mass ratio it can be seen (Figure 3, right) that in the groups with a mass ratio around 1 (0.8 to 0.99 and 1.0 to 1.19) the injury risk was similar. However, there was a higher injury probability in vehicles with a mass ratio be-

tween 0.6 and 0.79 (the vehicle opponent was heavier) compared to the group with a mass ratio 1.2 to 1.39. It is believed that the numbers for the groups with a mass ratio beyond are too small.

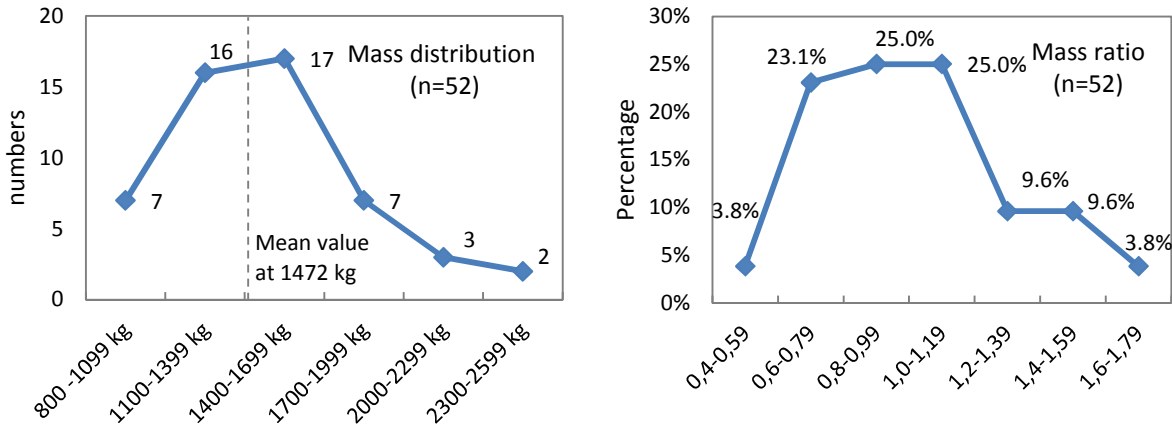


**Figure 3** Distribution (left) and ratio (right) of the mass for the vehicle opponents (n=52); vehicle opponent is heavier (ratio < 1), vehicle opponent is lighter (ratio > 1)

The influence of intrusion to the passenger compartment with regard to the mass ratio was evaluated and is illustrated in Figure 4. Intrusion is defined as stability loss in the a-pillar or the firewall. In general passenger compartment intrusion is observed in a small number of cases of car-to-car accidents only – when intrusion was observed it was mainly in accidents against objects and Heavy Goods Vehicles (HGV). Looking at the car-to-car impacts there were 4 cases in crashes with a mass ratio > 1 (the opponent vehicle was lighter) and 2 cases in crashes with a mass ratio < 1 (the opponent vehicle was heavier).

When looking at the 13 cases with a large weight difference between the accident vehicles (mass ratio between 0.6 and 0.79) in only one accident vehicle intrusion was observed. This indicates that intrusion seems not to be the major injury factor when a heavier vehicle crashes against a lighter vehicle as already postulated by Thompson et al. [2].

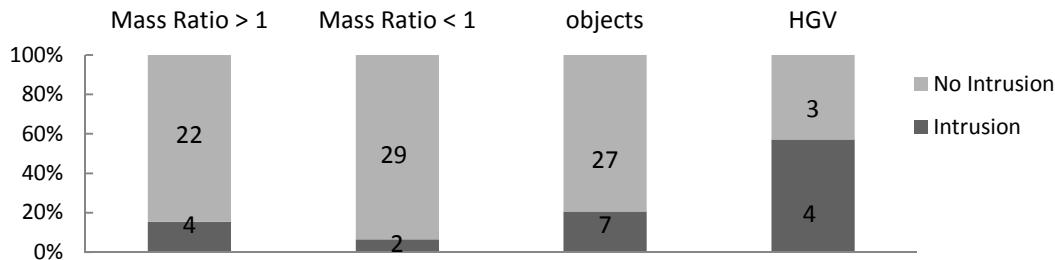


**Figure 4** Influence of intrusion in regard of the passenger compartment identified for the vehicle to vehicle accidents with a certain mass ratio and the vehicle to object accidents

Figure 5 illustrates the number of injured front seat occupants categorized in slightly injured, seriously injured and killed according to their own vehicle mass. As only cases with MAIS 2+ injuries were selected there were no uninjured occupants in this data set. On the left side there are crashes against all opponents (vehicles and objects). There were almost more than double of seriously injured occupants in lighter vehicles compared to heavier vehicles. While the left side of Figure 5 shows all accident scenarios the right side considers only car-to-vehicle accidents (including car-to-HGV). The data suggest that the injury risk is increasing when the vehicle is

lighter than the mean mass. However, there is a bias because heavier vehicles are more likely to be newer. Also, heavier vehicles are more likely to be a luxury vehicle having a more advanced restraint system.

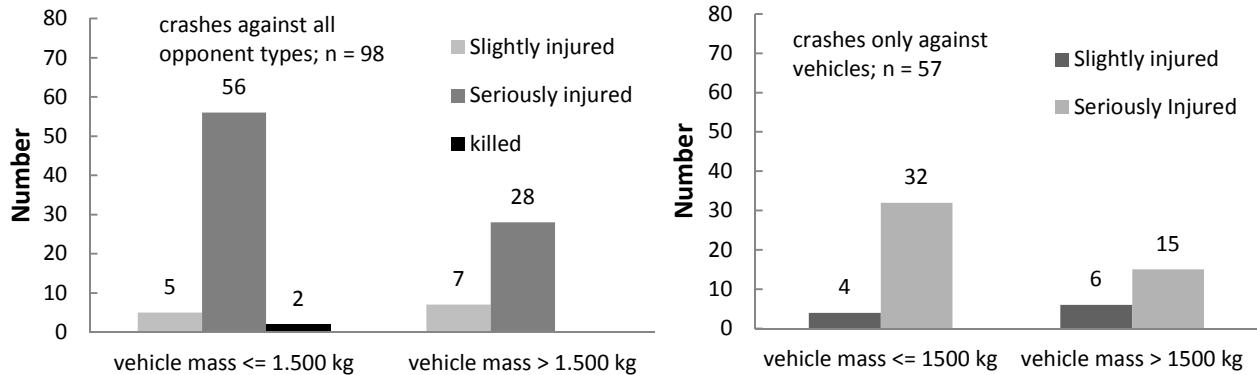


**Figure 5** Number of vehicles with MAIS2+ car occupants in regard to their injury categorization and their own vehicle mass; left: against all opponent types (n=98), right: only vehicle to vehicle crashes (n=57)

The analyses of real world accident data suggests that occupants in smaller vehicles (less than 1,500 kg) have a higher probability on injuries in frontal impacts compared to occupants in vehicles heavier than the crash trolley. Although the numbers were low in regard to the mass ratio, the numbers were very clear when only the own vehicle mass was considered. The accident data also suggest that the higher injury probability is not due to the passenger compartment stability, but rather due to the occupant loading due to the crash pulse and the restraint system.

### Crash Test Data

To compare the loading on the vehicles in the different test configurations the maximum acceleration measured at the b-pillar driver side, the OLC and the maximal plastic deformation measured in x-direction at the upper a-pillar were evaluated.

Figure 6 shows the acceleration together with the OLC for the different crash tests. There is a strong linear correlation between OLC and maximum cabin b-pillar acceleration ( $R^2=0.93$ ). It is important to note that the OLC was developed and is mainly valid for full frontal tests. However, for the MPDB tests, the maximum acceleration has a relatively higher increase compared to the OLC. The OLC values for the fixed barrier tests (FWRB and ODB) were in a range between 22.3 g and 32.4 g. The values were for lighter vehicles in the mobile barrier tests (MPDB) much higher 34.8 g and 46.6 g.

Eickhoff [21] has evaluated the OLC values for different vehicles using the NHTSA database. There, the majority of values were between 25 g and 38 g, which indicates that the OLC values for the lighter vehicles in the MDPB test are relatively high compared to conventional design levels.

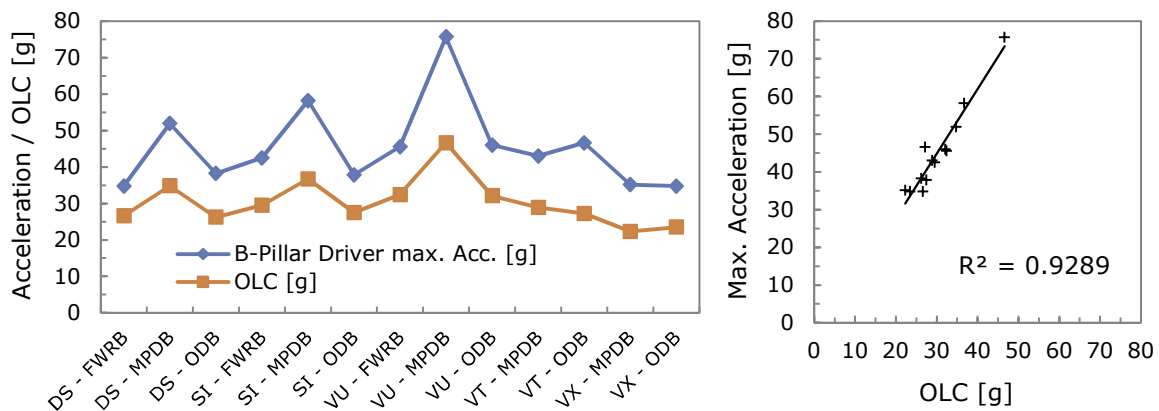


**Figure 6** Vehicle accelerations and occupant loading criterion (OLC)

The maximum accelerations measured at the b-pillar driver side are shown in Figure 7. It is apparent that the maximum acceleration levels for vehicles lighter than 1,500 kg were much higher in the test against a mobile barrier (MPDB) compared to the test configurations with a fixed object (ODB, FWRB). Acceleration values for the vehicles in the ODB and FWRB test were in general between 30 and 40 g, while the acceleration values for the lighter vehicles in the MPDB test were over 50 g and in one case reaches up to 76 g. However, the acceleration values for the heavier vehicles were similar when comparing MPDB test and ODB tests for the same car. Previous research showed that the acceleration level for fixed PDB tests are considerable higher compared to ODB even for heavy vehicles [5]. The combination of PDB barrier face and mobile barrier with a fixed weight could explain why the acceleration of the heavy cars is similar between ODB and MPDB. This is most likely due to the different barrier stiffnesses (ODB vs PDB) and the fact that the vehicles are not optimized for the MPDB test procedure. The vehicle VX had a test mass of 2,400 kg and had almost no differences in the MPDB accelerations compared with the ODB test. The vehicles front structure is differently loaded by the PDB element comparing to the FWRB or the ODB tests. This counts in particular for vehicles with an inhomogeneous vehicles front (Figure 7, right).

Note: In previous projects it was criticized that the mobile barrier would not generate enough loading for the heavier vehicle which could potentially lead to insufficient compartment strength in single vehicle accidents [5].

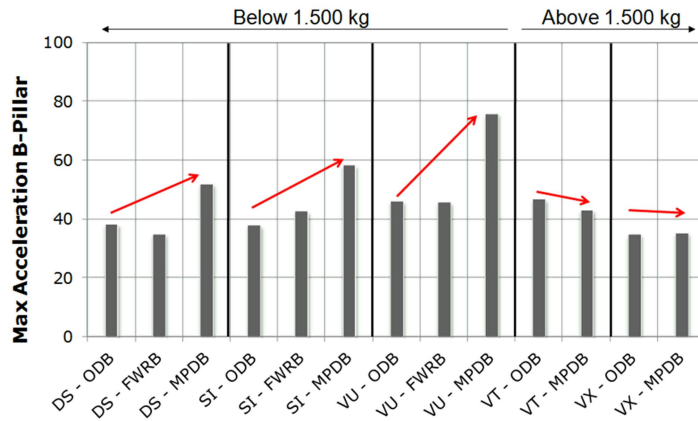


**Figure 7** Maximum vehicle accelerations for the vehicles measured at b-pillar driver side; right: example of the vehicle structure which is not optimized for the PDB barrier

In Figure 8 the a-pillar displacement on the driver side measured at waist line is shown. Almost no deformation was measured for the vehicles in the FWRB tests. This was expected as the objective of this test is to generate a high acceleration pulse to assess the restraint systems. The vehicle's front structure is symmetrically loaded in the FWRB and the crash structures can deform in a perfect manner. Even for the other configurations the deformation was relatively small. The vehicle DS had the largest deformations between 40 mm (ODB) and 50 mm (MPDB). Generally there is no clear trend which test set-up (MPDB vs. ODB) results in higher compartment intrusions – for some tests larger intrusions were measured for the MPDB and for others in the ODB test. Previous research [5] furthermore indicated that the deformation patterns are different between ODB and PDB (i.e. the PDB appears to load the upper region of the car more than the ODB test). Therefore the intrusion depth might be influenced by the combination of deformation pattern and barrier stiffness.

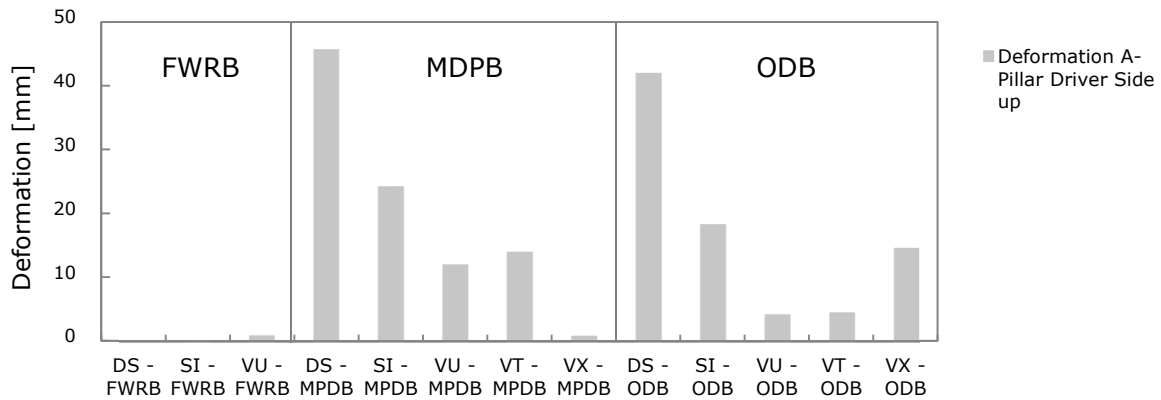


**Figure 8** Deformation of the vehicles measured in millimeter at the a-pillar of the driver side in the height of the waist line.

The maximum vehicle acceleration was compared to the thorax acceleration [3ms], pelvis peak acceleration and the belt force measured at the outer lap belt (B6). As expected the acceleration measured at the dummy is similar to the vehicle acceleration and therefore a possible indicator for evaluating the loading on the dummy in the crash test. Nevertheless, the force measured on the belt had even a higher correlation ( $R^2=0.84$ ) in regard to the vehicle acceleration.

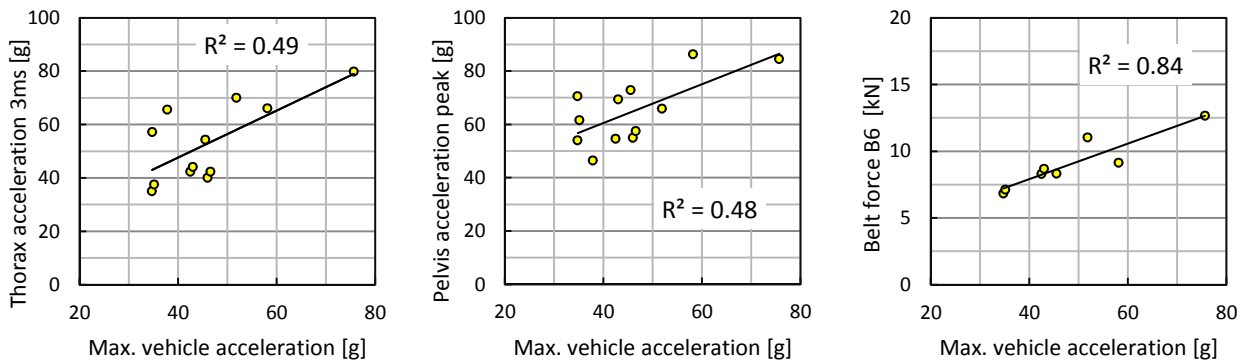


**Figure 9** Vehicle acceleration measured at a-pillar versus thorax acceleration, pelvis acceleration and lap belt force (B6).

The injury criteria measured at the dummy are shown in Figure 10. In general the head acceleration was higher in the MPDB test procedure compared to the fixed barrier tests for all vehicles. It should be noted that the values in particular for the two lighter vehicles (VU and DS) were much higher, up to  $a_{3ms} = 136$  g. Nevertheless, head bottoming out and chest contact with the steering wheel was not observed. Also the thorax deflection was higher in the MPDB than in the FWRB test (approximately 10 to 20 %), while the thorax deflection in the ODB test was the lowest. The thorax and pelvis acceleration were much higher in the mobile barrier test and, in general, very close to or above the IARV.

For the heavier vehicles (VT and VX) the dummy values were equal or slightly higher in the MPDB test procedure. For the lighter vehicles the relevant IARVs in regard to UN-R 94 ( $HIC_{36}$ ,  $a_{3ms}$ , thorax deflection) were slightly higher in the FWRB test, but still well below the limits. However, the pelvis and thorax acceleration were much closer or above the limits. The stronger loading on the lighter vehicles in the mobile barrier tests can be clearly seen in all IARVs. It has to be noted, that the restraint systems are optimized for Euro NCAP and are not adopting to the new crash pulse.

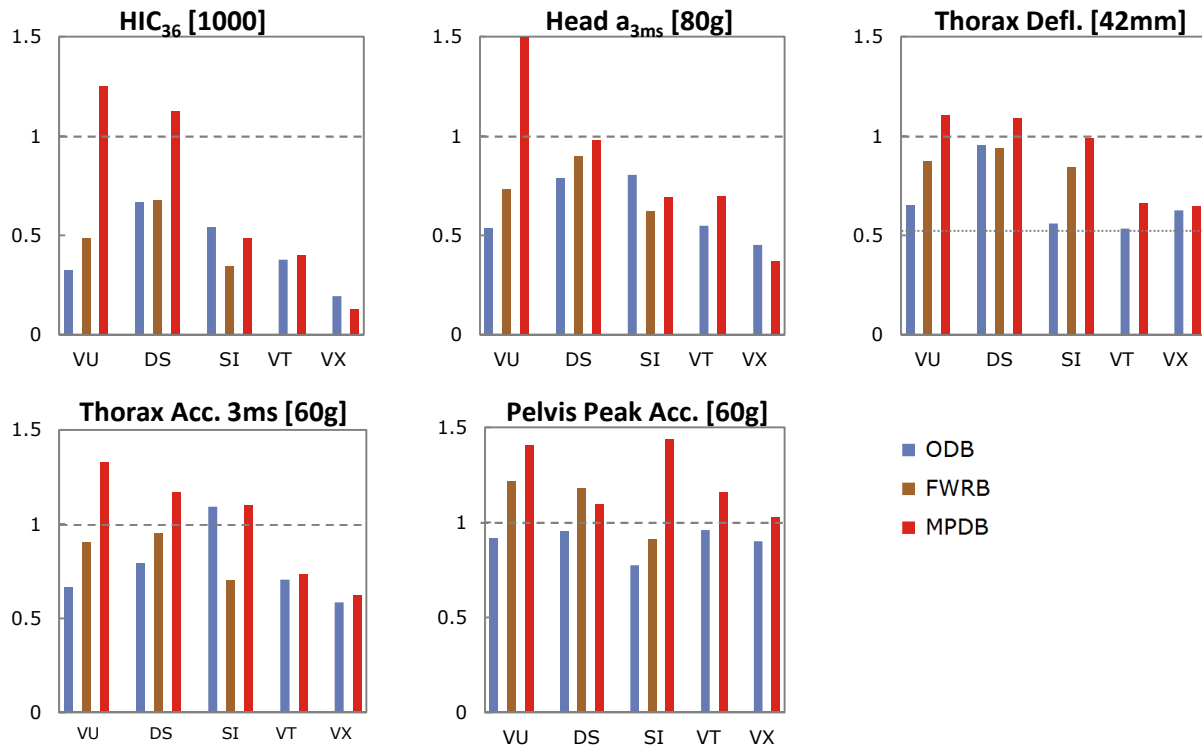


**Figure 10 Ratio of relevant injury assessment reference values for the vehicles in the test configurations ODB; FWRB and MPDB.**

The different loading in terms of vehicle structure, vehicle acceleration and injury assessment values for vehicles with a mass lighter and heavier than the mobile barrier should be investigated with the help of crash test data. It is assumed that lighter vehicles experience a higher loading with a frontal mobile offset barrier compared to a fixed barrier test (FW / ODB) and that heavier vehicles show a lower loading.

The vehicle crash test data with regard to vehicle deformation, vehicle acceleration and injury assessment values were analyzed. It has been shown that the assumption that lighter vehicles are subjected to a higher loading in a frontal mobile offset barrier test, compared to a fixed barrier test (FW / ODB), can be supported not only with regard to vehicle structural performance but also in regard to injury assessment values. On the other hand it has been that the vehicle acceleration and the injury assessment values were not substantially lower for the heavier vehicles. The delta-v is much lower for the heavier vehicles in MPDB tests but the PDB barrier is much stiffer and most of the vehicles are not designed for this test.

## LIMITATIONS

It has to be noted that the number of tested vehicles was limited. Furthermore, only one test per configuration was carried out.

It is important to note that not all vehicles were tested in the same test laboratory which could result in minor differences. However, the test configurations for the ODB test (Euro NCAP protocol) and the MDPB were among themselves the same.

With regard to the analyses of accident data, the data sample was carefully selected to address the appropriate accident configurations. However, this leads to a limited number of accident cases.

## CONCLUSIONS

The accident data show that the injury severity of car occupants is higher for lighter vehicles in car-to-car, car-to-HGV and car-to-object accidents. The influence of intrusion seems not to be the major factor for injuries in particular for car to car accidents. Accidents with large overlap are dominant. For impacts with a small overlap it is important to separate between impacts including one vehicle edge and centered impacts.

With the mobile deformable barrier test the loading conditions were seen more realistic in terms of real world car-to-car accidents. This was in particular true for the lighter vehicles. However, the loading on the light and stiff vehicles produces a very high acceleration pulse in the mobile barrier test procedure. The acceleration pulse was also influenced by the different deformation of the vehicle front structure when crashing against the PDB barrier. With regard to the IARVs, the vehicles had much higher head accelerations and thorax deflections in the mobile barrier test procedure. The data suggests that thorax and pelvis accelerations could be important and relevant indicators if the loading due to the vehicle pulse needs to be evaluated.

It was seen that the crash test with the mobile crash barrier induced a rotation to the vehicle which occurred relatively late in the impact. This motion induces high accelerations at the dummy head in the rebound phase, when the head hits the b-pillar. A dummy movement during the forward motion apart from the driver airbag due to the rotational effects of the MPDB test procedure has not been identified, though.

The benefit of the mobile deformable barrier test is the higher loading for smaller vehicles in particular in regard to the crash pulse. In addition, the PDB offers potential for the compatibility assessment of the vehicles structure. The trend of increased vehicle stiffness (especially illustrated by tests with the MPDB and small cars) shows the need of a further improvement of passive restraint systems to reduce the occupant loading and with it the injury risk.

As the measurement of the thorax loading with the chest deflection of the HIII dummy is not ideal, the evaluation of the loading in the mobile barrier test procedure with a more appropriate dummy is recommended.

## ACKNOWLEDGEMENTS

The authors would like to thank Euro NCAP for making the use of additional crash test data available.

## REFERENCES

- [1] Richards, D.; Edwards, M.; Cookson, R. *Technical assistance and economic analysis in the field of legislation pertinent to the issue of automotive safety: provision of information and services on the subject of accident analysis for the development of legislation on frontal impact protection*, **2010**.
- [2] Thompson, A.; Edwards, M.; Wisch, M.; Adolph, T.; Krusper, A.; Thomson, R. In: *FIMCAR: Frontal Impact and Compatibility Assessment Research*. Johannsen, H., Ed.; Universitätsverlag der TU Berlin: Berlin, **2013**; Vol. *DI.1*.
- [3] Saunders, J.; Parent, D. *Assessment of an Oblique Moving Deformable Barrier Test Procedure*: Seoul, **2013**.
- [4] Ratzek, A.; Sandner, V.; Kolke, R. Der ADAC-Kompatibilitätscrashtest 2013. *Verkehrsunfall und Fahrzeugtechnik*, **2014**, 1/2013(5), 170–178.
- [5] Johannsen, H., Ed. *FIMCAR: Frontal Impact and Compatibility Assessment Research*; Universitätsverlag der TU Berlin: Berlin, **2013**.
- [6] Schram, R.; Versmissen, T. *The Development of a Mobile Deformable Barrier Test Procedure*, **2007**.
- [7] Uittenbogaard, J.; Versmissen, T. In: *FIMCAR: Frontal Impact and Compatibility Assessment Research*. Johannsen, H., Ed.; Universitätsverlag der TU Berlin: Berlin, **2013**.
- [8] Versmissen, T.; Welten, J.; Rodarius, C. In: *FIMCAR: Frontal Impact and Compatibility Assessment Research*. Johannsen, H., Ed.; Universitätsverlag der TU Berlin: Berlin, **2013**.
- [9] Family Cars trump luxury models in rigorous new crash test. *IIHS Status Report*, **2012**, 47(10).
- [10] Murri, R.; Caviezel, S. Relevanz des IIHS-Small-Overlap-Crashtests in Europa. *Verkehrsunfall und Fahrzeugtechnik*, **2013**(6), 226–236.

- [11] Bean, J.; Kahane, C.; Mynatt, M.; Rudd, R.; Rush, C.; Wiacek, C. *Fatalities in Frontal Crashes Despite Seat Belts and Air Bags*: Washington, DC 20590, **2009**.
- [12] Adolph, T.; Eggers, A.; Pastor, C.; Damm, R. *New Requirements in Frontal Impact and Future Research for a Phase 2*: München, **April 08, 2014**.
- [13] UN/ECE. *Regulation No 94 — Uniform provisions concerning the approval of vehicles with regard to the protection of the occupants in the event of a frontal collision*; Official Journal of the European Union, **January 26, 2012**. <http://eur-lex.europa.eu/LexUriServ/LexUriServ.do?uri=OJ:L:2012:254:0077:0135:EN:PDF>.
- [14] Otte, D.; Krettek, C.; and Zwipp, H. *Scientific Approach and Methodology of a New In-Depth- Investigation Study in Germany so called GIDAS*: Japan, **2003**.
- [15] Adolph, T.; Wisch, M.; Edwards, M.; Thomson, R.; Stein, M.; Puppini, R. In: *FIMCAR: Frontal Impact and Compatibility Assessment Research*. Johannsen, H., Ed.; Universitätsverlag der TU Berlin: Berlin, **2013**; Vol. *FIMCAR VIII*.
- [16] Lazaro, I.; Vie, N.; Thomson, R.; Schwedhelm, H. In: *FIMCAR: Frontal Impact and Compatibility Assessment Research*. Johannsen, H., Ed.; Universitätsverlag der TU Berlin: Berlin, **2013**; Vol. *V*.
- [17] Kübler, L.; Gargallo, S.; Elsässer, K. In: *Airbag 2008*; Vol. *2008*.
- [18] Adolph, T.; Eggers, A. *Full Width Test – ECE-R 94, Evaluation of test data, Proposal for injury criteria, Way forward*: Bergisch Gladbach, **2013**.
- [19] Kramer, F.; Appel, H. In: *IRCOBI Conference 1990*.
- [20] Mertz, H.; Irwin, A.; Prasad, P. In: *Stapp Car Crash Journal*; Vol. *47*; pp. 155–188.
- [21] Eickhoff, B. *Analyse, Mechanismen und Reduktion gurtinduzierter Thoraxbelastungen im Frontalcrash*. Dissertation, Universitätsbibliothek der Helmut-Schmidt-Universität: Hamburg, **January 29, 2013**.

# A STUDY of GAS FLOW BEHAVIOR in AIRBAG DEPLOYMENT SIMULATION

**Hitoshi Ida**

**Masashi Aoki**

**Michihisa Asaoka**

Toyoda Gosei Co., Ltd.

Japan

**Kiyonobu Ohtani**

Institute of Fluid Science, Tohoku University

Japan

Paper Number 15-0081

## ABSTRACT

Airbag deployment simulation has been utilized as an important technique to predict the occupant protection performance in the development and design stages. One of the key elements of airbag deployment behavior is the gas flow behavior of jets from inflator. In this study, in order to understand the gas flow behavior of disk type inflator for driver side airbag, visualization experiments were conducted using the schlieren method. The gas flow from the inflator with a retainer has been found to have a strong directivity. Then, the gas flow simulation was conducted with a general purpose finite element program, LS-DYNA, it was possible to obtain a good reproducibility. For reproduction, it was found that jet direction and cone angle of gas diffusion were essential elements. Furthermore, comparison between simulation and experiments were conducted for deployment behavior of driver side airbag, the effect of gas flow on deployment behavior was analyzed. It was found from the results that the reproduction of gas flow from inflator was a major factor for reproduction on deployment behavior of driver side airbag.

## INTRODUCTION

To evaluate the occupant protection performance of the airbag, the airbag deployment simulation is an important and efficient one approach. The first developed approach was uniform pressure method, which obtained pressure from mixed jet gas property of inflator and equation of state was applied to entire inside of airbag. This method could evaluate energy absorption of airbag and used for occupants protection analysis combined with kinematic analysis.[1] However, Since the gas flow was not considered in this method, there were some issues that behavior and energy absorption of airbag in deploying process could not be obtained accurately. To resolve the issues, fluid and structure coupling method, ALE (Arbitrary Lagrangian-Eulerian) method has been introduced.[2]

When this method was applied to airbag deployment analysis, to represent the deployment of the folded airbag, enormous computational resources and cost were necessary.[3] To overcome the issue, a general purpose finite element program, LS-DYNA, implemented a new method CPM (Corpuscular Particle Method) which replace gas flow as particle movements. In this method, the gas was not treated as continuum and followed gas molecular dynamics. Instead of all models of the gas molecules, the overall translational kinetic energy are replaced with a number of particles to be equivalent.[4, 5]

It was not necessary to descrete entire space as same as ALE in this method, the deployment simulation has been executed in available computational resources and cost. When the gas flow in narrow tube such as curtain airbag, it was possible to predict the deployment behavior and an impact force property. The prediction is currently applied to products development.[6] However, the difference has occurred in actual phenomena and simulation results when the gas was evolved in large space such as driver side airbag. We focused the gas flow in the airbag, tried to visualize the gas flow from inflator using schlieren method. In the past study, there was a observation of the gas flow only inside the inflator.[7] Very few attemps have been made at such observation of the gas flow outside the inflator for airbag deployment behavior.

In this paper, the visualization experiments of the jet gas flow were conducted and reproduced the gas flow by CPM. Then we applied the study results to deployment simulation of driver side airbag, and present the deployment behavior was reproduced properly.

## METHODS

### Visualization Experiments of Gas Flow

To understand the jet gas flow from inflator, the visualization experiment using schlieren method was conducted in open atmosphere space. It was hard to perceive clearly the jet gas flow with high speed camera. There was a PIV method to observe velocity of marker particles which mixed in gas flow.[8] In this method, observation area was local and it was hard to visualize the range of gas flow. Therefore, we selected the schlieren method to visualize clearly and directly. The schlieren method is one method of observation for gas flow using difference of light refractive index. The method has been used to visualize a shock wave of explosion or aircraft.[9,10] The configuration of experiment apparatus are shown in Figure 1. A light from point light source was parallelized by parabolic mirror, object inflator gas was ejected in the parallelized light. The light was condensed by parabolic mirror again. The defocused light by difference of refractive index was removed by iris at focal point. Images of difference of light contrasting were recorded with a high speed camera. In generally, Although a knife edge was used in schlieren method, to observe the diffusing gas from the center of inflator, iris was used to capture the gas clearly. To take a picture of gas flow in range of airbag deployment, the world's largest class parabolic mirror with a diameter of one meter and focal length of eight meter was used in this experiments. This apparatus could be visualized at least 3kPa pressure waves such as sound from trombone.[11] For driver side airbag, the gas flow from inflator with or without a retainer was recorded with a high speed camera.

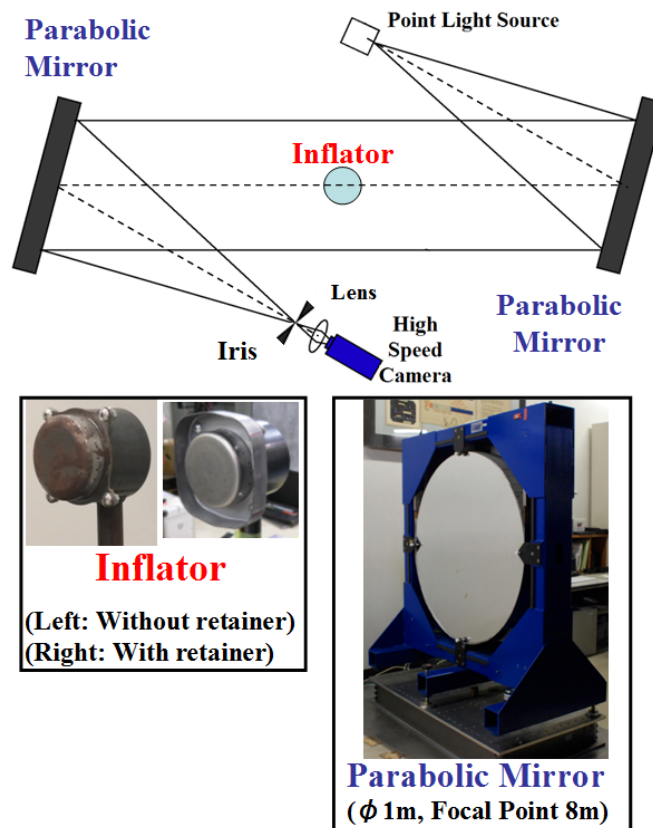


Figure 1. Gas flow visualization apparatus of schlieren method at Tohoku University.

## Gas Flow Simulation of Inflator

Gas flow simulation with or without a retainer using CPM of the LS-DYNA were conducted to reproduce the observed jet gas flow by visualization experiment. The research of seven CPM parameters is examined to reproduce the real gas flow. The examined parameters are shown in Table 1.

*Table 1.*  
*Parameters of gas flow simulation*

No.	Parameter	Without retainer	With retainer
1	Initial direction of gas inflow	Radial	Radial / Axial
2	Cone angle from orifices	Inactive / 16° / 25°	Inactive / 0.1 ~ 25°
3	Friction factor	0 (default)	0 ~ -0.2
4	Dynamic scaling of particle	Inactive / Active	Inactive / Active
5	Initial gas inside airbag	CV method / Particle	CV method / Particle
6	Number of orifices	16 (Inflator pinholes)	16 / 4 (Retainer corner)
7	Number of gas components	Mixed / Multiple	Mixed / Multiple

## Deployment Experiment of Driver Side Airbag

The static deployment behavior of driver side airbag was observed in an experiment. The experiment setting, the airbag configuration and deployment appearance are shown in Figure 2.

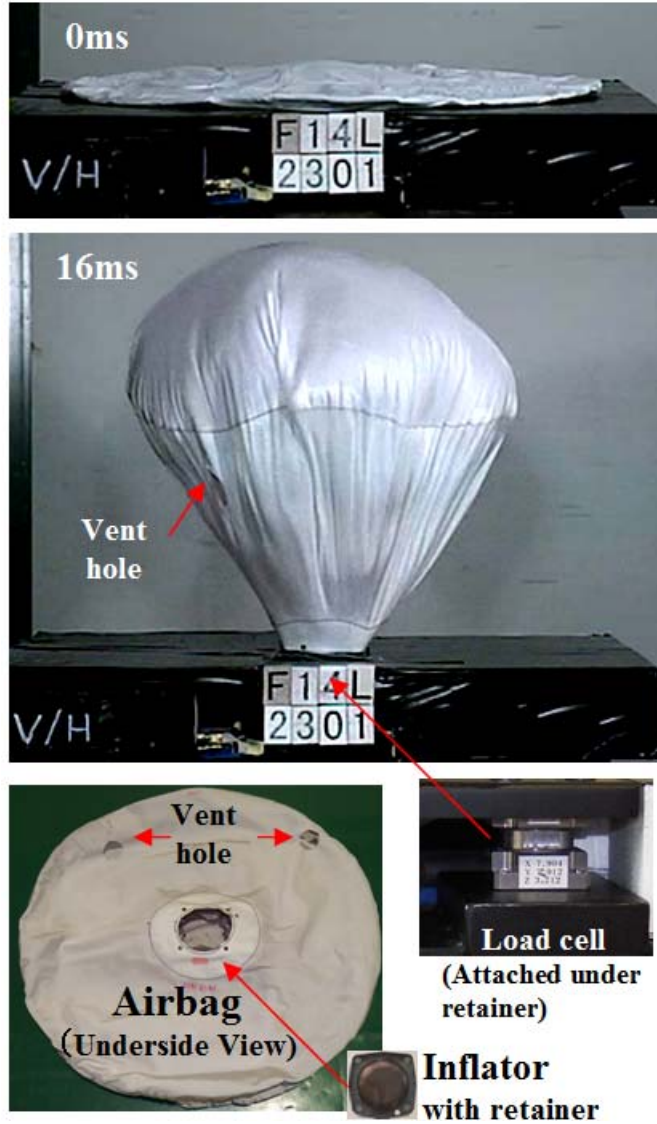


Figure 2. Static deployment experiment of driver side airbag.

The unfolded tether less airbag with retainer was installed for the experiment. A load cell was set under the retainer to measure a deployment force at installation point.

### Deployment Simulation of Driver Side Airbag

A reproduce simulation shown in Figure 2 was conducted. A mechanical property of airbag fabric was from tensile, shear test and reflected to the property of input deck. A gas temperature and a mass flow rate were identified by tank test simulation. The parameter values of CPM were selected default condition on atmosphere space and the best conditions on Table 1 to reproduce the gas flow. The effect of gas flow reproduction in atmosphere space was examined to airbag deployment.

## RESULTS

### Visualization Experiments and Simulation of Gas Flow

The gas flow from inflator was clearly visualized as a dark image in schlieren method. The results of visualization are shown in Figure 3. The large distortion parts of parallel light were removed and observed as shadow. Since the inflator gas had a high temperature and a high pressure, the gas produced a distinct distortion that was different from the atmosphere. In these results, the difference of the flow with or without retainer was clearly observed. The gas tended to be released radially and vertically from orifices on the inflator for without a retainer. On the other hands, for with a retainer, the flow along the wall of retainer was observed. Additionally, the flow along the wall did not diffuse immediately after release.

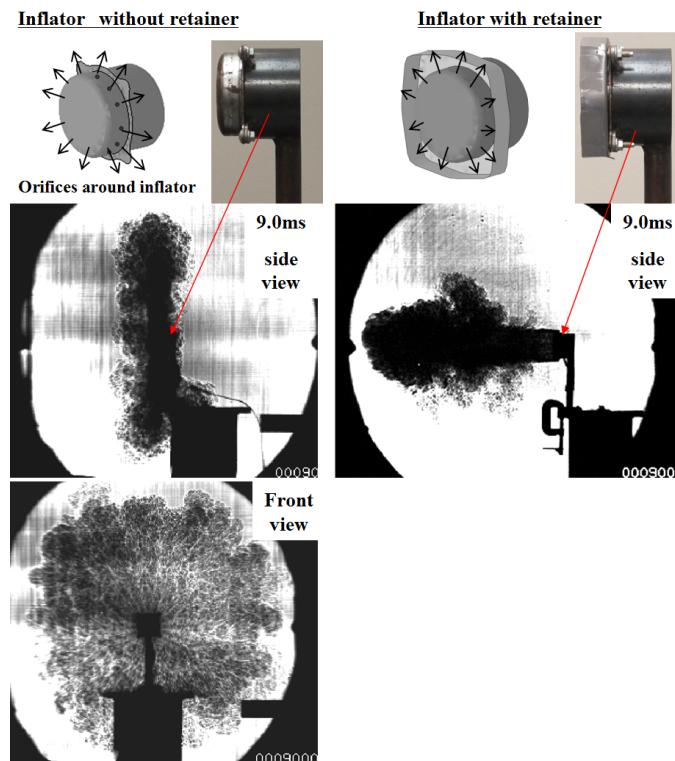


*Figure 3. Visualization of inflator gas by schlieren method (Left: without retainer, Right: with retainer).*

The gas flow of simulation by CPM for without the retainer in atmosphere space tended to be diffused randomly. The behavior of particles did not show radial flow. (See Figure 4A)

To reproduce this trend, when the cone angle parameter in Table 1 was set appropriately, radial flow was shown in Figure 4B.

On the other hands, for with retainer, the gas flow of simulation did not reproduce the experimental result. (See Figure 4C) The parameters from No. 3 to No. 7 in Table 1 did not affect to gas flow behavior. (See Figure 4D)

For with retainer, when jet direction was set as axial jet along the wall of retainer, the diffusion range of flow was slightly narrowed, however a directional flow was not reproduced. (See Figure 4E)

When additional parameter cone angle was set appropriately, the flow was reproduced as same as the experimental result. (See Figure 4F)

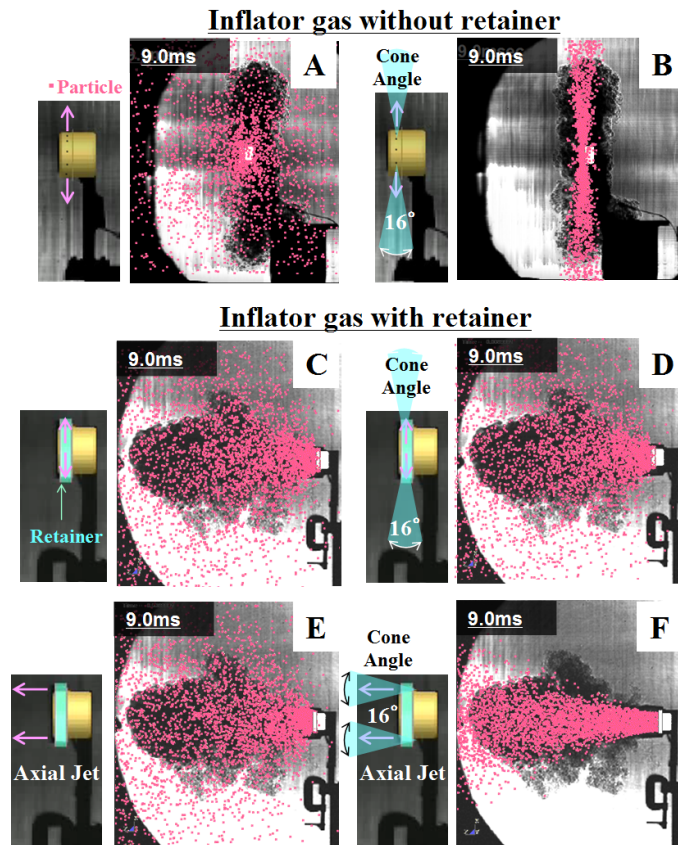


*Figure 4. Gas particle distribution of simulation result with retainer.*

### Deployment Experiments and Simulation of Driver Side Airbag

Comparison between deployment experiment and simulation of driver side airbag was conducted. When the jet direction was set radially and vertically of the inflator in simulation, the result shows that the deployment behavior was delay against experiment. Approximately half force of the experimental result occurred in retainer fixed points. (See Figure 5A)

When the jet direction was set as axial and along the wall of retainer and cone angle was set appropriately, the deployment time and deployment force were almost reproduced the experimental results. (See Figure 5B)

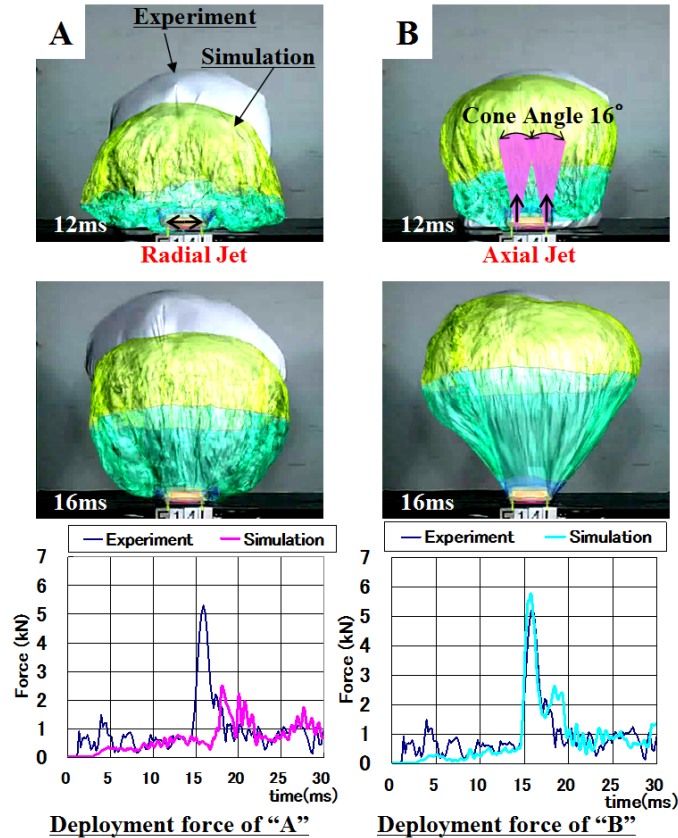


Figure 5. Comparison of deployment behavior & deployment force between experiment and simulation (Left: Radial jet, Right: Axial jet with Cone angle).

## DISCUSSION

According to the result comparison between experiment and simulation, when the particles were released to relatively wide space, random movement of each particle is dominant, the gas flow was found to be not sufficiently reproducible by CPM.

The actual gas flow from orifices on the inflator is released in vertical direction on orifices. When the gas flow from inflator with retainer is released, if it is assumed that the gas flow outlet faces open side of the retainer, the gas is released perpendicular to the open side of the retainer.

In CPM, because the particles diffuse randomly from orifices of the inflator, it should apply correction function such as cone angle.

## CONCLUSIONS

The visualization experiment and simulation of the gas flow from inflator provide the following findings.

Using schlieren method, the gas flow to atmosphere space is radially released perpendicular to orifices on the inflator. When the retainer is installed on inflator, the gas flow along wall of retainer is produced and the gas flow is perpendicular to open side of the inflator.

In simulation of CPM, particles from inflator behave randomly. To reproduce the actual radial flow, it should have a correction function, such as a cone angle. When the gas flow with retainer is reproduced, it should set the jet direction from open side of retainer and cone angle.

Applying the above conditions to deployment simulation of driver side airbag, the deployment behavior and the deployment force property are reproduced the experimental results.

## ACKNOWLEDGEMENTS

We wish to acknowledge valuable experiments and discussions with honorary Prof. Takayama at Institute of Fluid Science, Tohoku University.

## REFERENCES

- [1] Wang, J. T., & Nefske, D. J. (1988). A new CAL3D airbag inflation model. SAE Technical Paper 880654.
- [2] Fokin, D., Lokhande, N., & Fredriksson, L. (2003). On airbag simulation in LS-DYNA with the use of the Arbitrary Lagrangian-Eulerian method. 4th European LS-DYNA Users Conference.
- [3] Zhang, N., Shi, L., & Tzeng, B. (2006). Issues on Gas-Fabric interaction in airbag simulation using LS-DYNA ALE. 9th International LS-DYNA Conference.
- [4] Olovsson, L. (2007). *Corpuscular method for airbag deployment simulations in LS-DYNA* (Report R32S-1). Huddinge, Sweden: Impetus Afea AB.
- [5] Feng, B., & Coleman, D. (2008). Gas dynamics simulation of curtain airbag deployment through interior trims. 10th International LS-DYNA Conference.
- [6] Sugaya, H., Imura, K., & Mae, H. (2014). Development of Side Curtain Airbag Deployment Simulation Technology Using CPM. *Honda R&D Technical Review*, Vol. 26, No. 1.
- [7] Kratz, H., Pührer, C., Takazono, K., & Yano, K. (2008). Shockwave characterisation, parameter studies and visualization for a cold gas curtain inflator. Airbag2008.
- [8] Lee, J. S., Jang, G. Y., Kim, S., & Kim, S. C. (2006). Dynamic PIV measurement of a compressible flow issuing from an airbag inflator nozzle. *Journal of Thermal Science*, Vol. 15, No. 4, pp. 377-381.
- [9] Mizukaki, T., Miura, A., & Takayama, K. (2004). Experimental simulation of large-scale explosion using a micro-charge explosion (1) - Behavior of shock waves in a complicated closed-space -. *Science and Technology of Energetic Materials*, Vol. 65, No. 5, pp. 180-188
- [10] Ukai, T., Ohtani, K., & Obayashi, S. (2015). Validation of measurement accuracy for near-field pressure around supersonic projectiles in a ballistic range. *Measurement, Journal of the International Measurement Confederation*, Vol. 67, pp. 24-33.
- [11] Takayama, K., Ohtani, T., Ogawa, T., Kikuchi, T., Takayama, R., & Takahashi, T. (2011). Visualization of weak shock waves emitted from trombone. *The Journal of the Acoustical Society of America* 2011. doi:10.1121/1.3588692

# The Force Measurement of Primary Parts in Frontal Vehicle Crash Test

## - by Strain Gauge Calibration -

Park Un-chin

Song Ha-jong\*

Kim Hyun-chul\*

Florian Ganz\*\*

Sudar Sankar\*\*

Mario Wohlfahrt\*\*

### ABSTRACT

In this research, the new calibration component test methodology and converted forces from strain gauge will be proposed about measuring real time force of frontal NCAP crash powertrain mounting and structure like front side member.

**Key Word** : Strain Gauge, Vehicle Crash, Force Calculation, Structure Force Distribution

## 1. Introduction

Strain gauges are commonly used in Aerospace and vehicle durability tests but not for the vehicle dynamic crash so often. Recently some vehicle crash institutes are applying the strain gauge to predict the vehicle deforming time in case of accelerometer measuring failure or dummy ribs displacement but not for the force measurement.<sup>1)-4)</sup>

To know the force distribution of structure in vehicle crash test is very important because all the strength design of each part can be changed by it. In the CAE, we can easily measure the value it but it's not easy in the real car crash test because the most of structure and inner steel parts like front side member and knee support bracket are in plastic deformation. If we insert the load cell device replacing measuring parts it is possible but this way cannot be used in so many developing tests because those device will influence the test result.

So in this research we will find how to attach strain gauges efficiently to know the component system level real-time force distribution in vehicle crash test with considering avoiding its plastic deformation area. To avoid the trial and error we also developed some component tests which can be tested easily and measured the force. It is very good to find force vs strain voltage synchronizations.

All the measurements are measured again in 14MY Kia YD real vehicle crash test. We could find the synchronization with dynamic component test. Also, we can compare the difference static and dynamic breakage force.

## 2. Main Subject

### 2.1 Powertrain Mounting Breakage Force

#### 2.1.1 Mounting breakage phenomena

Breakage itself cannot be judged as a bad thing because sometimes it helps vehicle crash pulse to stay in low level. But how to control is important if too easily broken there will too much deformation in the passenger compartment. This is the one purpose of this measurement research.

The used YD vehicle is the US model of 1.8 Nu engine auto transmission. Its mountings are 3 points-engine mounting, transmission mounting and roll rod. In case of roll rod the breaking direction and point are too various so we selected measuring position the engine mounting and transmission mounting. Also in the other mounting breakage measuring HKMC has measured its bolt z-direction force so this time we concentrated to these 2 mountings.

In case of YD vehicle crash the chain cover in the engine mounting side is broken. In case of transmission mounting side, there is no broken parts but during the crash the applied force angle is changed from 0 deg to 45 deg.



Fig.1 Post picture of YD engine mounting

\* Safety Performance Team 1 : Author or Co-Author

\*\* Crash Simulation Team : Co-Author

\*\*\* ACTS (Advanced Car Technology System) : Co-Author

2.1.2 Component test set-up

To make similar static tensile test of breakage condition with vehicle crash as static condition, we used side door strength test bench. The chain cover of engine is mounted on the jig and the engine mounting is connected to it with engine mounting bracket. We attached 3 strain gauges with x,y and z direction on the bracket considering its load path and flat surface to attach. The other test case is the usage of 3 axis loadcell, replacing the engine mounting bracket.

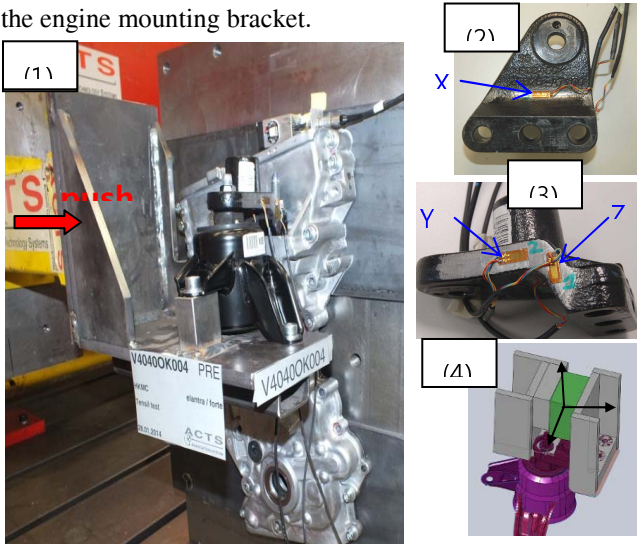


Fig.2 Chain cover breakage tensile test(1)/ Strain gauge position(2),(3)/3 Axis Load cell (4)

In case of transmission mounting breakage component test, we also used jig to mount transmission bracket and the transmission mounting,

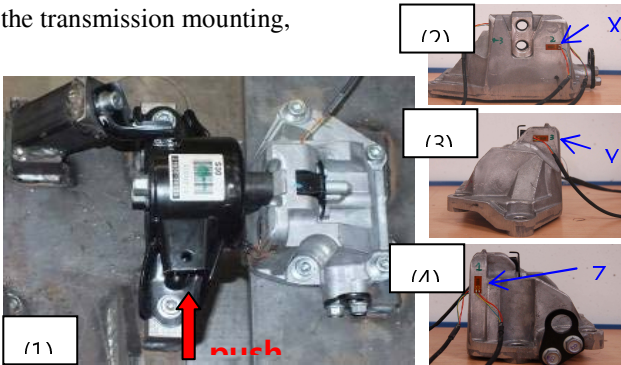


Fig.3 Transmission bracket breakage tensile test(1)/ Strain gauge position(2),(3),(4)

Also, in the crash CAE animation we already know the pushing angle is changed from 0 degree to 45 degree so we made another test chain pulling bench with seatbelt component test device.

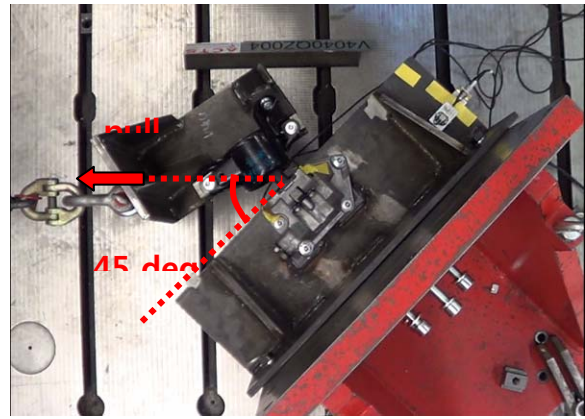


Fig.4 Transmission bracket breakage test with 45 degree (with loadcell, without loadcell)

2.1.3 Component test result of engine mounting

We pushed the mounting jig in all case except first trial test with 200mm/min. The force limit was 10 ton at pushing test device. The result summary is below.

Tests	Pushing Force (t)	Loadcell (t)			Strain (0.01%)		
		x	y	z	x	y	z
ENG	1. Loadcell	2.1	2.1	-	-	-	-
	2. Strain gauge	2.7	-	2.2	4.5	2.3	-
	3. Loadcell jig	3.0	-	-	-	-	-

Table 1. Summary of engine mounting breaking force

At the 1st engine mounting test, we used 3 axis load cell to confirm pushing force is equal to the force applied to the engine mounting bracket. Even if there was some breakage failure on the load cell mounting 4 bolts, we can check pushing force and load cell force was exactly same as 2.1 ton.

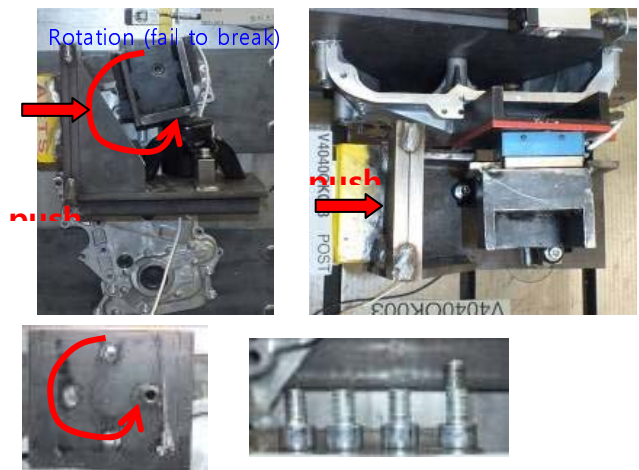
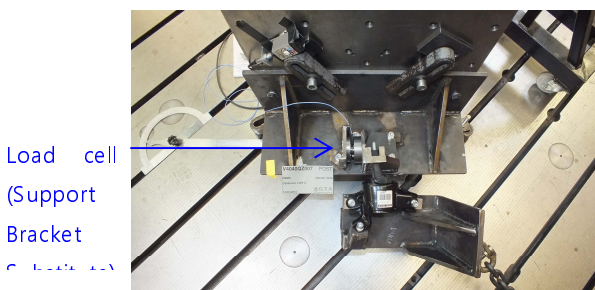


Fig.5 Engine mounting tensile test1 post picture



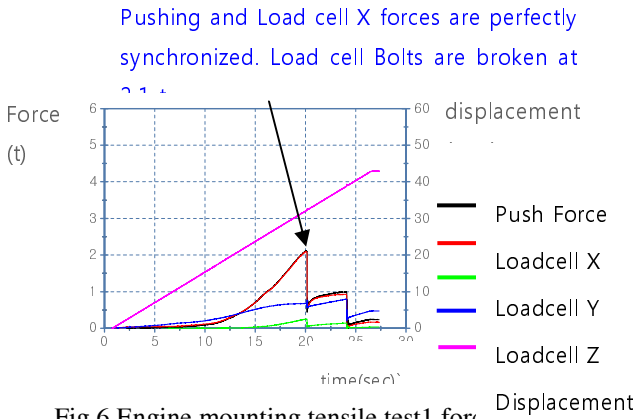


Fig.6 Engine mounting tensile test1 force graph

At the 2nd strain gauge test, we used the engine mounting bracket as the vehicle with 3 strain gauges attached. As a result, the chain cover rear hole is broken at 20mm displacement with 2.7 ton force. This breaking phenomena was very similar to the broken chain cover in high speed crash vehicle because the broken sequence is from the rear and the section surface is mostly vertical to y and z plane of vehicle.

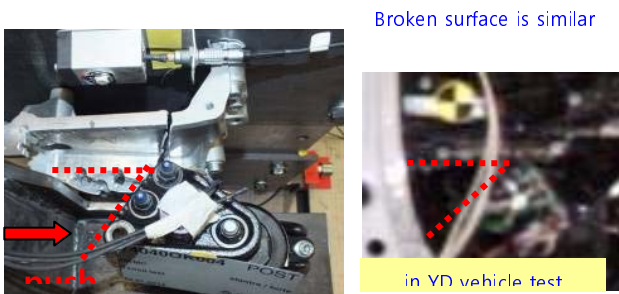


Fig.7 Engine mounting tensile test2 post picture

In this test the all the strain gauges are activated but x and y direction strain gauges activation was too small and the shape is not correspondent. The mode of z direction strain gauge is really synchronized very well to the pushing force. Now we can know this position is good elastic deforming place to measure its load and the load path is very unexpected because its direction is z.

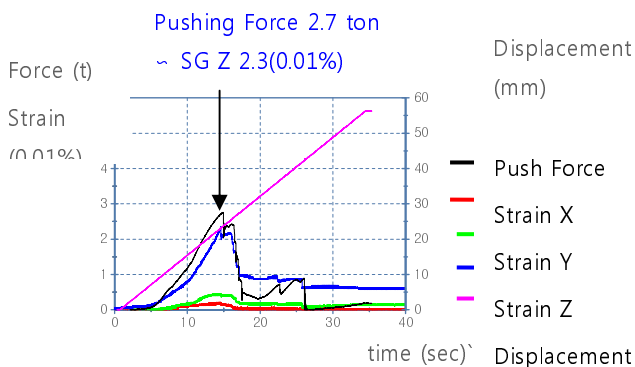


Fig.8 Engine mounting tensile test1 force graph

Also even if we have some rubber material like engine mounting bush on the calibration system we can use strain gauge to find the applied real time force. Now we can use this strain gauge position to fine the force in the vehicle crash test. This would be helpful to adjust the value of breaking force to improve the crash performance.

At the 3rd engine mounting test, we used 3 axis load cell jig again to check the variety of chain cover breaking force. Aluminum die casting breaking force tolerance is well known because it has a lot of air pouch inside when it is created. It has average 175~270Mpa tolerance at 1% strain-stress curve and to the amount of 310 MPa in case of 2% strain.

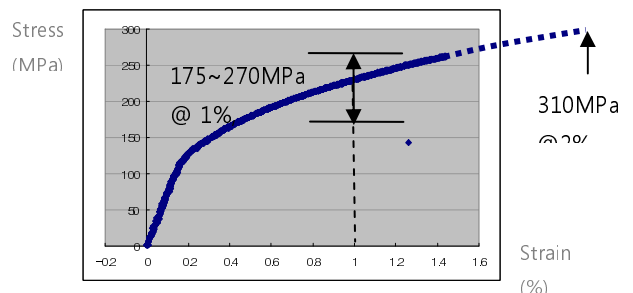


Fig.9 Aluminum die casting strain-stress curve

Because the load cell bolts were broken we attached 3 tucks to resist the breaking moments. As a result of 3rd engine mounting test, chain cover is broken at 3 ton pushing force with similar section surface to the test2. This is just 10% tolerance from 2.7 ton of 2nd test. So this kind of load cell can be used in the vehicle crash test to measure the breaking force instead of the engine mounting bracket only if it is not broken and deformed. The strong point of this load cell application is that it is possible to measure y and z direction force also. Most of engine rotates in y axis so there would be also z direction force.



Fig.10 Engine mounting tensile test3 post picture

### 2.1.4 Component test result of engine mounting

We pushed the mounting jig in all case except first trial test with 200mm/min. The force limit was 10 ton at pushing test device and 7 ton at pulling test device. The

result summary is below

Tests		Pushing Force (t)	Loadcell (t)		Strain (0.01%)	
			x	x	y	z
TM	1. 0 deg) Strain gauge	5.0	-	4.3	5.5	3.4
	2. 45 deg) Strain gauge		3.6			

Table2. Summary of transmission bracket breaking force

At the 1st transmission bracket test, we used the transmission supporting bracket as the vehicle with 3 strain gauges attached. As a result, the bracket is broken at 50mm displacement with 5.0 ton force. This breaking phenomenon did not happen in YD crash test but in case of next model of Elantra happened. So we can use this component test for both cases of transmission supporting broken or not broken to measure the real time force.

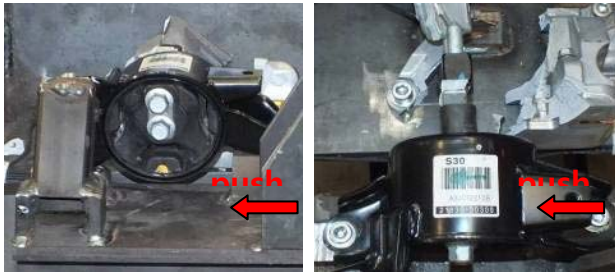


Fig.11 Transmission mounting tensile test1 post picture

In this test the all the strain gauges are activated but x and z direction strain gauges peak was delayed some. we can think this comes from the rubber bush absorbed the force till 23ms because x and z direction strain gauges are attached adjacent to the rubber bush. The mode of y direction strain gauge is really synchronized very well to the pushing force. The only differences are after being broken the smaller fall of strain y and the curve shape in detail. There seem to be come from the elastic system in including rubber but not difficult to see the peak force in transmission bracket.

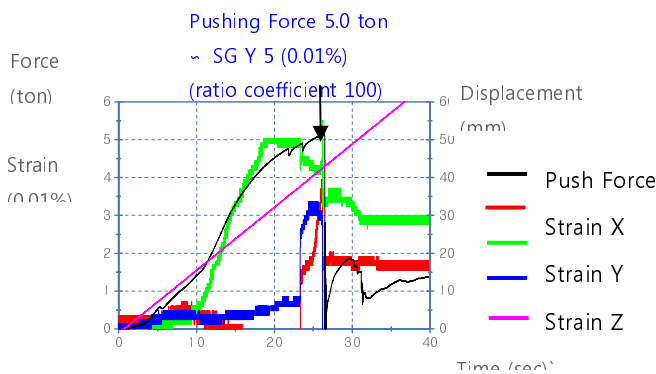


Fig.12 Transmission mounting tensile test1 force graph

Now we can know this position is good elastic deforming place to measure its load. In this case the load

path is as expected because its direction is y. Also even if we have some rubber material like transmission mounting bush even there are hard steel bolts inside on the calibration system we can use strain gauge to find the applied real time force. Now we can use this strain gauge position to fine the force in the vehicle crash test. This would be helpful to adjust the value of breaking force to improve the crash performance.

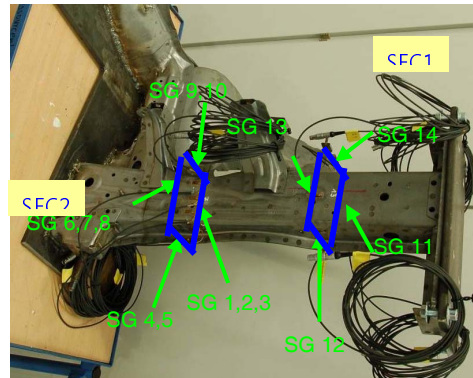
Also we can see at test2 the pushing force is almost same as loadcell value like engine mounting breakage test.

## 2.2 Front Side Member Crushing Section Force

### 2.2.1 Calibration Condition

To calibrate the front side member its straightness is very important. In case of YD, the rear lower of front side member has some bending to be connected to the floor side member. So we cut the front side member at the end of its straightness.

To measure YD's front side member we selected 2 x-direction sections which were almost no deformation during the US NCAP crash because if there is some deformation strain gauge value doesn't show the actual applied force. We attached 4 x-direction strain gauges at section1 for each surface one and 10 x-direction strain gauges at section2 for each surface 2~3.



Vehicle front

Fig.13 Front side member calibration sections

### 2.2.2 Calibration Result

We pushed front side member with 3 kinds of force- 2.5ton, 5ton and 10 ton because we already know the fact in RCAR frontal barrier test with load cell inserted to the member section the yielding force of the similar grade

compact car next model of Elantra front side member is 16 ton. As a reference in NCAP test its yielding force s 29 ton.

Force		Strain (mV)			
SG No		11	12	13	14
1st	2.5t	0.05	0.7	0.47	0.26
2nd	5t	0.08	1.36	1.08	0.63
3rd	10t	0.26	2.73	2.13	1.33
Ratio coeffi.		0.98	1.00	1.00	1.00

Table3. SEC1 Summary of front side member calibration

Force	Strain (mV)										
		1	2	3	4	5	6	7	8	9	10
1st	2.5t	0.12	0.07	0.08	0.03	0.95	1.08	0.55	0.56	0.5	0.03
2nd	5t	0.18	0.14	0.15	0.2	1.71	2.07	1.08	0.96	0.94	0.23
3rd	10t	0.51	0.25	0.25	0.1	3.29	4.01	2.12	2.09	2.02	0.43
coeffi.		0.99	1.00	0.99	0.55	1.00	1.00	1.00	1.00	1.00	0.98

Table4. SEC2 Summary of front side member calibration

The correlation was so linear except strain gauge4.

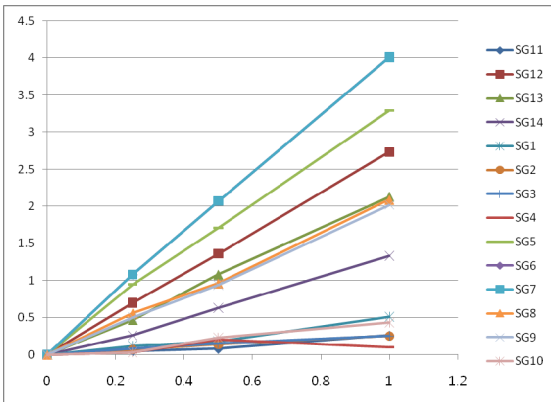


Fig.14 Front side member calibration result

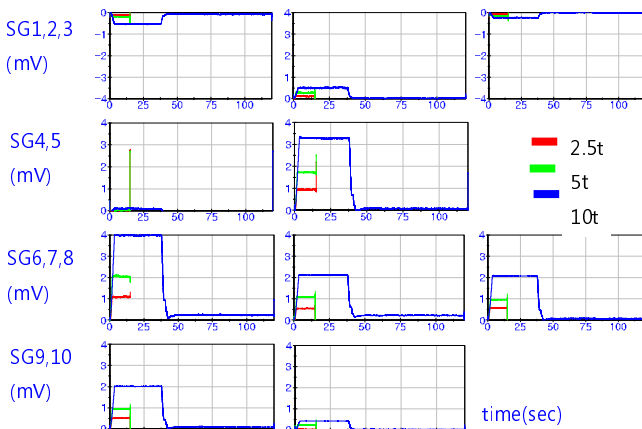


Fig.15. SEC2 calibration result of each strain gauges

The interesting thing is the ratio of each section strain peak average was similar for all 3 forces' test at section2 calibration. But in case of section1 calibration this ratio was not constant because we attached only 1 for each

section. This can be useful to find initial yielding direction of the member and can be used to control the vehicle crash dipping value. In case of this YD member we can know the initial principle deformation surface is "inner" and "bottom". When we see Fig12, we can check the member was deformed mostly at inner and secondly at bottom.

Force	outer	bottom	inner	upper
2.5t	1	4	8	2
5t	1	4	9	2
10t	1	3	8	2

Table5. The ratio of each surface strain at SEC2

### 2.2.3 Member Dynamic Component Test Condition

There are two frontal high speed modes in official crash tests. One is 56kph frontal to wooden flat barrier of US NCAP and KNCAP. The other one is 64kph 40% offset to aluminum honeycomb of EuroNCAP which are used in many country's NCAP. In case of 64kph offset there are some tolerance of honeycomb strength so 56kph frontal mode is better for the research of front side member characteristic.

To realize the YD 56kph frontal in component level, is we used 800kg rear half trolley. At the frontal center of barrier we attached YD's left frontal side member. We attached transmission with its linkage and subframe front mounting link because these have big influences to the member deformation in the real vehicle NCAP crash. as half rigid parts. We also attached 70mm distance the part of YD's crash box because too much hard contact can make some strain gauge noise peak value.

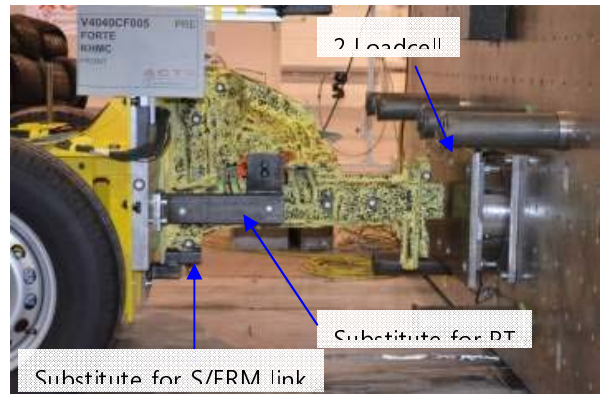


Fig.16. SEC2 calibration result of each strain gauges

It is well known fact when we should lessen the speed in the component level trolley test because the crushing energy is not absorbed by non-existing part. Experimentally we know in case of 56kph frontal, we use 35kph with same test weight for frontal member test. But in this test the trolley total weight was 940kg which is smaller than 1475kg of full car test and only left half hand side member was applied, we used 30.1kph after

calculating same energy. <sup>5)-6)</sup>

$$1/2m_1v_1^2 = 2 * 1/2m_2v_2^2 \quad m_1 = 1390 \quad v_1 = 35,$$

$$m_2 = 940 \quad \text{Then, } v_2 = 31\text{kph}$$

We also have the other experience, in case of frontal RCAR we use the same speed, 15kph at 70% mass. Even that is not full frontal mode, we know 30.1kph is appropriate number because 940kg is 64% of 1475kg.

At laser displacement measurement, we can know its dynamic peak collapsing was 352mm which is similar to acceleration calculation 372mm. When we compare the trolley x acceleration of the test with YD NHTSA official test x acceleration of rear side sill as a almost rigid part, those mode are similar at the 1st peak value.

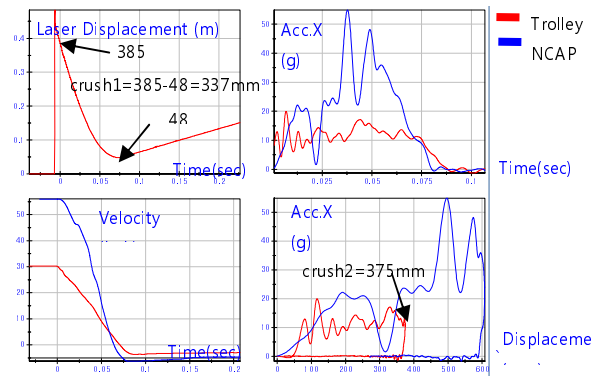


Fig.17. Member dynamic test characteristic

### 2.2.4 Measured and converted results in dynamic

By each trend line we did get the forces of the primary parts of frontal NCAP like the 2<sup>nd</sup> row of table.6.

Comparing the breakage force of powertrain mountings in the dynamic situation it seems to be needed 2.5~5 times more force to be broken.

Force	Eng Mt'g	TM Mt'g	FR MBR	
			SG5	SG6
Vehicle	6.9~7.3t	25t	19.7t	23.1t
MBR Dynamic	-	-	15.4t (Loadcell)	21.5t
Static Component	2.7t	5t	-	-

Table.6 Max Force results

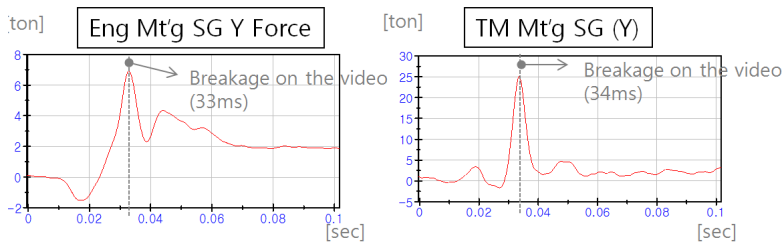


Fig.18. Powertrain breakage force converted from SG

For the member dynamic test, although we attached strain gauges in section1 and crash box there was no effective data but in section2 strain gauge 5 and 6 we got

some valuable results when we converted the voltage to the force by previous calibration equations. Especially in strain gauge6, the synchronization is almost perfect. The time based curve shape matching and peak value similarity prove this strain conversion is right. So we can know the section 2 peak force is 21.5 ton. The raw data of barrier load cell has some oscillating we applied CFC60. Because the load was measured in the barrier and the strain conversion to force is for the member section2, the peak values don't have to be same. As we see fig.14 these were the most sensitive strain gauge positions among all the section2 strain gauges.

For the NCAP test measurement, the Force shape is similar to member dynamic test fom 25ms but before 20ms there is no value. We think the force is distributed to other components like hood and fender so there is no value on SG6, even section 2 has some compressing force. As a result we were successful to measure only the 1<sup>st</sup> highest force 23.1t in the real crash. Even if member dynamic test is not perfect.

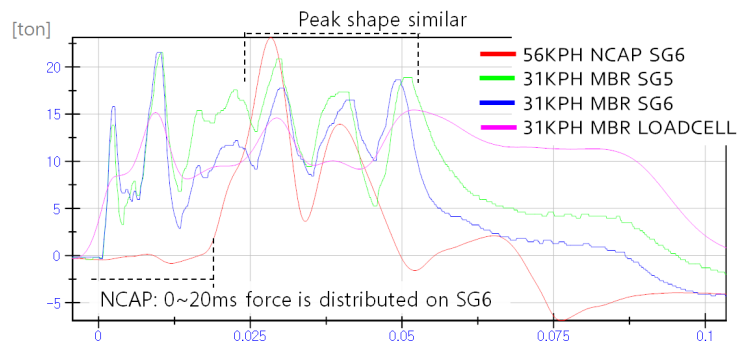


Fig.19. SG 5 and 6 Synchronization with load cell

### 3. Conclusion

As we discussed at the introduction, knowing the force of each part is very important. If we know, we can optimize the parts' weight and design for the good performance. To this time, those works were in the area of CAE but with this research we can also try more from test data. We expect test numbers frontal NCAP could be reduced half. For one vehicle development the developing cost saving would be over \$120,000. We are planning this methodology adaptation from PD project.

We reviewed the component test method of powertrain mountings and front side member with those characteristics. Also we found how to measure the real time force in powertrain mounting breakage tests and front side member dynamic crush test. The YD's chain cover breakage force in static test was about 3 ton and transmission 5 ton but 7ton and 25ton in dynamic. Front side member max force was 23.1t. These methods can be used in the full car crash tests.

If we stack these measurement and analyze we could

improve the prediction for the crash performance.

■ **Patent:** Be submitted "Powertrain load cell substitute"

### References

1. A. Muniappan, "Computational and Experimental Study on Lift Characteristics of Flapping Wing Micro Air Vehicle" MIT, 2006
2. P. K. C. Wood, " An Improved Test Procedure for Measurement of Dynamic Tensile Mechanical Properties of Automotive Sheet Steels" IARC, University of Warwick, 2007
3. P. K. C. Wood, " Characterising Dynamic Tensile Mechanical Properties of Automotive Materials at High Strain Rate" University of Warwick, 2007
4. Paul Lemmen, "Development of an Advanced Thorax / Shoulder Complex for the THOR Dummy" Paul Lemmen and Bernard Been, 2013
5. Karl Hoffmann, "Eine Einführung in die Technik des Messens mit Dehnungsmeßstreifen", Herausgeber: Hottinger Baldwin Messtechnik GmbH, Sarntadt
6. Herausgegeben von W.Beitz und K.-H., "DUBBEL TASCHENBUCH FÜR DEN MASCHINENBAU" 20. AUFLAGE

### ■ Author ■



Park Un-chin



Song Ha-jong



Kim Hyun-chul



Florian Ganz



Sudar Sankar



Mario Wohlfahrt

# The tracking method of vehicle point or dummy point in the vehicle crash by calculating linear accelerometer and angular velocity

Park Un-chin

Song Ha-jong\*

Kim Hyun-chul\*\*

Florian Ganz\*\*\*

Sudar Sankar\*\*\*

Christian Santos\*\*\*

## ABSTRACT

From the mathematical equations we can get the point coordinates with 3 axis linear accelerometer and 3 axis angular velocity by integration. In this research, we will introduce two unique algorithms-acceleration method and velocity method of Hyundai-Kia motors and ACTs and prove the accuracy from many kinds of dummy inboard or outboard tracking case and vehicle body point.

**Key Word** : Gyro, Tracking, Vehicle Crash, Dummy, accelerometer, angular velocity

## 1. Introduction

Target tracking is useful in the vehicle crash test analysis because we can check the contact of 2 objects and compare what is different on the moving among the several tests.

If we use video target tracking, it takes some more time than point tracking by calculating 3 axis linear accelerometer and 3 axis angular velocity because we should convert the high speed film file and analyze by video tracking program like TEMA. Also, the resolution of tracking data become lower because the resolution of high speed film is 1,000Hz and that of sensor data is 10,000 Hz. The most important thing is video target tracking time is restricted in case of the head tracking because the head is commonly covered by curtain airbag and passenger airbag by test modes or rotates so the target is untraceable.

But we cannot conclude the point tracking by calculating 3 axis linear accelerometer and 3 axis angular velocity is always more useful, because we cannot use it on the deforming area of crash vehicle. The vibration during the deformation makes a kind of noise so the calculation becomes inaccurate. Also there must be some tolerance in the calculation method. (IMU company says the maximum tolerance is about 12mm in case of frontal sled head tracking).<sup>1)-3)</sup>

So we should mix these two types of method for proper purpose. In this research we will introduce two unique algorithms-acceleration method and velocity method of Hyundai-Kia motors and ACTs. We need only

common 3 axis linear accelerometer and 3 axis angular velocity data and diadem software, not expensive sensor or software, so we believe this can be widely and easily used in crash analysis.

## 2. Main Subject

### 2.1 Theories and related formula in physics.

#### 2.1.1 The velocity relative to fixed system "S"

Considering two axis systems, "S" fixed to ground and "S'" moving relative to "S".

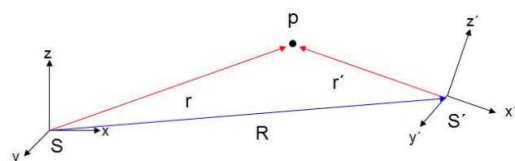
Considering a point in space, coordinates relative to the two systems are:

$$\text{To "S": } \vec{r} = x\vec{i} + y\vec{j} + z\vec{k} \quad (1)$$

$$\text{To "S'": } \vec{r}' = x'\vec{i}' + y'\vec{j}' + z'\vec{k}' \quad (2)$$

in velocity from position, the position must be differentiated through time.

$$\vec{v} = \frac{d\vec{r}}{dt} \quad (3)$$



To obtain the velocity relative to the fix systems "S",

\* Safety Performance Team 1 : Author or Co-Author

\*\* Crash Simulation Team : Co-Author

\*\*\* ACTS (Advanced Car Technology System) : Co-Author

the position has to be differentiated relative to the fix system "S".

$$(\vec{v})_s = \left( \frac{d\vec{r}'}{dt} \right)_s = \frac{dx'}{dt} \vec{i}' + \frac{dy'}{dt} \vec{j}' + \frac{dz'}{dt} \vec{k}' + x' \left( \frac{d\vec{i}'}{dt} \right)_s + y' \left( \frac{d\vec{j}'}{dt} \right)_s + z' \left( \frac{d\vec{k}'}{dt} \right)_s \quad (4)$$

The variation through time of the axis vectors represent the angular velocity of the axis. Therefore, the velocity of the point calculated relative to the fix system "S" is:

$$(\vec{v})_s = \left( \frac{d\vec{r}'}{dt} \right)_s + (\vec{\omega} \times \vec{r}') \quad (5)$$

To obtain the velocity variation through time of the axis vectors represent the angular velocity of the axis. Therefore, the velocity of the point calculated relative to the fix system "S" is:

$$(\vec{v})_s = \left( \frac{d\vec{R}}{dt} \right)_s + \left( \frac{d\vec{r}'}{dt} \right)_s + (\vec{\omega} \times \vec{r}') \quad (6)$$

But if S' is rotating in pitching sled, oblique or offset crash we should consider its velocity factor also.

$$(\vec{v})_s = \left( \frac{d\vec{R}}{dt} \right)_s + (\vec{\omega}' \times \vec{R}') + \left( \frac{d\vec{r}'}{dt} \right)_s + (\vec{\omega} \times \vec{r}') \quad (6')$$

### 2.1.2 The acceleration relative to fixed system "S"

To get acceleration, relative to the fix systems "S" the velocity has to be differentiated.

$$\vec{a} = \left( \frac{d\vec{v}}{dt} \right)_s = \left( \frac{d\vec{v}'}{dt} \right)_s + \left( \frac{d\vec{V}}{dt} \right)_s + \left( \frac{d(\vec{\omega} \times \vec{r}')}{dt} \right) \quad (7)$$

The third term differentiates as follows:

$$\begin{aligned} \left( \frac{d(\vec{\omega} \times \vec{r}')}{dt} \right) &= \left( \frac{d\vec{\omega}}{dt} \right)_s \times \vec{r}' + \vec{\omega} \times \left( \frac{d\vec{r}'}{dt} \right)_s = \left( \frac{d\vec{\omega}}{dt} \right)_s \times \vec{r}' + \vec{\omega} \times \left[ \left( \frac{d\vec{r}'}{dt} \right)_s + \vec{\omega} \times \vec{r}' \right] = \\ &= \left( \frac{d\vec{\omega}}{dt} \right)_s \times \vec{r}' + \vec{\omega} \times \left( \frac{d\vec{r}'}{dt} \right)_s + \vec{\omega} \times (\vec{\omega} \times \vec{r}') \end{aligned} \quad (8)$$

Remembering that from equation (5):

$$\left( \frac{d\vec{r}'}{dt} \right)_s = \left( \frac{d\vec{r}'}{dt} \right)_s + (\vec{\omega} \times \vec{r}')$$

Final acceleration relative to fixed system "S" is:

$$\vec{a} = \left( \frac{d\vec{V}}{dt} \right)_s + \left( \frac{d\vec{v}'}{dt} \right)_s + \left( \frac{d\vec{\omega}}{dt} \right)_s \times \vec{r}' + \vec{\omega} \times (\vec{\omega} \times \vec{r}') + 2\vec{\omega} \times \vec{v}' \quad (9)$$

Which is same as

$$\ddot{x}_{31} = \ddot{x}_{32} + \ddot{x}_{21} + \dot{\omega}_2 \times \vec{x}_{32} + \vec{\omega}_2 \times (\vec{\omega}_2 \times \vec{x}_{32}) + 2 \cdot \vec{\omega}_2 \times \dot{x}_{32} \quad (10)$$

### 2.1.3 Two methods - from velocity or acceleration

To obtain position from the velocity calculation, one integration must be done from equation (6). In case of a sled test, the calculated point acceleration has to be integrated two times (ax,ay,az) to obtain point position (x,y,z). Also sled acceleration has to be integrated one time to obtain sled velocity which is considered the moving system's velocity and angular velocity is given.

To obtain position from acceleration calculation, two integration must be done. in case of a crash test, the calculated point has to be integrated two times (ax,ay,az) to obtain point position (x,y,z). Sled acceleration does not need to be integrated. Angular velocity is given. Then, acceleration can be calculated from equation (8).

For velocity method calculation in a crash test, only one point acceleration needs to be integrated. In order to obtain position, one integration of the complete velocity needs to be done. Consequently 3 integrations are needed.

For acceleration method calculation in a crash test, only one point acceleration needs to be integrated. In order to obtain position, two integration of the complete velocity needs to be done. Consequently 4 integrations are needed.

Comparing these two method in a crash test, we can expect velocity method would be more accurate because its integration number are smaller one time.

For velocity method calculation in a sled test, point acceleration and sled acceleration needs to be integrated. In order to obtain position, one integration of the complete velocity needs to be done. Consequently 4 integrations are needed.

For acceleration method calculation in a sled test, only one point acceleration needs to be integrated. In order to obtain position, two integration of the complete velocity needs to be done. Consequently 4 integrations are needed.

Comparing these two method in a sled test, we can expect acceleration method would be more accurate because there is no integration of sled axis which has bigger value than the others.

### 2.2 How to insert channels in diadem macro

We should be careful about the polarity and each axis definition when we use this macro. The inserting

sequence can be list like Fig1.

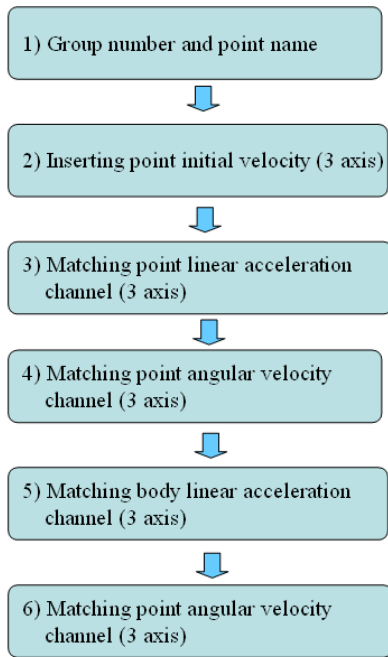


Fig.1 inserting sequence of the macro

Firstly, we should differentiate the group number and point name because when we do multi-calculation in one diadem file the previous calculation can be deleted unless we don't differentiate.

Secondly, we should insert point's 3 axis initial velocities because these are used to calculate the position. We should be careful for the macro unit, here we are using m/s, so NCAP x speed 56kph is 15.57 and Offset x speed 64kph is 17.78. The others be inserted as 0.

Thirdly, we should match the point's linear acceleration channels of 3 axis. We are using m/s<sup>2</sup> and the polarity is same as SAE1733's which deceleration is plus in case of dummy contact to front airbag.

Fourthly, we should match the angular velocity channels of 3 axis. We are using rad/s and the polarity is same as SAE1733's.

Fifthly, we should match the body linear acceleration channels of 3 axis. We are using m/s<sup>2</sup> and the polarity can be different by the case. In case of frontal sled test dummy head tracking the sled x axis pulse polarity is plus because when we compare and analyze it with video tracking the camera is onboard and it pushed the sled buck rear. In case of frontal crash test dummy head tracking the body x axis pulse polarity is minus because when we compare and analyze it with video tracking the camera is outboard and it pushed the car rear. If there is not y and z acceleration, we should match it with null channel which is automatically made by macro.

Sixthly, we should match the angular velocity channels of 3 axis. We are using rad/s and the polarity is same as

SAE1733's. This terms are from equation (6)' and used only for body rotating case like pitching sled, oblique or offset crash.

### 2.3 Usage and confirming accuracy

#### 2.2.1 Head tracking in YD NCAP sled and crash case

To confirm the accuracy, we chose YD US NCAP sled and crash case.

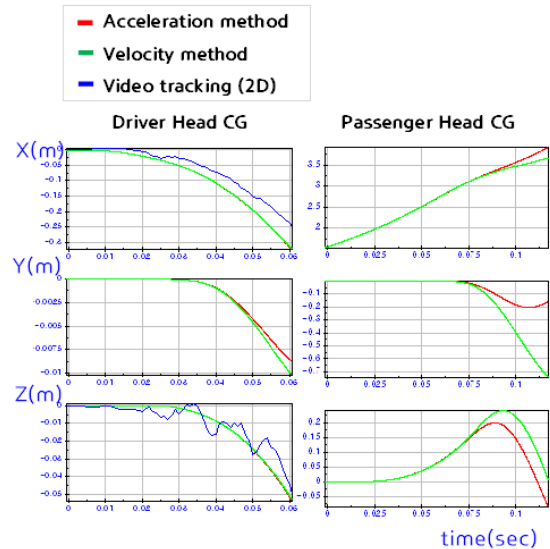


Fig.2 Head target tracking result in YD NCAP sled

When we review the sled target tracking, the acceleration method is very close to the velocity method till 100ms. But in case of passenger dummy the difference between them goes bigger (over 25cm), we can guess it comes from angular velocity tolerance which is 0.5°/sec in H3 50% percentile dummy but of 5°/sec in H3 5% percentile(10 times bigger tolerance).

The comparison with 2D video target tracking was not successful because there was big oscillation on the sled onboard camera. We compare it only for the driver.

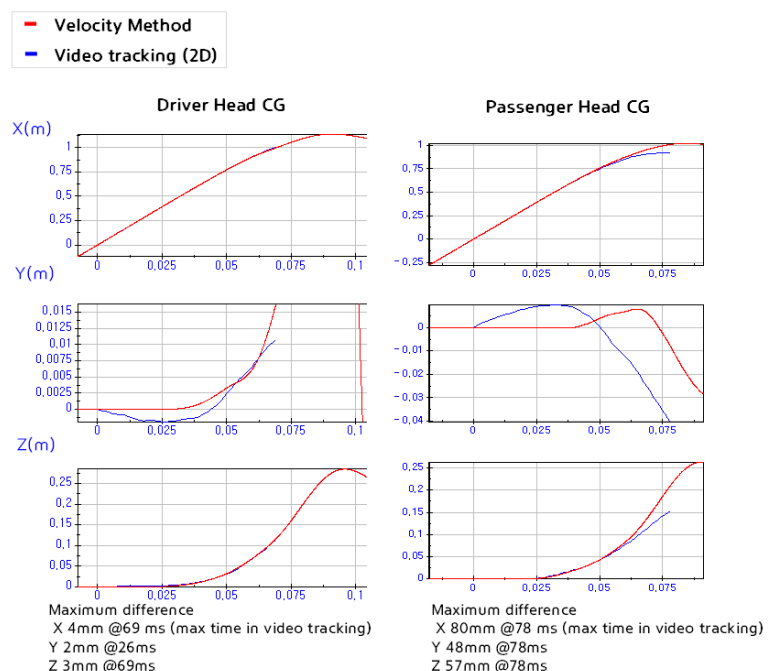


Fig.3 Head target tracking result in YD NCAP crash

In NCAP crash the comparison with 2D video target tracking was successful. The maximum tracking difference was 4mm below in driver. But in case of passenger it was much higher than driver, we guess this comes from also angular velocity tolerance which is 0.5°/sec in H3 50% percentile dummy but of 5°/sec in H3 5% percentile(10 times bigger tolerance).

Now the thinking in 2.1.3 that " we can expect acceleration method would be more accurate because there is no integration of sled axis which has bigger value than the others." in not so meaningful because the tolerance is too low in comparison with video tracking.

Comparison between sled and crash is not meaningful because sled test was done just as a base to confirm measuring method so we skip it here.

**2.2.2 YD smalloverlap trolley ACU tracking case**

In HKMC research with ACTs, we make YD smalloverlap trolley test for chassis and structure evaluation and its realization was quite close to the real crash. <sup>6)</sup>



Fig.4 YD smalloverlap trolley video@330ms

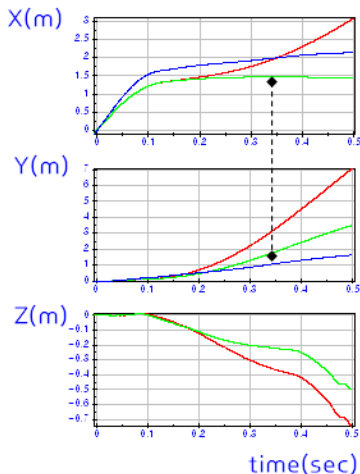


Fig.5 YD smalloverlap ACU position tracking

In this test, we attached 3 axis linear accelerometer and 3 axis angular velocity sensor to ACU (airbag control unit) position. Like NCAP sled head tracking result, acceleration method and velocity method tracking is close each other in 100ms but it becomes far. When we checked the video ACU position roughly which is possible to check to the time 330ms they matches to the tracking value x:1.5m and y:1.5m. We added similar place video tracking (cowl top tracking) in the graph, it is similar to the velocity tracking. So we can confirm the thinking in 2.1.3 that "we can expect velocity method would be more accurate because its integration number are smaller one time."

**2.2.3 YD IIHS side trolley CG tracking case**

In HKMC research with ACTs, we make YD IIHS side trolley test for the side structure evaluation and its realization was quite close to the real crash.



Fig.6 YD IIHS side trolley video@240m

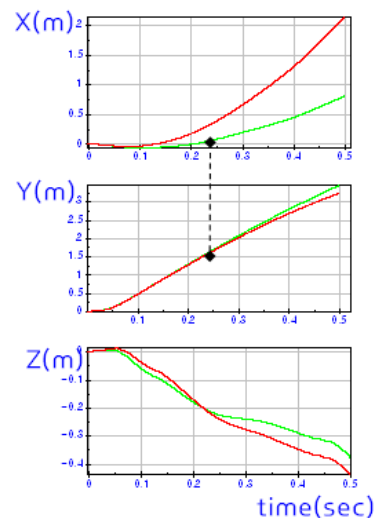


Fig.7 YD IIHS side trolley CG position tracking

In this test, we attached 3 axis linear accelerometer and 3 axis angular velocity sensor to trolley CG. Like NCAP

sled head tracking result, acceleration method and velocity method tracking is close each other in 100ms but it becomes far. When we checked the video CG position roughly which is possible to check to the time 240ms they matches to the tracking value x:0.1m and y:1.7m. There was no good video tracking position close to the trolley so we skipped to compare with video tracking. But we can confirm the thinking in 2.1.3 that "we can expect velocity method would be more accurate because its integration number are smaller one time."

#### 2.2.4 YD US NCAP crash ACU tracking case

For more usage, in HKMC research with ACTs, we run the YD NCAP crash test with 3 axis linear accelerometer and 3 axis angular velocity sensor to ACU position



Fig.8 YD NCAP ACU video@200m

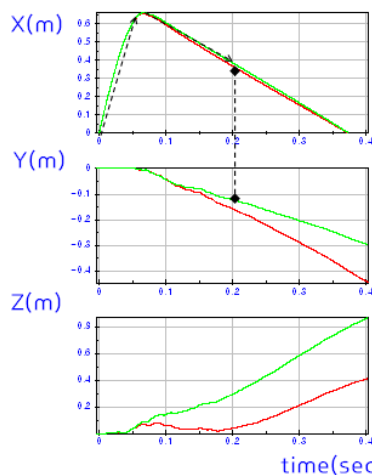


Fig.9 YD NCAP ACU position tracking

In this test, like NCAP sled head tracking result, acceleration method and velocity method tracking is close each other in 100ms but it becomes far. When we checked the video ACU position roughly which is possible to check to the time 200ms they matches to the tracking value x: once maximum 0.7m and rebound to 0.4m and y:0.12m. There was no good video tracking position close to the trolley so we skipped to compare with video tracking. But we can confirm the thinking in 2.1.3 that "we can expect velocity method would be

more accurate because its integration number are smaller one time."

### 3. Conclusion

As we discussed target tracking by calculating sensors is very useful in the vehicle crash test analysis because we can check the invisible area also. Now we developed HKMC and ACTs' unique calculating algorithm by the physical points moving vector equation. We did know below facts in this research.

- 1) The acceleration method is very close to the velocity method till 100ms.
- 2) The accuracy of velocity method was in 4mm in NCAP crash test H3 50% driver head tracking.
- 3) In case of passenger dummy the difference between them goes bigger (over 25cm), we can guess it comes from angular velocity tolerance which is  $0.5^\circ/\text{sec}$  in H3 50% percentile dummy but of  $5^\circ/\text{sec}$  in H3 5% percentile (10 times bigger tolerance).
- 4) For the body point tracking, only velocity method was accurate because its integration number are smaller one time than acceleration method.

■ Patent No. : Be submitted Diadme macro target tracking by 3 axis accelerometer and 3 axis angular velocity sensor

### References

1. Peter Björkholm, "Inertial Navigation of Crash Dummies Phase II", Imego 2011
2. Sangram Redkar, "USING INERTIAL MEASUREMENT TO SENSE CRASH-TEST DUMMY KINEMATICS" Arizona State University, 2010
3. Wolfgang Sinz. Simulation Based Analysis of Test Results Graz University of Technology, 2010
4. Karl Hoffmann, "Eine Einführung in die Technik des Messens mit Dehnungsmeßstreifen", Herausgeber: Hottinger Baldwin Messtechnik GmbH, Sarntadt
5. Herausgegeben von W.Beitz und K.-H., "DUBBEL TASCHENBUCH FÜR DEN MASCHINENBAU" 20. AUFLAGE
6. Park Un-chin "The trolley test way of IIHS small overlap and side test with minimized structure usage", HKMC, 2014

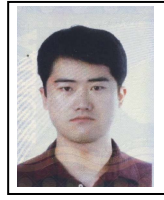
■ Author ■



Park Un-chin



Song Ha-jong



Kim Hyun-chul



Florian Ganz



Sudar Sankar



Christian Santos

# **OBJECTIVE EVALUATION METHOD OF VEHICLE CRASH PULSE SEVERITY IN FRONTAL NEW CAR ASSESSMENT PROGRAM (NCAP) TESTS**

**Chung-Kyu Park**

**Cing-Dao (Steve) Kan**

Center for Collision Safety and Analysis, George Mason University  
USA

Paper Number 15-0055

## **ABSTRACT**

In this study, the available metrics for evaluating the crash pulse severity are reviewed and their accessibility is evaluated by using the frontal New Car Assessment Program (NCAP) test data. The linear regression analysis and sled test simulations are conducted. The new approach is proposed to evaluate the full vehicle crash performance by quantifying the crash pulse severity and restraint system performance separately and objectively.

## **INTRODUCTION**

The safety of occupants in a vehicle crash is highly dependent on the performance of vehicle structure and occupant restraint system. In vehicle crash safety, the role of a vehicle structure is absorbing crash energy efficiently as well as protecting the integrity of the occupant compartment. In general, the performance of vehicle structure is described by the occupant compartment intrusion and vehicle crash pulse. Basically, the occupant restraint system is designed based on the performance of the vehicle structure. So, it is desirable to evaluate the performance of vehicle structure objectively and quantitatively.

In frontal vehicle crash tests, occupant compartment intrusion and vehicle crash pulse are the most fundamental responses of a vehicle's structure. The occupant compartment intrusion is considered as an objective metric for quantifying the deformation severity of a vehicle structure. In general, a large compartment intrusion increases the injury probability of lower extremity of occupants. The vehicle crash pulse is the time history of vehicle acceleration and is used to calculate the changes of velocity and dynamic crush of a vehicle by integration. The vehicle crash pulse is closely related to the head and chest injuries of occupants. However, the severity of the vehicle crash pulse is difficult to be quantified objectively because the injury responses of dummy head and chest are also closely associated with restraint system performance. The crash pulse severity should be an objective measure of how severely the vehicle crash pulse has an effect on the occupant injury. Basically, it is regarded that less severe crash pulses possibly lead to less severe occupant injury.

Recently, there have been many vehicle safety research activities by re-designing current vehicles. For example, a current vehicle is light-weighted by using light-weight materials, and enforced structurally to meet the requirements of new regulatory tests (e.g. IIHS small-overlap frontal test and NHTSA oblique frontal test). When a current vehicle is re-designed, its crash pulse is changed accordingly and existing restraint system is not performing as it was designed any more. Then, it is difficult to conclude how its crash performance gets better or worse than the original one, especially in terms of crash pulse.

Many metrics were introduced and utilized to evaluate the severity of vehicle crash pulse [1-11]. Those metrics are derived from vehicle crash pulse in the frontal impact and can be categorized into 4 groups in the way of how occupant responses are considered. However, their assessability of the crash pulse severity is still uncertain. The objective of this study is to evaluate the assessability of available metrics for quantifying vehicle crash pulse severity in front crash. The vehicle crash pulses of the front New Car Assessment Program (NCAP) tests are utilized. Also, a new approach to evaluate the full vehicle crash performance is proposed.

## **REVIEW OF EXISTING METRICS**

In this study, some of existing metrics for evaluating vehicle crash pulses in frontal vehicle crash are reviewed. The existing metrics can be categorized into four groups: (1) metrics based on vehicle crash pulse only, (2) metrics based on vehicle crash pulse with assumed occupant response, (3) metrics based on vehicle crash pulse with actual

occupant response, and (4) combined metrics with the aforementioned metrics. The velocity  $v(t)$  and displacement  $d(t)$  are obtained by integration and double integration of the acceleration  $a(t)$ , respectively.

### Category1: Metrics Based on Vehicle Crash Pulse Only

In the category1, the metrics are obtained from the vehicle crash pulse only. Dummy responses in the test are not considered. Therefore, these metrics are independent of occupant restraint system and represent an objective, quantified value of the vehicle crash pulse. However, they can hardly predict dummy responses.

- **Maximum acceleration**  $(a)_{\max}$  is simply the maximum value of a vehicle acceleration curve over the duration of the crash event.
- **Moving average acceleration**  $(\bar{a})^{\Delta t}$  is calculated as

$$(\bar{a})^{\Delta t} = \frac{1}{\Delta t} \int_t^{t+\Delta t} a(\tau) d\tau, \quad (1)$$

where  $t$  is time and  $\Delta t$  is a moving time interval. If  $\Delta t$  is the duration of the crash event, the moving average acceleration becomes the average acceleration. The upper bar indicates the average value. In general, **maximum moving average acceleration**  $(\bar{a})_{\max}^{\Delta t}$  is used.

- **Delta-V**  $\Delta V$  is the total vehicle velocity change over the duration of the crash event, as expressed by

$$\Delta V = (v)_{t=0} - (v)_{\min}. \quad (2)$$

- **Time To Zero Velocity** (TTZV)  $(t)_{v=0}$  is the time when vehicle velocity becomes zero.
- **Maximum dynamic displacement**  $(d)_{\max}$  is simply the maximum value of a vehicle displacement curve over the duration of the crash event.

### Category2: Metrics Based on Vehicle Crash Pulse with Assumed Occupant Response

In the category2, an occupant restraint system is assumed and the metrics are derived from the dummy responses with the assumed restraint system under a given vehicle crash pulse. So, these metrics are independent of actual dummy responses in tests, but they are dependent on a virtual, uniform restraint system. Hence, they represent the objective quantified value of vehicle crash pulse and can predict dummy responses.

In general, the vehicle crash model and the restraint system are simplified in the category2. The common simplified model is a Spring-Mass (SM) system as shown in Figure1. In the SM model, the occupant is assumed as a point mass and the restraint system is a simple spring system. Subscripts  $V$  and  $O$  stand for vehicle and occupant, respectively.  $M$  is the vehicle mass,  $m$  is the occupant mass,  $k$  is the spring stiffness, and  $\delta$  is the initial slack between the occupant and restraint system. The upper wave indicates the prescribed motion which is a given vehicle crash pulse. In the actual crash test, the spring is highly nonlinear to represent the operation of seatbelt and airbag.

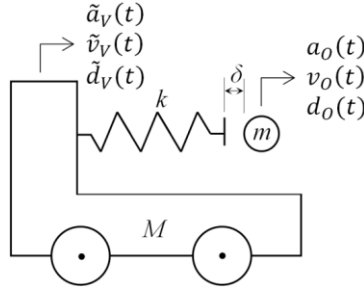


Figure1. The model of a simple Spring-Mass (SM) system.

- The Equation Of Motion (EOM) of the SM model is defined as

$$a_o(t) + \omega_n \cdot d_o(t) = \tilde{a}_v(t), \quad (3)$$

where  $\omega_n = \sqrt{k/m}$ . The analytical solution of the EOM  $a_o^{SM}$  is in the form of the convolution integral expressed as

$$a_o^{SM}(t) = v_v(0) \cdot \omega_n \int_0^t \tilde{a}_v(\tau) \cdot \sin\{\omega_n(t - \tau)\} d\tau. \quad (4)$$

- In the flail-space model [1], the spring stiffness  $k$  is assumed to be zero, which indicates that no restraint system is present. So, the occupant moves freely. The allowable moving distance of the point mass is assumed to be 0.6 m. At the instant of occupant impact with the occupant compartment interior, the largest difference in velocity is termed the Occupant Impact Velocity (OIV). Once the impact with the interior occurs, the occupant is assumed to remain in contact with the interior and to be subjected to any subsequent vehicular acceleration.

Figure2 shows the velocity curves in a frontal NCAP test. The black curve is the test vehicle velocity and the red curve is the test occupant (chest) velocity. The occupant is restrained by a certain restraint system. In special cases, it can be assumed that the occupant velocity is prescribed, like the blue dot curve in Figure2, by a special restraint system. In this special case, the occupant translates freely with the initial velocity  $v_o(0)$  until the point A. The point A represents the distance of the initial slack  $\delta$ . This phase is called free flight. After reaching the point A, the occupant is decelerating with a constant acceleration  $a_o$  until it reaches the point B. At the point B, the relative velocity  $v_{o/V}$  of the occupant to the vehicle becomes zero. This phase between the point A and the point B is called ideal restraint because the occupant has the constant minimum acceleration under a given crash pulse. So, this prescribed occupant velocity is the ideal velocity of the occupant in frontal crash and this special restraint system can be considered as the ideal restraint system. Compared to the SM model, the spring stiffness  $k$  will be nonlinear to maintain the constant deceleration of the occupant.

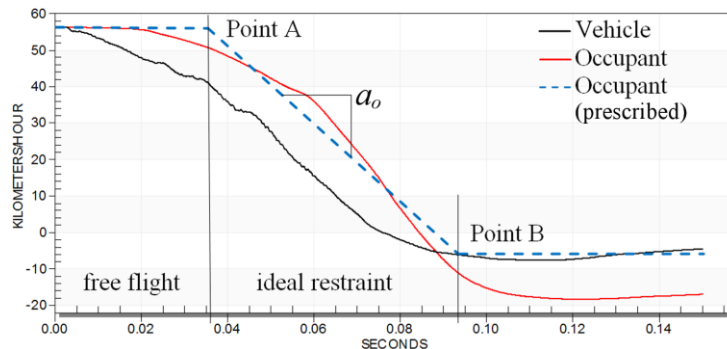


Figure2. Prescribed occupant response in the NCAP test.

- In the **Occupant Load Criterion** (OLC) metric [2], it is assumed that the initial slack  $\delta$  is 65 mm and the distance between the vehicle and the occupant at the point B is an additional 235 mm. Then, given the point A and the point B, the constant acceleration  $a_o$  becomes the critical occupant response which is called the OLC (G). Basically, the OLC means the minimum occupant acceleration induced by a given crash pulse under the protection of the ideal restraint system.
- In the **Maximum Chest Travel** (MCT) metric [3], it is assumed that the initial slack  $\delta$  and the constant acceleration  $a_o$  are predefined. Then, the distance between the point A and the point B is the critical occupant response. This distance is called the MCT (mm).

### Category3: Metrics Based on Vehicle Crash Pulse with Actual Occupant Response

In the category3, metrics are obtained from both vehicle crash pulse and actual dummy responses in the test. The metrics are dependent on the dummy responses and restraint system performance in tests. Basically, those metrics identify the contribution of restraint system performance to the full vehicle crash performance. So, they quantify the vehicle structure performance in terms of crash pulse and the restraint system performance, but they are not the objective, quantified value. In general, they are in percentage terms.

- Occupant restraint performance during vehicle deceleration is measured as the relative velocity of the occupant in vehicle divided by the maximum velocity change of the vehicle which is  $\Delta V$ . This ratio is called the **Restraint Quotient** (RQ) [4] expressed as

$$RQ_C = \frac{v_{OC/V}}{\Delta V}, \quad (5)$$

where

$$v_{OC/V} = v_{OC} - v_V \quad (6)$$

and the subscript  $C$  stands for chest. It normally varies between 0 and 1. A RQ value of 0 represents an occupant rigidly coupled to the vehicle interior and a value of 1 indicates that the occupant attains the total velocity change of the vehicle before impacting the vehicle interior. The lower the RQ, the better the restraint performance in a crash. The relative kinetic energy per unit mass is calculated using the maximum relative occupant velocity normalized by a velocity of 5 m/s, which is called **kinetic energy factor** ( $E$ ) [4] expressed as

$$E_C = \frac{(v_{OC/V})_{\max}^2}{5^2}. \quad (7)$$

- In the SM model in Figure1, the energy per unit mass (or energy density) of an occupant can be expressed as

$$e = \int_0^{d_v} a_o(x) dx_o = \int_0^{d_v} a_o(x) d(x_V + x_{O/V}) = e_{rd} + e_{rs}, \quad (8)$$

where

$$e_{rd} = \int_0^{d_v} a_o(x) dx_V, \quad (9)$$

$$e_{rs} = \int_0^{d_v} a_O(x) dx_{O/V} , \text{ and} \quad (10)$$

$$x_{O/V} = x_O - x_V . \quad (11)$$

$e_{rd}$  is called the ride-down energy density and  $e_{rs}$  is the restraint energy density [5-10]. The ride-down energy is attributed to the crush of the front structures of the car and the restraint energy is dissipated by the crushing of the restraint system components. Then, the ride-down efficiency  $\mu$  is obtained from

$$\mu = \frac{(e_{rd})_{\max}}{\{v(0)\}^2/2} . \quad (12)$$

This metrics reflect the percentage of total kinetic energy absorbed by the vehicle structure.

#### Category4: Combined Metrics Using the Aforementioned Metrics

In the category4, the metrics are defined as the linear combination of the aforementioned metrics. Mostly, certain metrics are combined to improve better prediction of occupant injury.

- In the Expanded  $\Delta V$  [11],  $\Delta V$  is expanded by combining with other metrics. Three expanded  $\Delta V$  metrics were proposed as

$$\text{Expanded } \Delta V-1 = a_1 \Delta V + a_2 \mu + a_3 E_c , \quad (13)$$

$$\text{Expanded } \Delta V-2 = a_1 \Delta V + a_2 (\bar{a})_{\max}^{\Delta t} + a_3 RQ_c , \quad \text{and} \quad (14)$$

$$\text{Expanded } \Delta V-3 = a_1 \Delta V + a_2 (\bar{a})_{\max}^{\Delta t} + a_3 E_c , \quad (15)$$

where  $a_1, a_2$ , and  $a_3$  are coefficients.

- In the OLC++ [2], OLC was augmented as

$$\text{OLC++} = a_1 \text{OLC} + \frac{a_2}{(t)_{v=0}} + a_3 (\bar{a})_{\max}^{\Delta t} , \quad (16)$$

where  $a_1, a_2$ , and  $a_3$  are coefficients.

#### DATA ANALYSIS

The aforementioned metrics' assessability of crash pulse severity is evaluated using frontal NCAP test data. A total of 60 frontal NCAP test data, collected from the MY 2012 vehicle test program, are analyzed. The linear regressions of each pair of all metrics and their  $R^2$  values are examined. The larger value of  $R^2$  indicates better fits. It is considered that the pair of two metrics has a linear correlation if the  $R^2$  is greater than 0.5.

It seems that the metrics in Category2 are the fairly appropriate metrics for evaluating the crash pulse severity since they are the objective metrics associated with both vehicle crash pulse and uniform restraint system. So, the relationship between the metrics in Category2 and other metrics are investigated.

Table1 summarizes the linear regression results between Category1 and Category2. The  $R^2$  values of each pair are shown in Table1. It is observed that the OLC and MCT have relatively high  $R^2$  values with maximum acceleration,

maximum moving average acceleration, TTZV, and maximum dynamic crush. However, OIV has low  $R^2$  values. Especially, Delta-V has very low  $R^2$  values with OLC and MCT. Interestingly, although the metrics in Category1 are purely obtained from vehicle crash pulse only without dummy response information, the metrics in Category1 have a good linear correlation with the OLC and MCT in Category2.

**Table1. Linear regression results between Category1 and Category2 (highlighted cell indicates that  $R^2$  is greater than 0.5).**

$R^2$	OIV	OLC	MCT
Max. Accel.	0.214	0.527	0.445
Max. Moving Average Accel. ( $\Delta t=25\text{msec}$ )	0.477	0.735	0.607
Delta-V	0.395	0.002	0.029
TTZV	0.281	0.859	0.793
Max. Dynamic Crush	0.051	0.678	0.704

Table2 summarizes the linear regression results between Category2 and Category3. It is observed that the OLC and MCT have high  $R^2$  values with the metrics in Category3, but OIV has very low  $R^2$  values. Basically, the metrics in Category3 describe the actual effects of the vehicle crash pulse and restraint system on the dummy responses in the test. So, the high linear correlation between OLC and MCT in Category2 and the metrics in Category3 indicates that the OLC and MCT are able to predict the effect of the vehicle crash pulse on the dummy response and assess the crash pulse severity adequately.

**Table2. Linear regression results between Category2 and Category3 (highlighted cell indicates that  $R^2$  is greater than 0.5).**

$R^2$		OIV	OLC	MCT
Driver	RQ <sub>c</sub>	0.051	0.669	0.679
	E <sub>c</sub>	0.098	0.705	0.680
	Ride-Down Efficiency	0.058	0.617	0.624
Passenger	RQ <sub>c</sub>	0.056	0.515	0.504
	Ride-Down Efficiency	0.120	0.474	0.447

Table3 summarizes the linear regression results between the aforementioned metrics and dummy injuries in the NCAP tests. It is observed that the  $R^2$  values of all pairs between metrics and dummy injuries are very low. The Delta-V is commonly used to address the crash severity, but it can hardly predict the dummy injuries as well.

**Table3. Linear regression results between metrics and occupant injury responses.**

$R^2$	Driver (H3 50% male)			Passenger (H3 5% female)			
	HIC <sub>15</sub>	Chest Peak Accel.	Chest Peak Deflection	HIC <sub>15</sub>	Chest Peak Accel.	Chest Peak Deflection	
Max. Accel.	0.000	0.043	0.057	0.003	0.125	0.015	
Max. Moving Average Accel. ( $\Delta t=25\text{msec}$ )	0.002	0.139	0.064	0.013	0.284	0.005	
$\Delta V$	0.003	0.007	0.019	0.005	0.001	0.055	
TTZV	0.005	0.101	0.060	0.018	0.339	0.016	
Max. Dynamic Crush	0.022	0.055	0.036	0.017	0.224	0.025	
OIV	0.023	0.070	0.039	0.001	0.186	0.002	
OLC	0.014	0.090	0.023	0.026	0.342	0.005	
MCT	0.021	0.075	0.016	0.026	0.305	0.012	
Driver	RQ <sub>c</sub>	0.009	0.086	0.056	0.028	0.178	0.069
	E <sub>c</sub>	0.013	0.084	0.044	0.030	0.196	0.042
	Ride-Down Efficiency	0.010	0.113	0.052	0.052	0.201	0.081
Passenger	RQ <sub>c</sub>	0.002	0.036	0.034	0.026	0.109	0.075
	Ride-Down Efficiency	0.001	0.106	0.067	0.020	0.137	0.120
Expanded $\Delta V$ -1	0.012	0.082	0.037	0.024	0.192	0.030	
Expanded $\Delta V$ -2	0.005	0.110	0.053	0.022	0.220	0.042	
Expanded $\Delta V$ -3	0.010	0.096	0.043	0.025	0.217	0.030	
OLC++	0.014	0.092	0.043	0.019	0.310	0.010	

Based on the linear regression of the metrics shown in Table1 and Table2, it is found that some of metrics fairly can assess the crash pulse severity. Especially, it seems that the OLC has the high accessibility of crash pulse severity according to its high linear correlation to many metrics in Category1 and Category3. However, none of metrics can predict dummy injuries. Every vehicle has its own uniquely designed restraint system, and the dummy responds very

sensitively to various restraint system performances. Moreover, crash tests have very high dispersion errors in dummy injuries in general. In these circumstances, it is very difficult to predict dummy injuries in frontal crash using existing metrics.

### SLED TEST SIMULATIONS

In order to identify the effect of vehicle crash pulse and restraint system on dummy responses, sled test simulations with Hybrid III 50th male dummy FE model are conducted using all different 60 NCAP crash pulses. Two cases are considered for each sled test simulation; (1) fix dummy clearance dimensions and (2) adjust some of dummy clearance dimensions, such as CS (chest to steering hub), SCA (steering column angle), and KD (knee to dash). The uniform generic restraint system (seatbelt and airbag) is utilized for all sled test simulations. The dummy responses in sled test simulations are monitored.

Figure3 shows the linear regressions of chest peak accelerations in NCAP tests and sled test simulations. They show little correlation between two tests. Since the sled test simulations utilize the NCAP crash pulses, main difference between two tests is that all the different restraint systems are used in NCAP tests and one uniform restraint system is used in sled test simulations. It can be interpreted as the data dispersion is mainly caused by the various restraint system performances in the NCAP test vehicles.

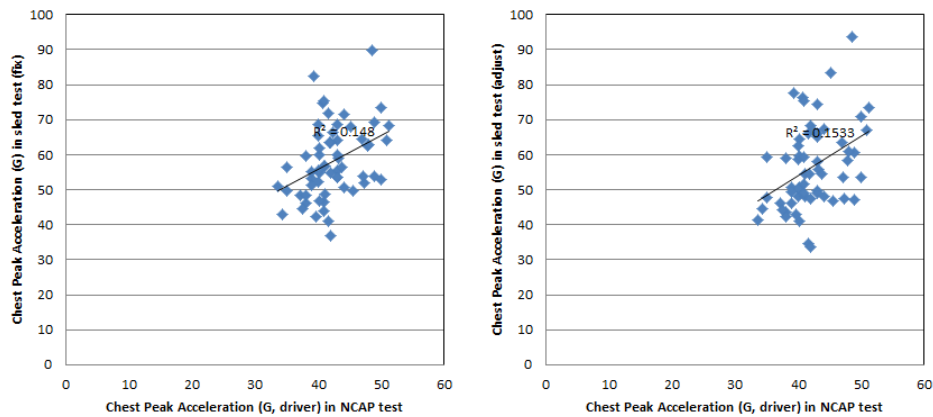


Figure3. Data distribution of chest peak acceleration in NCAP tests vs. chest peak acceleration in sled test simulations

Figure4 shows the linear regressions of chest peak accelerations in sled test simulations and the OLC metric. They show high correlation between two metrics. In other words, the OLC metric is able to predict dummy responses and injuries if the uniform restraint system is used in all test vehicles. Also, it can be observed that the different dummy clearance dimension makes the degree of data dispersion increase, but the linear correlation is still high.

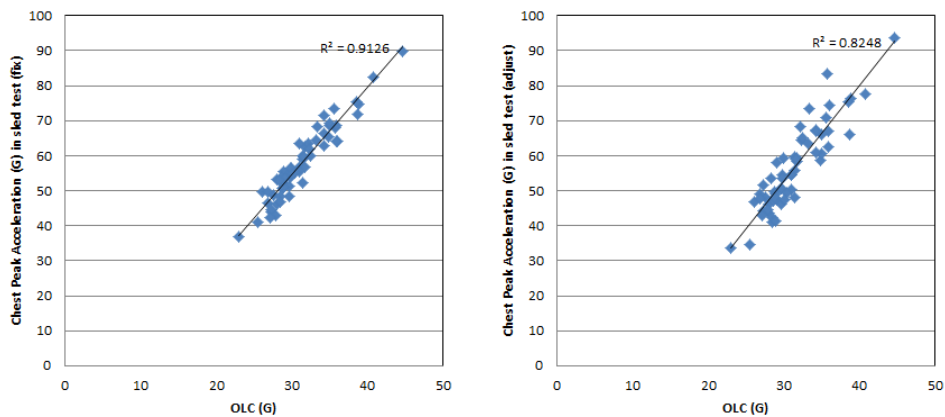


Figure4. Data distribution of OLC vs. chest peak acceleration in sled test simulations

## DISCUSSION

It seems that the Category3 provide an ideal approach to evaluate a full vehicle crash performance by quantifying both the vehicle structure performance and restraint system performance separately, where the vehicle structure performance includes only the crash pulse severity, but not the occupant compartment intrusion. However, the metrics in the Category3 are objective. The performance of the restraint system in vehicles are various in frontal crash tests. Moreover, the restraint system performance is dependent on the crash pulse severity, which means that the restraint system performance is coupled with crash pulse severity. So, it is difficult to quantify the restraint system performance objectively by de-coupling from the effect of a vehicle crash pulse. In this study, a new approach is proposed to evaluate the full vehicle crash performance by quantifying the crash pulse severity and restraint system performance separately and objectively. The new approach makes the restraint system performance de-coupled from the effect of the vehicle crash pulse.

Figure5 shows the three datasets of occupant chest peak accelerations with respect to maximum moving average acceleration of vehicles. The first dataset, red squares, is the OLC values. This dataset shows good linear correlation with high  $R^2$  value. Basically, the OLC metric indicates the minimum occupant acceleration under a given crash pulse. Therefore, the OLC data forms the lower boundary in Figure5. The second dataset, green triangles, is the occupant peak accelerations obtained from the analytical solution (Eq. 4) of the SM model with the constant spring stiffness  $k$ . This dataset also shows good linear correlation with high  $R^2$  value. Because the restraint system is regarded as a simple linear spring, the occupant response in the SM model under a given crash pulse is likely worse than the one with actual restraint system. Maybe the occupant response in the SM model with the linear spring will be the worst under the given crash pulse. Hence, it can be seen that the occupant peak acceleration in the SM model forms the upper boundary in Figure5. The linear regression slopes of two datasets (red squares and green triangles) are actually very close. So, the OLC metric with respect to maximum moving average acceleration of vehicles is considered as the crash pulse severity metric and the crash pulse severity index is defined by normalizing the crash pulse severity metric.

In Figure5, the third dataset, blue rhombuses, is the chest peak accelerations (driver) in the frontal NCAP tests. These data points are distributed between the lower and upper boundaries formed by two datasets (red squares and green triangles). Some data points are close to the lower or upper boundaries, that is, those data points are close to their minimum or maximum values in their crash pulse severity levels. The rational explanation of the data dispersion between two boundaries is because the different restraint system performance in every vehicle in the frontal NCAP tests. So, in order to de-couple the restraint system performance from the crash pulse effect, the third dataset is mapped to the OLC-axis plane and normalized to generate the restraint system performance index.

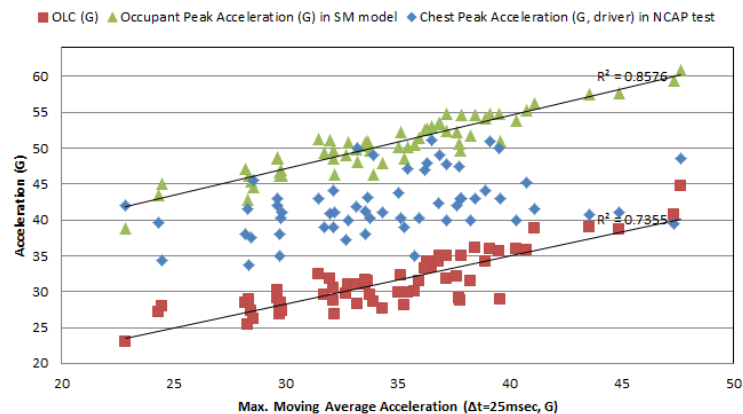


**Figure5. Data distribution of max. moving average acceleration vs. OLC, occupant peak acceleration in SM model, and chest peak acceleration (driver) in NCAP test.**

The crash pulse severity index and restraint system performance index are objective and independent each other. Two indices describe the full vehicle crash performance in the frontal NCAP test. Figure6 shows the data distribution of the full vehicle crash performance in two indices plane, which is very informative. For instance, the point A in Figure6 means low crash pulse severity but poor restraint system performance, and the point B indicates

high crash pulse severity but good restraint system performance. Practically, when the vehicle crash pulse is known, the plot in Figure5 shows the crash pulse severity and the range of the dummy chest peak acceleration, and the plot in Figure6 tells the performance of the current vehicle's restraint system in the frontal crash.

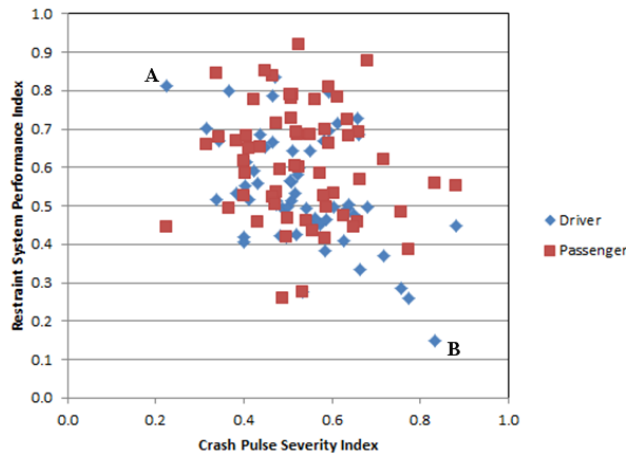


Figure6. Data distribution of crash pulse severity index vs. restraint system performance index.

## CONCLUSIONS

In this study, the existing metrics for evaluating the crash pulse severity are reviewed and categorized into four groups: (1) metrics based on vehicle crash pulse only, (2) metrics based on vehicle crash pulse with assumed occupant response, (3) metrics based on vehicle crash pulse with actual occupant response, and (4) combined metrics with the aforementioned metrics.

Their accessibility of crash pulse severity is evaluated by using the frontal NCAP test data. A total of 60 frontal NCAP test data, collected from the MY 2012 vehicle test program, are analyzed. The linear regression analysis shows that some of metrics fairly can assess the crash pulse severity. Especially, it seems that the OLC has the high accessibility of crash pulse severity according to its high linear correlation to many metrics in Category1 and Category3. However, none of metrics can predict dummy injuries.

The sled test simulations are conducted using the NCAP pulses. The uniform generic restraint system (seatbelt and airbag) is utilized for all sled test simulations. The results conclude that the various restraint system performances in the NCAP test's vehicles cause a big variation in dummy responses and make it difficult to predict dummy injuries in the frontal NCAP test.

The new approach is proposed to evaluate the full vehicle crash performance in the frontal NCAP test by quantifying the crash pulse severity and restraint system performance separately and objectively. The crash pulse severity index is defined by normalizing the OLC metric, and then the restraint system performance index is defined by decoupling the restraint system performance from the crash pulse effect. Two indices describe the full vehicle crash performance in the frontal NCAP test. The new approach provides a quantitative and objective way to analyze the crash performance of a vehicle in the frontal NCAP test.

## ACKNOWLEDGEMENTS

The authors are grateful to Eun-Young Kim for data processing.

## REFERENCES

- [1] J.D. Michie, "Collision risk assessment based on occupant flail-space model," *Transportation Research Record*, 1981, 796:1-9.

- [2] L. Kübler, S. Gargallo, and K. Elsäßer, "Frontal crash pulse assessment with application to occupant safety," *ATZ worldwide*, 2009, 111(6):12-17.
- [3] S.J. Song, S. Kim, and S. Bilkhu, "Front impact pulse severity assessment methodology," SAE Technical Paper #2005-01-1416.
- [4] D.C. Viano and S. Arepally, "Assessing the safety performance of occupant restraint systems," SAE Technical Paper #902328.
- [5] H. Katoh and R. Nakahama, "A study on the ride-down evaluation," *Experimental Safety Vehicles, Proceeding of the 9<sup>th</sup> International Technical Conference on Experimental Safety Vehicles*, pp. 190-195, 1982.
- [6] N.C. Evans, L.M. Furton, and D.A. Cok, "Occupant energy management technique for restraint system analysis and design – theory and validation," SAE Technical Paper #922082.
- [7] K.J. Bonello, "Occupant energy management technique for restraint system analysis and design - understanding the physics of the system," SAE Technical Paper #922083.
- [8] M. Huang, J. Laya, and M. Loo, "A study on ride-down efficiency and occupant responses in high speed crash tests," SAE Technical Paper #950656.
- [9] J. Wu, G.S. Nusholtz, and S. Bilkhu, "Optimization of vehicle crash pulses in relative displacement domain," *International Journal of Crashworthiness*, 2002, 7(4):397-414.
- [10] J. Wu, S. Bilkhu, and G.S. Nusholtz, "An impact pulse-restraint energy relationship and its applications," SAE Technical Paper #2003-01-0505.
- [11] D.J. Gabauer, "Predicting occupant injury with vehicle-based injury in roadside crashes," Dissertation, Virginia Polytechnic Institute and State University, 2008.

# ESTIMATION OF FRONT UNDERRUN PROTECTOR EFFECTIVENESS IN TERMS OF FATALITY REDUCTION

**Asao Koike**  
**Yoshiaki Okami**  
**Atsushi Miyamae**  
**Ryota Yamamoto**  
ISUZU Advanced Engineering Center  
Japan

**Peter de Coo**  
Coo-Consult  
The Netherlands

**Sjef van Montfort**  
TNO Integrated Vehicle Safety  
The Netherlands

Paper Number 15-0041

## ABSTRACT

Frontal collisions between cars and trucks lead to high fatality rate of the car driver. Therefore the Japanese road administration established a directive, conformity to ECE-R.93 (2000/40/EC), compulsory since September 1st, 2011. As known, this directive describes a 'rigid' Front Underrun Protection (FUP) device installed on a truck. New developments are in the direction of energy absorbing devices in order to manage more severe impacts between both vehicles. The question is how to estimate the effectiveness of these devices.

Using a virtual car fleet, the effect of different FUP devices installed on or integrated with a truck front end can be estimated by simulation, in terms of injury severity and crash severity. The relationship between both makes it possible to estimate injury severity via crash severity. By transferring injury severity to AIS scale and fatality rate, a coupling can be made with real accidents and their effects on injuries. The other subject is to indicate the car severity by replacing a specific car fleet to a general device, in order to simplify the evaluation. The paper shows the steps from the simulations, to the analyses and simplifications, transfer to AIS scale and mapping on the real accident database, to predict the reduction of fatalities by using different types of energy absorbing FUPs (e.a.FUP).

In order to represent the car fleet, the Moving Progressive Deformable Barrier (MPDB) was selected. The MPDB was modelled to collide to a truck with an e.a.FUP. By this method, number of fatalities, or fatality reduction rate of the car for a certain e.a.FUP was estimated from the MPDB crash severity.

The processes in this study are based on simulations and accident investigation and analysis. The vehicle models used in the simulations are mainly validated on NCAP frontal impact tests. Some cars were validated at higher speeds, up to 90 km/h.

In this paper the prediction of injury levels is only based on the HIC to show the concept/principle of the method, but the method can be extended with other injury parameters.

The method described in this paper uses the Acceleration Severity Index (ASI) of a car-to-truck frontal collision in order to determine the probability of injury and fatalities. It uses AIS scaling and mapping on a matrix of relevant car to truck accidents. This simplified method can be applied to predict the e.a.FUP effectiveness in terms of injury reduction, and especially the fatality reduction.

## INTRODUCTION AND METHODOLOGY

New designs of safety structures need intensive testing and assessment before being realized and installed on vehicles on the road. However, the development of a realistic test setup is often a problem. Another problem is to find a way to value the usefulness and impact of the design on the society. In a previous paper [1] ways to test these structures, i.e. energy absorbing truck front underrun protection devices, were indicated. It was also suggested to use a generic test device instead of passenger cars with dummies for the final evaluation and assessment of newly designed truck front structures, and in particular an energy absorbing front underrun device. Using crash severity and accident severity information, the effect of a new design truck front structure can be estimated in terms of fatality reduction (See Figure 1).

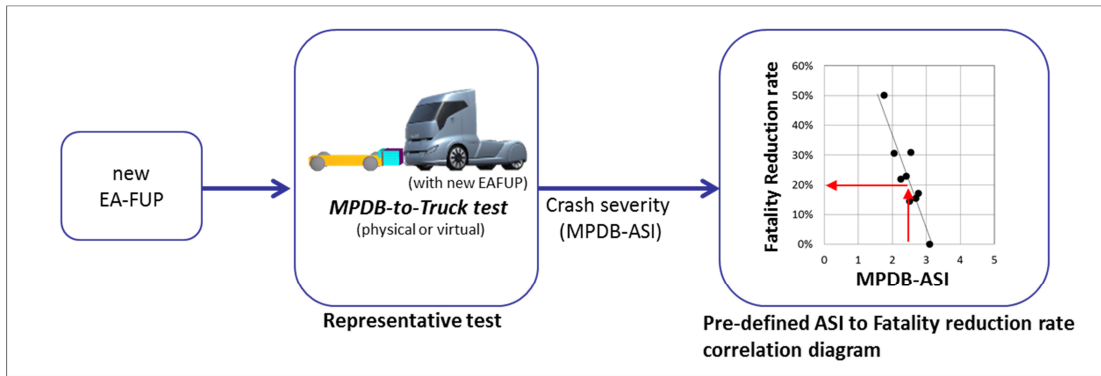


Figure 1. General concept of estimating FUP effectiveness

A similar idea but slightly different in implementation is given in [12]. The first steps to realize the above concept were made in [1]. In brief it boils down to the following. Based on accident investigation, vehicle registration and available test data a car fleet was selected and modelled. Also a 'standard set of FUP devices was defined, consisting of one 'rigid' FUP (fulfilling legal requirements) and 2 sets of 4 energy absorbing FUPs. Simulations of car-to-truck frontal collisions were carried out taking into account various accident parameters like relative speed and offset. This resulted in information about crash severity and injury severity. It appeared that a correlation can be indicated between the ASI and several injury parameters, like Head3msG, HIC, Thorax3msG, Chest deflection and Pelvis3msG. It also appeared that injury limit values for these injury parameters (e.g. HIC 1000) show an ASI limit value of 3 on an exponential curve. This process is visualized in the blue box, Figure 2-I.

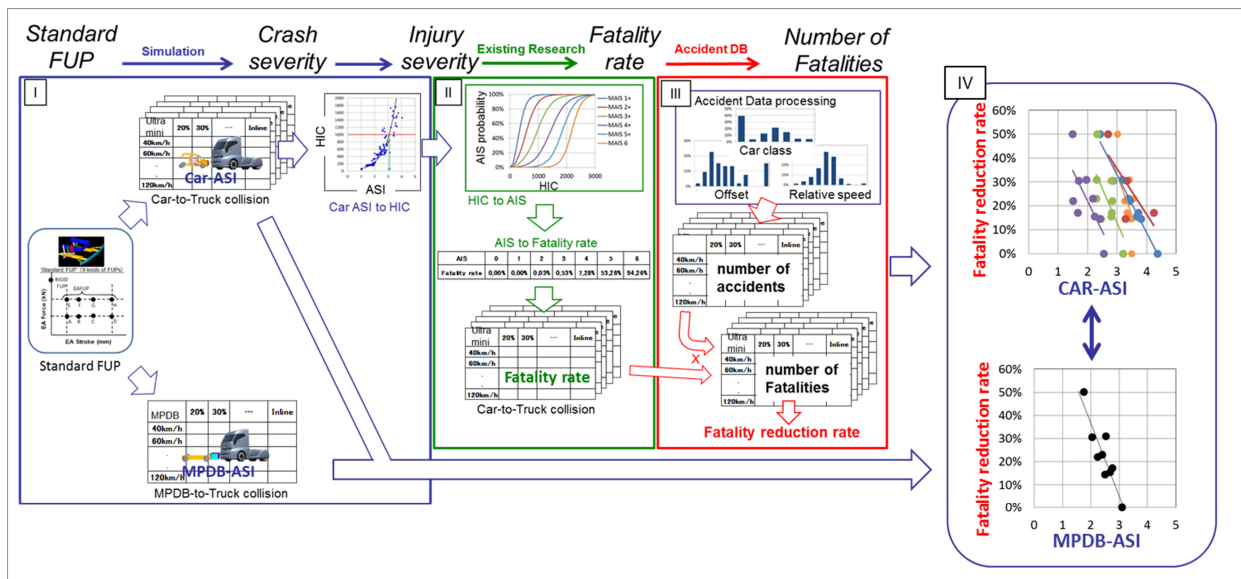


Figure 2: Outline of the method

The green box (Figure 2-II) shows how injury severity is transferred to Abbreviated Injury and subsequently to a Fatality Rate, which allows to transform the individual simulation data (Figure 2-I, blue box) to individual fatality data (Figure 2-II, green box). The next step is to associate this information with the information from accident data and fatality numbers (Figure 2-III, red box), resulting in a relationship between accident severity (CAR-ASI) and fatality numbers / fatality reduction rate (Figure 2-IV). In another line (bottom of Figure 2-I) the same batch of simulations is applied using a generic test device (MPDB) leading to a similar relationship between accident severity (MPDB-ASI) and the same fatality numbers / fatality reduction rate (Figure 2-IV). The relationship between CAR-ASI and MPDB-ASI will be shown in this paper, as well as the description of the consecutive steps mentioned above, starting with the green box.

### HIC TO FATALITY RATE

For the quantification of occupant head injury (HIC), the Abbreviated Injury Scale (AIS) is used. Formulas for the HIC versus injury probability for the 6 AIS+ levels are given in [5]. In a similar way as described in [3], the correlation between HIC and AIS can be developed (See Figure 3). Combining this figure with the AIS 6 (fatal) curve, the probability of fatality can be determined (See Figure 2-II and Table 1). The probability of fatality is used to transform all injury data from the simulations to a fatality rate for the individual simulated accident cases (See Figure 2-II, bottom picture in green box).

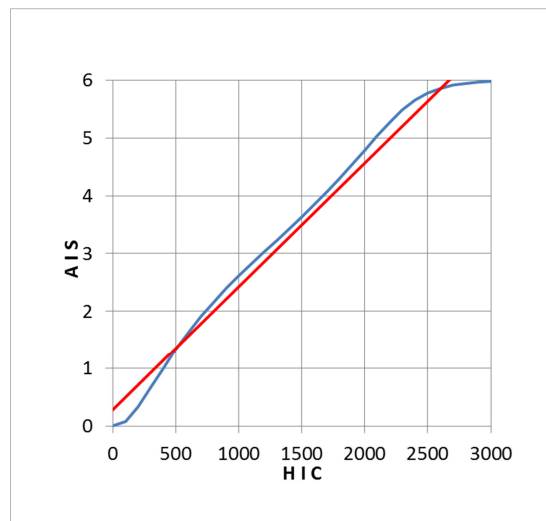


Figure 3: HIC-AIS relationship (trendline red)

Table 1. Relationship between AIS, HIC and fatality rate

AIS	0	1	2	3	4	5	6
HIC	0	329	798	1267	1736	2206	2675
HIC range	~ 93	94 ~ 562	563 ~ 1031	1032 ~ 1501	1502 ~ 1970	1971 ~ 2439	2440 ~
Fatality rate	0,00%	0,00%	0,03%	0,53%	7,28%	53,28%	94,26%

## STATISTICS

The road vehicle registration database provides information about the amount of vehicles in different classes on the road. The traffic accident database provides information about the vehicle types involved in accidents and global information about collision type and injury. From in-depth accident analysis, more specific information on type of accident, speed and injury are known and can be rated in more detail.

### Car distribution in car-to-truck head-on accidents

From the national accident database (2007 – 2011) [8] the representation of vehicles involved in car-to-truck head-on accidents can be obtained. As a standard for this database, the following classes have been defined: Ultra mini passenger car, ultra mini non passenger car, Sedan 1, Sedan 2, Mini vans, 1 box vehicles, SUV. In Figure 2-III the distribution of the cars in the different classes is shown. In the current study, however, another class definition was adopted: Ultra mini, Super mini, Small family, Saloon, SUV. This definition is more or less based on the one used by Euro NCAP. These vehicles represent 77% of the total registered cars. The numbers of vehicles in the 5 classes has been extrapolated to sum up to 100%.

### Truck data

In the national accident database [8] most of the trucks were not supplied with a FUP (compulsory from September 2011 on new trucks). In the current paper it is assumed that trucks are fitted at least with a rigid FUP for determining the fatalities in these accidents. Therefore corrections were made on the number of fatalities, based on a study described in [4].

### Relative speed

In the national accident database the traveling speeds of car and truck in the accidents is available. The relative or closing speed, however, is always lower than the sum of both speeds (braking). In this paper the relative speed is determined on the basis of an internal study by ISUZU. The distribution of the relative speed is shown in Figure 2-III. The relative speed concentration is around 80-100 km/h.

### Offset distribution

From in-depth studies of special cases in the national accident database the offset distribution is estimated (See Figure 2-III). Especially in the high offset range this estimation is not always very precise. Offsets between 60% and inline can be everywhere in this range. Offsets collisions lower than 30% may result in a different event: the vehicle slides off instead of crashes into the truck front. Together with the offset limitation caused by the PDB width, the offsets in this paper range from 30% to 60%.

## NUMBER OF FATALITIES AND FATALITY RATE

From the national accident database a total number of 433 fatalities in car-to-truck head-on collisions in the period 2007 – 2011 could be subtracted. From this number of 433, 53 cases were selected for in-depth analysis. The analysis resulted in allocation of these fatalities in the above mentioned categories of vehicle class, relative speed and offset. With this classification, including all 433 fatalities, and using the fatality rate with AIS score, a number of fatalities could be associated with each type of collision. This resulted in the graph of Figure 4. Taking the number of fatalities using a rigid FUP as the standard, a fatality reduction rate can be determined along the vertical axis of this graph, ranging from 0% (FUP performance identical to rigid FUP) to ~60% (FUP performance better than rigid FUP).

It should be noted that the trendlines for the 5 selected vehicles almost have similar slopes. This means that it does not matter which trendline is used to determine the amount of reduction.

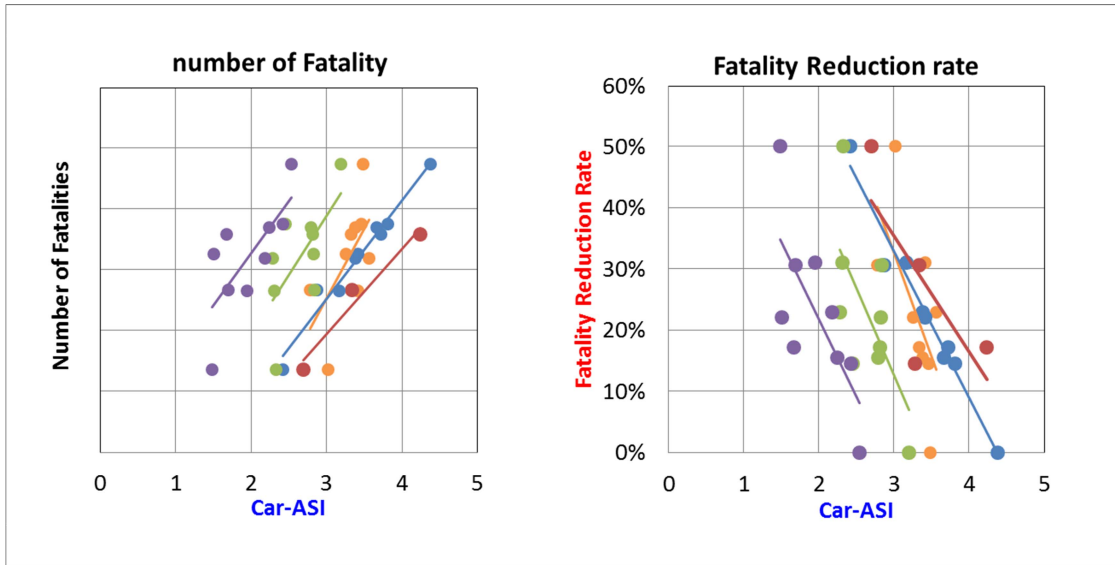


*Figure 4: Car-ASI versus Number of Fatalities and versus Fatality Reduction Rate for the vehicle fleet*

### MOVING PROGRESSIVE DEFORMABLE BARRIER

The assessment of an energy absorbing front underrun protection device in terms of fatality reduction can be done by using a passenger car with dummies in a car-to-truck frontal collision. Instead, a Moving Progressive Deformable Barrier (MPDB) will be used for simplicity reasons, cost reduction and generalization. The MPDB was investigated within the FIMCAR project [11] in frontal offset car-to-MPDB collisions with the purpose of assessing self-protection and partner protection of passenger cars. Focusing on partner protection, the MPDB may be used in frontal offset MPDB-to-truck tests. The MPDB is then used as a loading device, replacing the impacting passenger car. Based on the results, a statement can be given on crash severity, injuries to passengers and the compatibility of the e.a.FUP and the passenger car's front structure.

#### New PDB

The geometrical conformity between a MPDB (Progressive Deformable Barrier installed on a trolley) and a passenger car and between a MPDB and a truck is shown in Figures 5a and 5b.



*Figure 5a: Car front versus MPDB*



*Figure 5b: Truck front versus MPDB*

The size of the PDB [10] (especially the height) is hardly of influence on the outcome of the test with the passenger car. However, in a test with a truck the upper part of the PDB may contact the stiff longitudinal members, tilt mechanism or cabin floor. This will not happen in a car-to-truck collision, or at least at a much later stage. The current size of PDB may lead to incomplete contact between the PDB lower part and the e.a.FUP. Therefore the conditions of a resized PDB have been evaluated, in such a way that they do not affect the current stiffness properties of the PDB.

The misalignments of the PDB have also been recognized in other research [6]. In relation with a truck front end, a number of modifications are suggested. The current height of the (M)PDB (700mm + 150mm ground clearance) might not be realistic for interaction with trucks. In [6] suggestions for adjustments and tests are made, see Figure 6a.

From studies by GRSP ECE-TRANS-WP29-GRSP-2007-17e and VC-COMPAT [9], this barrier front face includes nearly all stiff structural components of a selection of passenger cars. The depth of the barrier, especially with the stiff 90mm honeycomb at the back, is adequate for impacts with passenger cars, due to the load spreading capability in the car front structure. When impacting a truck front structure with mainly a FUP beam, this may lead to bottoming out of the barrier. Therefore the bumper structure from the Offset Deformable Barrier (ODB) was used on the PDB (See Figure 6b) to spread the local load from a single FUP beam into the PDB.

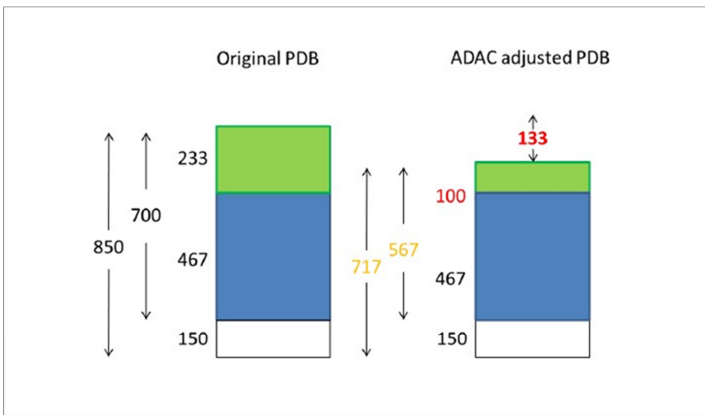


**Figure 6a: Original and alternative front of PDB**

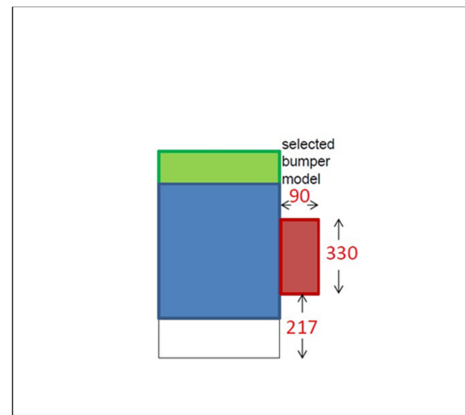


**Figure 6b: Alternative PDB front with bumper**

It is clear that the bumper structure does not allow aggressiveness assessment according to the standard PDB protocol. However, the modified PDB reflects better the load spreading by an average passenger car.

Regarding the width of the PDB, the MPDB-to-truck collision with the current barrier width of 1m limits the overlap of the car by approx. 60%. (see Figure 7). So higher overlaps and in-line collisions can not be tested in this way.

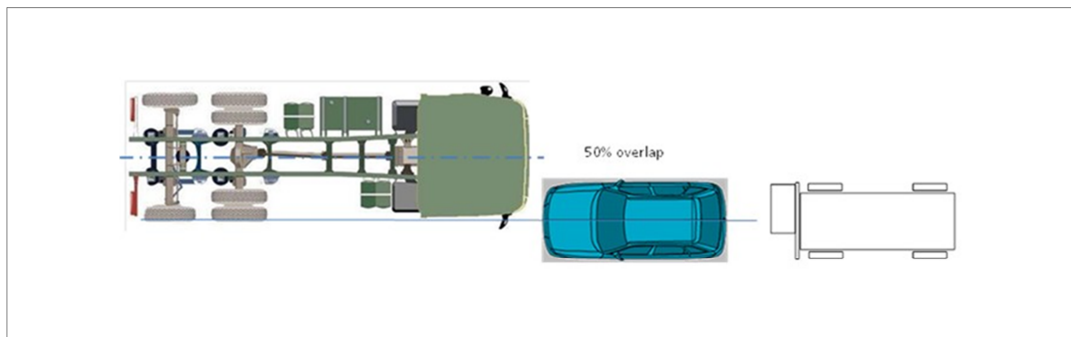


**Figure 7: Overlap of passenger car and MPDB**

## MPDB simulations and ASI comparison

Using the modified PDB, a batch of simulations was carried out. The parameters relative speed, offset and FUP type were varied. The results of these simulations produced an accident severity value ASI for each case. Combining these MPDB-ASI values with the CAR-ASI values obtained from the batch of car simulations, the graphs of Figure 8 can be composed. It appears that a linear relationship can be indicated between car and MPDB ASI.

A linear relationship allows a transformation from the Fatality Reduction vs CAR-ASI graph to the same graph with the MPDB-ASI on the horizontal axis.

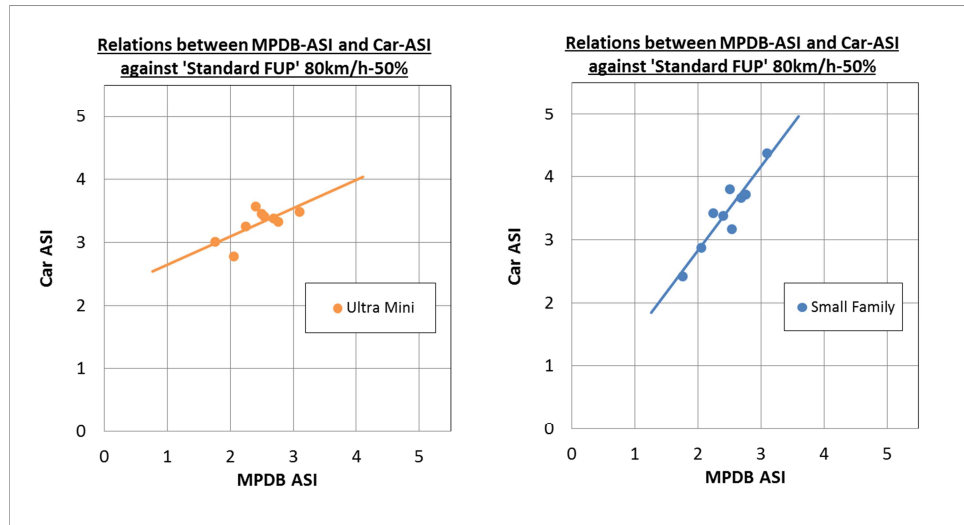


Figure 8: Relationship between CAR-ASI and MPDB-ASI

## SELECTION OF TYPICAL ACCIDENT

In order to estimate the effectiveness of a new FUP design, in terms of fatality reduction, relative to a legal rigid FUP, many simulations can be carried out and studied. These include ranges of relative speeds and offsets. From the accident investigations it appears that most accidents and fatalities occur in a speed range of 80-100 km/h. Collisions with relative speeds up to 90 km/h show that damage to the vehicles is large and that the energy absorbing capabilities of the vehicles are fairly to fully utilized. The offset concentration is around 40-50%. Close to 30% may lead to different impact behavior. Therefore a typical accident is chosen with relative speed of 80 km/h and 50% offset.

## EVALUATION NEW FUP DESIGN

The introduction of a rigid FUP on new trucks by enforcement through rule making is a very good step to reduce the seriousness of car-to-truck frontal collisions. Many studies, however, have shown that energy absorption by the truck front end is a good way of reducing the seriousness even further. By applying the method developed in this study the reduction can be quantified. A simulation of a collision (80 km/h, 50% offset) between the MPDB and the truck supplied with the new front structure results in an ASI value indication the severity of the crash. In Figure this value is put on the horizontal axis. When being left of the intersection of the trendline with the horizontal axis, the new front structure has a benefit on the fatality reduction. The reduction rate is determined by vertical intersection

with the trendline. An ASI value of 2.5 for instance results in a reduction rate of 20% with respect to a rigid front underrun protection device.

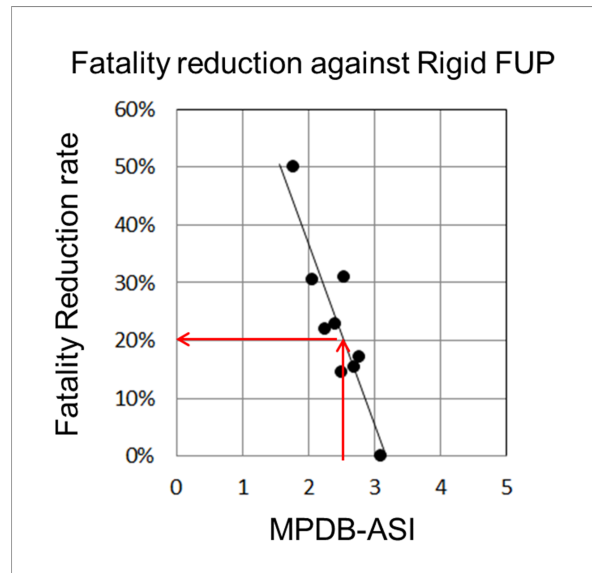


Figure 9: Determination of FUP effectiveness in terms of fatality reduction rate.

## DISCUSSION

There are a number of limitations to the study. The selection of car models which are defined as representative for the classes in the fleet is based on the availability of crash test results (from NCAP tests or private tests). Except for the in-house tests, which are carried out at high speeds, up to 90 km/h, the NCAP tests are normally carried out at speeds from 56 km/h to 64 km/h. In case overload situations (high speed impacts, up to 90 km/h) are simulated, the results may be different for models which have been validated against lower speed impacts. Therefore, the simulations outside the validation range are handled with care.

The width of the PDB is limited to 1000mm. As a consequence, only overlaps up to 60% be realized. Small overlaps are limited to approx. 30%. The PDB is uniform over the barrier width and smaller overlaps typically result in a different collision phenomenon. The MPDB is not representative for all type of cars.

Each simulation results in a set of injury values (head, chest, pelvis, etc.) for the occupant in the passenger car. In the study above only the HIC value is used to determine fatality via AIS. Other injury values can be involved in a similar way. However, AIS is a measure in accident investigation that describes the injury to a human per body region in real-world crashes. The different AIS values per body region can be combined to one overall injury criterion, known as the Injury Severity Score (ISS). The ISS predicts a percentage of mortality [7].

In this research, the interval in which the HIC reaches a maximum value was set to 36ms. This time interval affects the HIC calculation. In case of hard contact impacts this interval can better be 15ms, which is also applied in [5].

## CONCLUSIONS

The project described in this paper originally started with the aim of reducing injuries in car-to-truck frontal collisions by improving the compatibility of the truck front structure. Evaluation of a new truck front design is usually done by full scale testing using a passenger car with a dummy installed. This is a limited, costly and complicated way to obtain a feeling about possible reduction of injury to car occupants. Therefore a simplified and less costly method was developed by using a generic loading device replacing car and dummy, and by

doing computer simulations of these crash tests in order to evaluate more parameters which are involved in these collisions.

Although the national accident database includes 5 years of data, the amount of data related to car-to-truck frontal collisions is relatively low (433). Especially the number of in-depth cases from which detailed information about the accident is subtracted is low (53). This has consequences on the accuracy of the number of fatalities and on the fatality reduction rate. However, it is also recognized that by inclusion of new data (additional years) from the national accident database, the composition and distribution of the fatalities will also change, because of introduction of newer car and truck designs, new roads and road design, etc. In the current method the use of an MPDB replacing the car is therefore an advantage, but the influence of new statistic information should be faced.

The size of the standard PDB was adapted and a bumper element was added. The size was changed in order to have a better structural interaction with the energy absorbing front of the truck (the FUP). The influence of height reduction of the PDB may be small for the application in assessing car self-protection and partner protection. The bumper element was added to the PDB in order to have better load spreading from the (isolated and limited contact area) FUP to the MPDB. Especially in the lower offset cases the FUP, without any adjacent structures, may penetrate the honeycomb of the PDB till the end, resulting in bottoming out. A bumper element may reduce this, however, the possibility of aggressiveness evaluation is abolished.

The method described in this paper allows a quick evaluation of new truck front designs with respect to fatality reduction. Assuming that the accident statistics do not change abruptly from one year to another, the estimated reduction of fatalities might be valid for some time, especially when the fatality reduction rate is used.

## REFERENCES

- [1] A. Koike, K. Toyofuku, N. Iguchi, K. Yamaguchi, R. Yamamoto, P. de Coo. "A new assessment method for car to truck compatibility". DEKRA Symposium Safety of Commercial Vehicles, November 2012.
- [2] A. Krusper. "Structural Interaction between Vehicles". Thesis for the degree of doctor of Philosophy in Machine and Vehicle System. Dept. of Applied Mechanics, Chalmers University of Technology, Gothenburg, Sweden, 2014.
- [3] M. Shojaati. "Correlation between injury risk and impact severity index ASI". 3rd Swiss Transport Research Conference, Ascona, March 2003.
- [4] Y. Sukegawa, H. Kubota, T. Hirase. "Japan's Approach for Car to Truck Compatibility in head-on Collisions". Japan Automobile Manufacturers Association, ESV Paper Number 7-0989.
- [5] NHTSA. "Injury Risk Curves". <http://www.nhtsa.gov/cars/rules/rulings/AAirBagSNPRM/PEA/pea-III.n.html>
- [6] A. Radzek. "ADAC Compatibility-Crashtest". Advanced Automotive Front-end 2012. Landsberg, November 2012, Munich.
- [7] F. Leneman, on behalf of the VC-COMPAT truck leg consortium. "Assessment of Energy Absorbing Underrun Protection devices". DEKRA Symposium Safety of Commercial Vehicles, October 2004.
- [8] "Domestic accident statistics data (Macro data)". Institute for Traffic Accident Research and Data Analysis (ITARDA).
- [9] VC-Compat: <http://vc-compat.rtdproject.net>
- [10] J. Saunders, P. Delannoy. "Results of NHTSA's Comparison of the Offset Deformable Barrier and the Progressive Deformable Barrier Test Procedures". Paper Number 09-0549
- [11] FIMCAR: <http://www.fimcar.eu>
- [12] J. Winnicki, R. Eppinger. "A Method For Estimating The Effect Of Vehicle Crashworthiness Design Changes On Injuries And Fatalities". DOT HS 808 680, February 1998.